PHYSICAL AND NUMERICAL ANALYSIS OF FRACTURE IN FLAT PLATES ARISING FROM TRANSLATING LOADS

By

© Jonathan Howell, B.Eng.

A thesis submitted to the School of Graduate Studies

in partial fulfillment of the requirements for the degree of

Master of Engineering

Faculty of Engineering and Applied Science

Memorial University of Newfoundland

Oct 2018

St. John's Newfoundland and Labrador Canada

Abstract

Previous work with moving loads showed a significant decrease in structural capacity of samples subjected to moving loads that caused plastic damages, however did not investigate loads which incited fracture. The state of the art in material science for ductile metals indicates that fracture can be predicted by a locus of triaxiality, Lode Angle Parameter and effective plastic strain. However, in the case of stationary loads*, effective fracture strain* has been used to accurately predict fracture.

Collision analysis for loads which incite fracture is more frequently being completed using non-linear finite element analysis, commonly using the *effective plastic strain to fracture* method. However, real collisions are often oblique, and as such, it can be assumed that some horizontal translation is realistic and should be modelled as a moving load.

This thesis explores the effects of moving loads which incite fracture in plate samples using experiments and corresponding numerical models. The results of this thesis found a significant loss in ability to resist fracture during the horizontal translation of a load along a plate sample as well as a clear inability to accurately characterize a moving load numerically using the *effective plastic strain to fracture* method. In particular, this thesis presents: the results of laboratory experiments using the Moving Load Apparatus involving two distinct indenters (cutting and rolling wheel) designed to induce different stress states; a discussion of calibrated numerical models as well as triaxiality and Lode Angle Parameter for the point of fracture of these models.

Acknowledgements

Dr. Bruce Quinton – my supervisor. Thank you for the incredible amount of time spent on my work, discussing various other topics which came up during research, support and supervision, in addition to sparking an interest to pursue further study in the first place.

Technical Services – Billy Bidgood, David Snook and any others involved in fabrication of samples and the cutting wheel. In particular, we "bent" the MLA approximately half way through testing, over half the samples had to be recut to allow installment within the apparatus. This was done extremely fast by the crew and allowed us to continue testing nearly immediately.

Technical Staff – Matthew Curtis, Craig Mitchell, Trevor Clark and work term student Phil Malone. Thank you for your expertise with the MLA and its operation, patience and the incredible amount of help and support and guidance provided.

My parents and grandparents for putting me in a position to continue my studies.

Finally, Emily for the immense amount of support and understanding you've met me with over the previous two years.

This research was supported through the NSERC Discovery Grant project "Effects of Moving Ice Loads on Damage to Hull Structures" and the RDC (InnovateNL) Ignite R&D project "Advanced Arctic Structural Engineering".

Table of Contents

List of Tables

List of Figures

List of Symbols, Nomenclature or Abbreviations

Elastic deformation/loads	Response of a plate sample that is loaded within its nominal elastic region where no permanent damage occurs.
Plastic damages	Response of a plate sample that is loaded past its nominal yield point where permanent damage/deformation will occur
Horizontal/Lateral direction	Any direction in plane with a plate specimen, however for this thesis refers to the direction aligned to the long axis of the plate sample. Both terms are used synonymously due the direction of travel of the plate sample corresponding to its long axis.
Vertical/Normal direction	The orthogonal direction to the plane of the plate sample or out of plane loading perpendicular to the plate sample. For this thesis, both are used interchangeably.
Moving load	Any load which includes lateral or horizontal motion along the plate sample.

Moving load effect	The phenomena associated with the reduced structural capacity (the ability to resist force or displacement) during a laterally translating load. Please note that the moving load effect refers loads which incite fracture and plastic level damages.
Moving load capacity	The structural capacity to resist a moving load. Please note that in this thesis, how the plate samples are loaded is separated into displacement and force controlled loadings. As such, any references to moving load capacity are in reference to their ability to resist the measured response (i.e. force for displacement control and displacement for force control).
Stationary load	Any load which is only loaded in the normal direction to a plate sample.
Stationary load capacity	The structural capacity to resist a vertical or normal load. For the purposes of this thesis, the stationary capacity is often compared to the moving load

	capacity in both the vertical and horizontal directions to assess the loss in capacity.
Effective plastic strain to fracture	The combined measure of strain through an element, analogous to equivalent stress.
Effective Fracture Strain	A value of effective plastic strain used to dictate the point of fracture of elements in numerical simulations

List of Appendices

Chapter 1 Introduction

In accidental collision or grounding scenarios, vessels or offshore structures can experience loads which induce fracture or tearing of the plating and structural members. Often, these fractures occur longitudinally along the hull as the load translates along the vessel and are a type of moving load. Quinton (2015) used numerical and physical experimentation to show that moving loads which induced plastic damage had a clear influence on the sample's response to load, significantly decreasing the capacity of a hull plate and frames structures when compared to identical stationary loading. Due to the path dependent nature of both plastic damage and fracture, there is reason to suspect that the fracture capacity of steel hull plating is also dependent on load movement.

The moving load scenario is important for both analysis of collisions after they occurred and for the further understanding of ships and offshore structures which operate in ice infested waters. Using the Coupled Model Intercomparison Project Phase 5 global climate model, analysis by Melia, Haines and Hawkins (2016) predicted that on average usage of Arctic trade routes would decrease shipping times by 4 and 13 days by late 21st century for Asian bound vessels from North American and European ports respectively. Further, the analysis predicted that moderately ice strengthened vessels (Polar Class 6 and above) would likely be able to transit the Arctic for 10-12 months annually in the same time period. Additionally, the work predicts trans-Arctic shipping (accessible for open water vessels) for a season ranges of 2-4 months and 4-8 months for low and high emission assumptions respectively. As such, Arctic shipping is clearly desirable for both ice classified and non-

classified vessels and with the prospective increase in ability to do so, it is necessary that the limits of these vessels in accidental scenarios is properly characterized.

It has also been shown that ductile fracture for various types of ductile metals, classic J2 theory is insufficient to describe the phenomena and is in fact dependent on triaxiality and Lode Angle Parameter. These two parameters were originally used to predict fracture in rock and soil samples (Bardet 1990) with advancements including three invariants for the Sandia GeoModel (Fossum and Brannon 2006). Thus, the development of geomaterial science has far outstripped that of ductile metal plasticity and fracture. Bao & Wierzbicki (2004) showed that for varying ductile metals, in particular 2024-T351 Aluminum Alloy, triaxiality defined a ductile fracture curve with fracture strain, and give a fracture criterion as well as conditions which determine the nature of fracture. These fracture criterion were determined through standard upsetting tests and were centered about a cut-off value of -1/3 under which fracture could not occur, and a transition value of 0.4 where the fracture changed from shear fracture to void formation. Xue (2007) proceeded to show that the fracture criterion for ductile metals could be further refined into a fracture surface, known as a 3D locus with the inclusion of Lode Angle for certain types of metals. The fracture criterion are normalized values of -1, 1, which when combined with triaxiality, describe many specific load conditions. The three major states of stress, axial symmetric compression, plastic plane strain and axially symmetric tension correspond to $\theta = -1, 0, 1$ respectively with plane stress occurring in intermediate values. It should be noted that the theory was extended by Bai & Wierzbicki (2008) for A710 steel and later by Bai, Teng and Wierzbicki (2009) for 1045 and DH36 steel.

This thesis tests the hypothesis that the movement of the load affects the values for triaxiality and Lode angle, allowing for fracture at significantly lower capacities in comparison to hull samples subject to similar stationary loading. This is explored using physical experimentation in conjunction with corresponding, calibrated numerical models.

1.1 Background

Ship collisions have been analyzed extensively, through empirical or analytical methods with great effort put forth to determine a solution space which properly characterizes generalized situations for full scale ship hulls (Minorsky 1959). This has mainly been completed through the development of various energy methods and collapse mechanisms to characterize the absorbed energy during collision. The scope of the research is wide, however most neglect the movement post indentation.

Very little information of the movement post indentation exists for loads on ship hulls. Experimentally, Rodd & Sikora (1995) completed quarter scale tests with an inclined indenter to observe the damage patterns, and gather some quantifiable results based on impact energy and maximum deformation for two distinct frame sections. The work provided significant insight towards the nature of fracture mechanisms of the inner shell rupture of a double bottomed vessel and distinctly showed the need for further investigation to refine the nature of the response.

Following this Alsos (2008) divided the concept of a moving load into two problems; grounding and fracture onset. This study investigated two material instability criterion, which were implemented into numerical models and compared to experimental results for

stationary loading. The work identifies the necessity for a simplified method to accurately predict fracture for grounding ship loads, as well as the difficulty involved with meshing and implementing fracture. In addition to this work, Hong, Amdahl (2012) prepared a numerical model to a typical double bottom section in response to very light sliding loads during grounding (i.e. over a large surface area) termed as sliding loads. From this, a simplified, semi-empirical methodology for assessing the resistance of the sliding motion was presented based on separate analysis of the primary failure modes of the three major structural components.

The concept of a moving load was then analyzed in depth by Quinton (2015). It was shown that moving loads caused reduced structural capacity for loads resulting in plastic damages. A series of hull plate and frame experiments were completed which showed a reduced vertical force (or capacity) for moving loads in comparison to identical stationary tests and the nature of the moving load effect was further investigated through a set of calibrated numerical models.

Ship collisions causing tearing damages have been examined in great detail, with significant efforts placed in developing analytical solutions describing the observed responses, particularly for plate samples. Various authors have approached the subject, both empirically and analytically. Vaughan (1980) , Lu & Calladine (1990), Paik (1994) and others used experimental testing to develop formulae or methodology to describe the phenomena, while Zheng (1994) and Wierzbicki (1995) described the collision event theoretically, with the later developing a closed form solution describing the various mechanisms contributing to the cutting force. The ideas were further developed by

Simonsen & Wierzbicki (1998) who refined and simplified the solution, as well as Simonsen (1998) who developed for a cone shaped indenter. In each case, the load movement was not compared to a similar stationary load with respect to capacity, but instead focused on developing analytical expressions to describe the cutting forces, particularly from the deformation pattern of the collision. Additionally, much work was completed to integrate these analytical expressions into known energy collision methods as previously outlined, where internal work (structure response) is equated to external energy (colliding object).

1.2 Methodology

To investigate the possible moving load effect on fracture and the theorized connection to the fracture parameters, Lode angle and triaxiality, laboratory experimentation were conducted. These tests were designed to confirm the applicability of moving load effects to fracture, to clarify the factors which influenced the moving load effect, and to provide a base comparison for the corresponding numerical experiments presented in Chapter 5.

1.3 Thesis Organization

This thesis is divided into the following sections:

1. Introduction – Briefly introduces the concept of moving loads and fracture, including previous work and current knowledge. Displays the need to further investigate the effects of moving loads on fracture capacity, particularly due to accidental loads.

2. Literature Review – Identifies and explains the relevant literature to collision assessment, moving loads and fracture mechanics including the gaps which the thesis addresses in the current understanding of the topics.
3. Experimental Setup – Discusses and displays the Moving Load Apparatus setup and corresponding test procedures.
4. Experimental Results – Details the results found from the performed moving load experiments.
5. Numerical Analysis – Presents the corresponding numerical models for various experimental cases. Describes the calibration of the models and comparison to the respective experimental case.
6. Conclusions and Recommendations for Future Work – Reviews the research, presents the conclusions and recommendations for future work in moving loads which result in fracture.

Chapter 2 Literature Review

There is increasing financial motive to travel into Arctic waters for both ice strengthened and open water vessels, and as these transits become commonplace, the probability of scenarios which result in accidental damages causing plastic damages will increase. This thesis posits a decrease in fracture capacity in flat plates due to the moving load effect. In such situations, where loads translate along the hull, there is a clear potential for fracture to occur. Therefore, it is necessary to examine the phenomena as to properly understand its impact and apply the knowledge gained to further understand the risks involved with Arctic transit.

There is very limited work exploring moving load effect, most completed by Quinton (2015). His work focused on displaying its impact on plastic load cases as well as verifying elastic load inciting an elastic response can be treated as stationary loads. Outside of this work, Hong and Amdahl (2012) and Hong (2009) investigate the specific scenario of sliding loads causing plastic damage are the only other works which directly investigate moving loads. Of these studies, none explored the effect of horizontal load translation on fracture initiation. The work by Alsos (2008) explores moving loads to induce fracture, however fail to quantify the losses experienced due to horizontal translation.

In addition to the newly described moving load phenomena, there has been much recent advancement in the material science of fracture, specifically the work considered by Bao and Wierzbicki (2004), Bai and Wierzbicki (2008) and others on triaxiality and Lode angle dependence. This work has largely focused on the generation of three dimensional fracture locus' to predict fracture of T351-2024 aluminum alloy & 1045, A710 and DH36 steel. The

work has shown that fracture of ductile metals has a clear dependence on one or both of the parameters and therefore should be considered in analysis.

In addition very little application to the numeric modelling of fracture exists. Currently, no work considers both the application of the fracture terms (stress triaxiality and Lode Angle Parameter) and moving loads. The sole work in this field is the consideration of stress triaxiality (or biaxiality for shell elements, where through thickness is neglected) in the modelling of ship hull fracture was completed by Alsos (2008) but neglects Lode Angle Parameter and moving loads.

The literature review was developed to discuss the existing research completed in areas which can be applied to moving loads causing ship hull rupture or can be used to benchmark and compare the results of the numerical portion of this experiment. This includes relevant research on current collision analysis, moving loads, tearing and fracture, specifically triaxiality & Lode angle dependence.

2.1 Collision Analysis

This section of the literature review was developed to outline the current state of collision analysis, including the basic understanding behind the numerical and analytical modelling. The literature was fundamental in the development of a firm understanding of the current technologies and techniques used in similar analyses which in turn assisted in the development of the results of this work.

2.1.1 Ship Impacts

Ship impacts resulting in serious plastic damage can typically be broken into three different categories. The first is ship to ship allisions or collisions, where the movement of one or both vessels results in an impact, respectively. The second is known as grounding or shoaling, which occur when a ship makes contact with the seabed or submerged objects, commonly due to sudden changes in the topography of the ocean floor. The third is ice/iceberg to ship impacts, which do not commonly result in severe deformation. Due to the similarity of all three, there is an extensive amount of available literature for all types of impacts with focuses on collisions by Minorsky (1959), and Rosenblatt (1975) and while Hong (2009), Alsos (2008) and Hong & Amdahl (2012) have pioneered work on grounding impacts. The findings of this report are applicable to all impacts which potentially result in hull rupture (including any which are outside the three categories listed above).

2.1.2 Non-Rupture and Rupture Impacts

When considering any type of impact, the amount and type of resulting damage is often the goal of analysis. As such, impacts can again be sub-divided to impacts that result in some level of plastic deformation but do not experience rupture, and those that do rupture. It should be noted that several types of impacts, particularly ice-ship may result in deflection in the elastic region, which will reverse with unloading and result in no permanent deformation. These impacts causing elastic response carry no significance regarding the subject of this research, and as such will not be discussed further.

Innovations into the characterization of rupture impacts was completed in the past century, with the development of Minorsky's Method (1959). The methodology was created to

empirically describe a collision or grounding through the use of the conservation of energy. This was done simply relating the impact energy of one or more vessels to the volume of displaced steel observed in the crash.

The major shortcoming of this method is the inherent assumption that membrane stress in the hull plating prior to rupture is negligible (MSL 2000) and as such, the methodology is unsuitable for low speed collisions. The method has been expanded significantly as a result of further analysis of exclusions found when applying the original to broader empirical data sets. In particular, Rosenblatt (1975) expanded the work for low energy impacts not resulting in rupture by rectifying the shortcoming addressed above through the introduction of progressive plastic damage, which is simply the concept of the hull section possessing a reserve of plastic "strength" which is exhausted before rupture occurs.

2.1.3 Collision Mechanics

The mechanics of ship collision or grounding is mainly developed from typical particle collision physics, expanded for the structures and hydrodynamic components involved in a ship collision. As such, collision analysis is typically divided into external and internal components, which can be either decoupled or coupled, depending on the type of analysis. The external mechanics is the determination of the global rigid body motion and hull girder loads, and the resulting total energy that the deformation and friction will be required to absorb (Hong 2009). External dynamics have been studied in detail by various authors, including Pedersen and Zhang (1998) for collision purposes and Simenson and Wierzbicki (1998) for grounding situations. External dynamics are not the focus of this work and are therefore omitted from detailed discussion. Internal mechanics attempt to determine the

structural response given the required dissipation of energy dictated from the external dynamics. The following section covers the various research and methods currently used to analyze the internal mechanics of a collision or grounding.

2.1.4 Methodology

The advancement of collision analysis has been driven by industry trends since the late 1950's, with the aim of producing protected nuclear reactor cores for merchant ships, which would remain intact in the event of collision with another vessel. After the concept of nuclear merchant vessels was deemed unviable, the motivation for collision analysis shifted to focus on the protection of oil carriers to minimize pollution in the 1970's. Today, the focus remains focused on pollution, in conjunction with damage stability, and ultimate strength of damaged ships (Samuelides 2015).

The analytical and empirical models have been developed since the commencement of collision analysis with the analysis of the nuclear powered vessel Savannah, where the structure was designed to withstand an impact at 15 knots (670 MJ) without causing damage. The method used to develop the protective structure is known as the Minorsky Method, which relates the volume of damaged material elements that are in line with the impactor or indenter, through the use consideration of 26 collision incidents, giving the following expression:

$$E_D = 32 + 47 * R_T$$

Where E_D is the energy absorbed by damaged elements (in MJ), while R_T is the combined volume of damaged elements of both vessels (in m^3). The method is as result of actual

collision data, and is notably only applicable for high energy impacts, or those which cause rupture or fracture on the outer shell (Minorsky 1959).

Currently there are several viable methods to analyze ship collision, which include finite element analysis, simple formulae, analytical and empirical models, and experimental work. The utilization of simplified formulae result in a high level estimate of energy absorption by the damaged structure(s) and has been vetted through many iterations of experimental testing or real world data. These formulae offer basic result results for minimal effort and can easily be applied in general practice.

Experimentally, much scale work has been completed which investigates the collision process and reaction of the damaged structure. This includes large scale work completed by Woisin (1979) extending the Minorsky Method. Additionally, model scale tests have been completed by Paik & Pedersen (1996) on double hull penetration and Rodd & Sikora (1995) which is discussed in Chapter 2.2. Additionally, more experimental scale tests have been completed specifically to observe and describe the mechanics, such as (Wierzbicki 1995) which directly addresses tearing.

Tests were also completed by (Wang, Ohtsubo, and Liu 1997) to observe the behaviour of a double bottom during a grounding event. Here scale models were collided with five different conic indenters with varying radii to model scenarios from grounding on sharp rocks to shoaling or contact with flat seabed. An additional test scenario of contact with a vessel of a small bow angle colliding with the large bow of a generic VLCC was also explored. The results were characterized in simple theoretical models and from this, formulae were derived. The primary failure modes included membrane stretching of the

shell panel, onset rupture, crack propagation, folding of main supporting members and crushing of intersection of main supporting members. The main purpose of this work was to develop a simple analytical based method to describe the nature of the damage and then match with existing data.

Following the experimental work, there are a number of applicable works which use simple analytical formulae in attempts to characterize ship collisions. Examples of this include (Wang, Ohtsubo, and Liu 1997) which deals with raking damages, (Pedersen and Zhang 1998), which attempted to address the inherent issue with empirical derivation; the variability of the collision scenario, in particular the structural arrangement of the vessel and the low energy extensions of the Minorsky Method, by Rosenblatt.

One low energy extension of the Minorsky Method by Rosenblatt is known as the Tanker Structural Analysis for Minor Collisions method (or TSAMC) (Rosenblatt 1975). According to the author, 70-90% of the energy absorbed by a ship's structure results from plastic deformation of the side shell, and that as the shell begins to deform, significant membrane stresses occur. The TSAMC analyzes the energy required for tearing to occur, and to which depth the indenter will penetrate the hull from this energy requirement. The energy absorbed by the structure is divided into elastic and plastic portions, with the elastic including the hull girder vibrational response, classic bending of hull girder and local elastic deformation; while the plastic includes the deformation due to membrane tension in shell and deck, web frame shearing and plastic bending of sideshell plating (Rosenblatt 1975). In comparison, it was determined that the elastic portion was far smaller than the plastic energy absorbed, and the predominant contributor was the membrane stress in the sideshell.

The method is severely limited due to several assumptions and simplifications, which include a static collision, rigid bow, damage is limited to one area and the omission of tearing/rupturing. Due to these assumptions, the method poorly analyzes real collisions, as it fails to consider absorbed energy after penetration occurs (Calle and Alves 2011). It should be noted that Rosenblatt recognized the need to further investigate “cutting or puncture”, specifically the forces and energy associated with the failure mode.

Finally, finite element methods have become widely accepted as one of the most powerful tools moving forward when considering ship structural analysis (Hong 2009) with considerable efforts put into development of ship collision models and fracture propagation during collision. Early attempts at collision modelling were attempted including (Porter and Ammerman 1996), (Ammerman and Daidola 1996), with limited success. The early models all suffered from two major problems; the underestimation of the hydrodynamic contributions to the collision and the lack of a failure model, something still under investigation today. The hydrodynamic contributions have been corrected through proper vetting and comparison of the results, such as the work completed by Servis & Sameulides (2002) who simulated the lateral collision of a Ro-Ro vessel with a bulbous bow and compared with large scale experimental tests. Recent work has been completed by Alsos (2008) fracture of the material with validation to an experimental reference.

2.2 Moving Loads

Moving loads are simply loads which impact an object, then continue to slide along the impacted object, while remaining in contact. This phenomena is particularly applicable to ship hulls, where a majority of the collisions are oblique, or begin contact by moving

roughly normally to each other. A moving load is a distinct type of dynamic, transient load. With regards to this project, laterally moving loads causing rupture between frames (i.e. only hull plating is affected) are of interest. This includes both tearing and rupture due to material failure, both of which are commonly observed in collision and grounding. Other types of moving loads include non-rupture loads, which can be categorized as elastic or inelastic (Quinton 2015). As the focus is on rupture type loads, it can be assumed that any further discussion of moving loads refers to this type. It should be noted however, that a majority of the literature pertains to moving loads which do not result in rupture and provides both a clear justification along with significant background information to help facilitate this work.

The analysis of moving loads first began with the introduction of iron railway bridges in the mid-19th century by Willis, James and Galton (Timoshenko 1983). At the time, there was no consensus in the industry as to the impact of a moving load or force along a beam. There was considerable support for two sides, one supporting the idea that time was necessary to reach deflections seen in a static load, while others believed that the sudden loading would result in large deflections. Willis et al carried out realistic tests to investigate the nature of ultimate strength and moving loads, and discovered that the capacity was significantly reduced in comparison to static loading. The loading apparatus was essentially a pin-pin beam with a load moving laterally along the length. It was further discovered that these affects increased with an increase in speed.

Contrary to the ground breaking experiment, results from actual bridges showed a significantly lower increase in deflection due to a moving load. Willis repeated the

experiments again, simplifying the experimental setup and described the larger decrease in structural capacity as a result of the flexibility of the bars used in the original test. Further he developed an analytical solution describing the observations of both experiments, which is as follows:

$$W - \frac{W}{g}v^2\left(\frac{d^2y}{dx^2}\right)_{x=\frac{l}{2}} = W\left(1 + \frac{16\delta_{st}v^2}{gl^2}\right)$$

It was also determined that the path of the load was not symmetric about the center of the beam, and that it followed the following solution:

$$\frac{1}{\beta} = \left(\frac{16\delta_{st}v^2}{gl^2}\right)$$

An approximation of the solution was developed by Willis, but found to be inadequate for large β and was eventually solved by Stokes with good agreement to the experimental data. The two continued to advance the field eventually incorporating vibrational affects and considered several extreme cases. Various other authors further developed and explored moving loads for many load and structure types, many of which are explained in (Frýba 1972).

The application of moving loads to simulate grounding and other type damages on a ship hull, specifically plates has largely been pioneered by Rodd and Sikora (1995), Wang, Ohtsubo and Liu (1997), Alsos (2008), Hong (2009), Hong and Amdahl (2012) and Quinton (2008) and (2015).

Rodd and Sikora (1995) assessed the evaluation of the structural integrity of double hull tankers via experimental testing to simulate grounding and stranding, in an attempt to further the prediction of damage during these scenarios. Through the completion of several scale tests which involved a static indentation and moving collision with a “rock” indenter, two types of double hulls were assessed with the failure mechanisms analyzed. Regarding the moving load, one grounding case was addressed where a non-zero angle of attack was utilized. Here the leading edge of the “rock” indenter entered just below the inner shell of the double bottom, while exiting just above the inside inner shell. This was done to ensure that an optimum amount of data was collected, i.e. that the inner hull ruptured during the movement of the load, instead of the alternative where it either ruptured through the initial penetration (i.e. simulates a static load) or does not rupture at all. As such an angle of attack of 7.4 degrees was selected, which was further justified through a rough calculation which showed that this correlated to a collision at 2 to 3 degrees for 40 000 tons at full scale.

From the authors, it should be noted that the vertical damage was designed to occur in a shorter relative horizontal length than expected in a full-scale counterpart. Therefore, due to this geometric scale difference, the vertical measured forces were deemed artificially large. In terms of scalable results, Rodd and Sikora (1995) analyzed the parameters vertical distance before intrusion of the inner bulkhead and the amount of energy dissipated if an inner hull rupture occurred. It was found that due to significant plastic deformations, this distance increased drastically during collision.

For the conventional double hull design, it was found that the energy dissipated was 400 MNm. Further, their results presented some useful information on crack initiation. The

primary rupture of the inner hull initiated in the third transverse frame while the indenter was between the first and second frame, and that this crack propagates in the backwards, longitudinal direction, towards the indenter. When the indenter reaches the crack, extreme stress concentrations occurred resulting in immediate rupture of the inner shell. It was also noted as the indenter translated in the longitudinal direction, the distortion and subsequent tearing of the transverse frames caused a crack in the inner hull plating at the weld connection. These points are worthy of further investigation, as they may indicate and be influenced (or influence) Lode angle and triaxiality.

The raking damage tests by Wang, Ohtsubo, and Liu (1997) addresses global strength in the longitudinal direction for the bottom structure of vessels for horizontal penetration. Four failure modes were considered; deformation of the transverse structure, deformation of bottom plating immediately behind the transverse structure, tearing of the bottom plating, and tearing of the inner bottom plating. From these four modes, a methodology was described and checked against ASIS grounding experimental data and an actual grounding of a VLCC and found the method adequately predicted the results of the tests. This work had a similar purpose as this thesis; to access and potentially predict the capacity of bottom structures under horizontal loading, however focuses entirely on the determining the *horizontal resistance force* from penetration and completely omit the vertical loading on the bottom structure.

Alsos (2008) explored both fracture for grounding events. For fracture, the implementation of the BWH and RCTL failure criteria in numerical simulations was compared to a set of experimental results. This was completed to show the validity and necessity of additional

fracture criteria past simplified plastic strain to model grounding events. In addition, the resistance of indentation is explored as related to the size and shape of the seafloor, resulting in a series of characteristic scenarios. The resistance and resulting deformation during grounding during these scenarios was also explored.

Hong (2009) discussed a deformation mode for sliding loads when grounding, as well as identifying the large difference in deformation pattern between flat and sharp seabed obstructions. Additionally, a *wavy pattern* plastic mechanism for longitudinal bottom girders was proposed, and although the closed form solution was not determined, the problem was solved semi-analytically. Finally, an assessment tool for ship bottom structures during a grounding event was developed based on the plastic mechanisms presented and considered what was determined as the three major structural components; longitudinal girders, bottom plating and transverse floors.

Moving loads were separately addressed by Quinton (2008) addressed the lack of consideration in design codes for icebreaking and ice strengthened ships or installations. The work was focused on sliding damage due to ice-ship interaction, where it was predicted numerically that a significant decrease in plastic structural capacity would occur in both the shell plating and the frames of a vessel, when a progressive ice load that incited plastic damage was applied in comparison to a similar static ice load. However, it was also predicted that there would be no significant effect on elastic capacity. It was noted that a static load resulted in a symmetrical response throughout the structure, which promptly vanished as the load began moving.

The numerical experiments of moving loads involved a laterally translating indenter along a test hull to simulate sliding damage due to ice interaction. The loading of the test specimen was divided into three distinct stages; a vertical (out of plane) indentation, a lateral translation along the hull and a vertical unloading. Three categories of numerical tests were selected based on the travel direction and longitudinal start location of the indenter. These were longitudinally across multiple transverse web stiffeners, longitudinally between transverse stiffeners and transversely parallel to transverse web stiffeners. These categories were further expanded to include for a total of eight distinct scenarios based on the location of the loading in relation to the longitudinal stiffening. For the eight load scenarios, five levels of vertical displacement were tested, from 0.1% to 0.5% of the total length. The vertical force response found from these tests were then compared to the vertical force capacity of a static loading, where a general decrease in capacity was observed. It should be noted that the work did not consider element failure (fracture) and thus had infinite plastic capacity. Therefore, the higher loading cases are unrealistic and unsuitable to quantify structural capacity and can only be used to show the general trend of decreased capacity. Further, the *wavy pattern* mechanism outlined by Hong (2009) was not observed.

Quinton (2015) then continued to investigate the moving load effect experimentally and numerically, exploring several of the load scenarios from the previous work. This included the development of a novel Moving Load Apparatus and corresponding numerical models. The work quantified the loss of structural capacity during loading that incited plastic damage and showed numerically that elastic of pseudo-elastic damages can be modelled accurately as stationary loads. The experimental work considered six total factors; sample

type, starting location, vertical indentation, horizontal travel, vertical/horizontal speed and temperature. In addition, two types of loadings were used, force and displacement control. Finally, two indenters were used, a steel rolling wheel and an ice cone. This resulted in a total of 26 experimental tests.

Overall, the results of the displacement controlled testing showed a capacity loss of up to 40% for ½" plate specimens, 31% for ¼" specimen and 31% for frame specimens when compared to corresponding stationary loading. Further, the remaining factors of temperature and strain-rate were found to be largely insignificant at the ranges tested, regarding the vertical force capacity for moving loads. The frame tests also showed a huge increase in the vertical indentation during the force controlled experiments (up to 81% compared with similar stationary loads), thus indicating that typical frames poorly resist moving loads. The experimental tests also verified the early onset of plastic web buckling for moving loads on frames. Finally, the results of the ice cone experiments were unclear due to the small number of tests and variability of the ice, which resulted in a recommendation for future work. Following this, numerical tests were completed using the experimental results to calibrate and validate simulations for each of the sample types (½", ¼" and frame).

A response surface method (RSM) analysis of the various factors was completed, and showed that for all specimen types yield strength, boundary compliance and the interaction between the two, and boundary condition stiffness were the relevant factors, while the tangent modulus were only significant for the ¼" and frame tests. The results of all three RSM were found to be extremely sensitive to the boundary condition stiffness. This is

easily seen through the implementation of fixed boundary conditions which consistently resulted in an over prediction of capacity loss. Two suitable alternatives were found to correct this, the first by having the boundary far from the moving load, or to add corrections to simulate the imperfect nature of a real world fixed boundary. The first of these solutions is expensive computationally while the second was found to be difficult to estimate. Overall, the results were found to capture the moving load effect very well for the ½" and ¼" plate specimen, however the results for the frame samples were not compliant. With the frame tests, the post buckling behaviour was poorly predicted.

It should be noted that both Lode Angle parameter (Bai and Wierzbicki 2008) and stress triaxiality (Bao and Wierzbicki 2004) affect the development of plasticity and should be addressed in future work and analysis. The furthering development in this area would likely be widely applicable, due to the frequency of plastic deformation damages that do not result in rupture. For example, damages to ships operating in the ice infested waters of the Baltic Sea for the 2002-2003 shipping season were statistically suggested to typically to be permanent deformation in the shell plating as suggested by Hänninen and Rytkönen (2004).

Contrary to the work completed by Quinton (2015), this thesis will focus on the development of moving loads which result in plate rupture, i.e. fracturing of the shell plating, and the application of the Lode Angle and stress triaxiality parameters to explain the loss in fracture capacity for moving loads.

2.3 Tearing Mechanics

The goal of this section is to review and discuss the current state of the art of tearing mechanics applied to ship hull materials. Specifically of concern is the in-plane tearing of thin plates. While research exists which covers thick plates and block elements through the exclusion of membrane stress, they are not used in fabrication of ship hulls and as such will not be covered further. The current state of the science of tearing is fairly advanced with many empirical and analytical models covering analysis of damages. However, to date most of the analysis of tearing has been completed as to extend the theory and methodology for energy methods such as Rosenblatt (1975) for collision and grounding events.

Tearing analysis for shipping applications was first approached by Vaughan (1980), who first used data gathered by Akita and Kitamura (1972) to show that work done on a side shell by a wedge shaped indenter can be decomposed into bending and plate tearing components, and later conducted scale drop experiments to determine the quantities of each based on a number of factors. From these experiments, empirical relationships were generated to characterize both the bending and tearing work components. The work predicted that for small penetrations that tearing was dominant and bending a minor contributor, while the converse was true for large penetrations. The major limitation of the relation was the range of thicknesses tested, and it was eventually determined that the relation was only valid for steel less than 1.867 mm thick, and therefore the analysis only valid for thin plates.

Further experimental work to determine empirical relationships has been completed by Lu & Calladine (1990), Paik (1994), Simonsen & Wierzbicki (1998), Simonsen (1998) among

others, while further semi-analytical work was completed by Zheng (1994). These works were later incorporated into the energy expressions for ship collisions as a mode of damage by Pedersen & Zhang (1998), Zhang (2002).

2.4 Fracture Mechanics

This section of the literature review outlines the recent developments in fracture modelling and prediction for ductile metals. The goal of this paper is not to further the current state of the art regarding materials science, but to apply these techniques to ship collisions to further the state of the art in hull rupture prediction. As such, the literature reviewed was necessary to develop an understanding of the physical mechanisms which occur during fracture and thus allowed for the advancement of the predictive modelling of ship hull fracture.

2.4.1 Introduction

For isotropic materials, any stress state can be defined by the Cauchy Stress Tensor, σ_{ij}, also known as the stress tensor. The stress tensor can be divided into two components; hydrostatic and deviatoric, which can be defined as:

$$\sigma_{ij} = s_{ij} + p\delta_{ij}$$

where s_{ij} is the deviatoric stress tensor and $p\delta_{ij}$ is the mean hydrostatic stress tensor, $p = \frac{1}{3}tr(\sigma_{ij})$ is the hydrostatic stress (Malvern 1969), and δ_{ij} is the Kronecker delta function. The strain tensor, ε_{ij} can be divided similarly. Deviatoric stresses tend to change the shape of the yield surface, while hydrostatic loading results in a change in size.

The hydrostatic stress has a proven effect on fracture of ductile metals as shown by McClintock (1968), Rice & Tracey (1969) both through the study of void growth in various

sample types. Further, hydrostatic stress is related to the dimensionless hydrostatic pressure parameter, η, known as stress triaxiality, which can be defined as:

$$\eta = \frac{p}{\sigma_{vm}}$$

where σ_{vm} is von Mises equivalent stress.

Three invariants can be found for both the Cauchy Stress tensor, σ_{ij} and two nontrivial invariants for the deviatoric stress tensor, s_{ij}. For the deviatoric tensor invariants, it has been shown by Cazacu, Plunkett, and Barlat (2006), Racherla & Bassani (2007) that the second and third deviatoric invariants, have an impact on ductile fracture and plasticity of metals, and is usually normalized through the calculation of the Lode Angle, θ. Similar to stress triaxiality, it is frequently convenient to use a normalized parameter, known as the Lode Angle Parameter $\bar{\theta}$:

$$\bar{\theta} = \cos(3\theta) = \frac{27}{2}\frac{\det(s_{ij})}{\sigma_{vm}^3}, \bar{\theta} = [-1,1]$$

Both works developed models which included the strength difference between load states of compression and tension, however, ultimately both were unable to predict plane strain yielding.

2.4.2 Triaxiality

As stated previously, the fracture of ductile metals is strongly dependent on hydrostatic stress, and therefore stress triaxiality. This was first shown by McClintock (1968) and Rice & Tracey (1969) who demonstrated that ductile fracture is prominently dependent on

hydrostatic pressure through analysis of void growth in cylindrical and spherical voids respectively. This was continued by various authors, including Richmond and Spitzig (1984) who pioneered hydrostatic stress influence on aluminum alloys, Atkins (1996) who identified that fracture initiation criteria should be dependent on hydrostatic stress and Wilson (2002) who confirmed the Richmond & Spitzig's conclusions. Others, such as Norris et al. (1978), and others arrived at the conclusion that hydrostatic stress should be considered regarding fracture onset criteria. This was then furthered by Bao and Wierzbicki (2004) who highlighted that all current codes simply use equivalent fracture strain as a simplified criterion. To rectify this short coming, through fitting of experimental data, they found a relation relating stress triaxiality to fracture strain for Al 2024-T351.

Gurson (1977), Needleman & Tvergaard (1984), identified the concept of a shrinking yield surface with hydrostatic pressure. From here, the GTN model was developed, were equivalent strain to fracture was made dependent on the first invariant of the stress tensor, σ_{ij}. This fracture criterion was justified for ductile metals as yield will occur in the plastic range, and therefore any difference between strains will be much smaller in magnitude than for differences in stresses. Further, the GTN model describes tensile fracture, and therefore high stress triaxiality very well, but poorly predicts the shear failure mode seen in low triaxialities. Finally, the GTN model assumes that if the hydrostatic pressure is brought back to that of the undeformed stress state, the material will obtain its original strength.

Additionally, Bao and Wierzbicki (2004) observed that how fracture occurs depends on the levels of triaxiality experienced by the material and displayed the boundary between the fracture and no fracture regions for a wide range of stress triaxiailites through the revision

of the fracture criterion. From their experimental work for Al 2024-T351 it was shown that $\eta = -\frac{1}{3}$ (corresponded to uniaxial round bar compression), $\eta = 0$ (torsion test) and $\eta = \frac{1}{3}$ (uniaxial round bar tension) where $\eta = -\frac{1}{3}$ was the "cut-off" value below which fracture could never occur. It should be noted that triaxiality is not naturally bounded (i.e. can extend infinitely in either direction), however, the region of focus is about $\eta = 0$, as such, henceforth the region above $\eta = \frac{1}{3}$ are referred to as upper region while below $\eta = -\frac{1}{3}$ is known as the lower region.

Following this, Bao & Wierzbicki (2004) found that the mechanism for fracture varied from shear fracture in the negative triaxiality range to void formation in high triaxiality ranges. For the moderate triaxiality range between the two extremes, fracture may develop as a combination of the two, however it is currently unclear how the transition occurs. At the time, it was thought that a possible slope discontinuity could occur at some transition point between the two extremes. From the results, the transition point was approximated to be about $\eta = \frac{1}{3}$. Further, it was shown that the transition from one mode is material dependent (i.e. for 2024-T351 Aluminum alloy, $\eta = 0.4$ was the clear transition). Various other authors and models find a similar transition or cut-off value, however it is unclear at this time the nature of the irregularity.

Bao and Wierzbicki (2004) continued on to develop a two dimensional fracture locus for 2024 aluminum alloy to display the relation of fracture strain to stress triaxiality, for the three distinct regions. For the negative region, a vertical asymptote developed based on the experimental results of Kudo and Aio (1967) was used, while a simple parabola was

sufficient for the moderate (0-0.4) and high (0.4-0.95) ranges. Additionally, Bai, Teng and Wierzbicki (2009) developed a closed-form solution for the stress triaxiality in a flat grooved specimen and verified through the use of FE packages and experimental results of DH36 and 1045 steel.

2.4.2.1 Plasticity

Although not the focus of this work, the dependency of the yield criterion on hydrostatic pressure or triaxiality is worth noting and far precedes this work on ductile fracture. The concept was first explored by the application of the Coulomb-Mohr criterion by Drucker and Prager (1952). The concept was originally developed for analysis of brittle materials and is popular due to its accurate prediction in the elastic range as well as small strain plasticity. It has shown to be applicable to metal plasticity by Bai and Wierzbicki (2008), who demonstrated that it correctly characterizes fracture of ductile metals and extended the criterion to a spherical coordinate system. Hancock and Mackenzie (1976) also displayed that ductility of metals depended on the triaxiality of the stress state in high triaxiality regions through experimental studies.

The adapted Mohr-Coulumb (MC) criterion as proposed by Bai and Weirzbicki (2008) is appealing for the prediction of ductile fracture as it can be justified in the plastic region, through the relative resolution of stress and strain and is explicitly dependent on Lode Angle Parameter (discussed in the following section). Further, in contrast to the GTN model, it accurately predicts shear fracture in low triaxiality regions. Through transformation of the MC into a strain based criterion under monotonic loading, the criterion can accurately predict ductile failure.

Additionally, Gurson (1977), Needleman and Tvergaard (1984) also posited a model, known as the GTN model to describe hydrostatic dependent material softening due to various void growth mechanisms. The key difference between the theories is the posited mechanism for the softening of the material. The model implemented Bai & Wierzbicki (2008) assumes that the softening is due to the growth of material porosity, while the GTN (1977; 1984) assumes that the responsible mechanism is dislocation suppression. This concept assumes that the dislocation is reversible with changing hydrostatic pressure, or that if hydrostatically loaded and unloaded the material will retain its original strength. Bai & Wierzbicki (2008) planned and proposed a test to further investigate the two types of softening with controlled triaxiality. The proposed example would involve two tests on each notched round bar sample, where after some plastic deformation occurred, the sample was machined a second time to a larger radius.

2.4.3 Lode Angle Parameter

Although stress triaxiality results in greater accuracy in predicting fracture, Lode Angle must be incorporated into the yield criterion due to its clear influence on material ductility as shown by Bai and Wierzbicki (2008). Mathematically, it can be shown that the Lode Angle has a range of $0 \leq \theta \leq \frac{\pi}{3}$, and as such the normalized, Lode Angle Parameter, $\bar{\theta}$, has a range of $-1 \leq \bar{\theta} \leq 1$. From the inclusion of the two parameters, it is then possible to describe all stress states (or loading conditions).

The first major investigation into a deviatoric influence on fracture was completed by Wierzbicki, Bao and Bai (2005) who generated a new experimental technique to construct

a fracture locus and identified dependency on both stress triaxiality and an average deviatoric parameter (analogous to Lode Angle) for Al 2024-T351.

Material yield's dependence on Lode Angle Parameter was further described by Bai and Wierzbicki (2008) through a comparison of von Mises and Tresca yield criterion. The authors then continued to introduce Lode parameter into the Coulomb-Mohr yield criteria equation. There are four material calibration terms and three parameters which control the convexity of the yield surface. It is possible to obtain the two criterion from simplifications with the convexity parameters. Along with this, methodology to develop a 3D fracture locus in the space of fracture strain, triaxiality and Lode Angle Parameter was presented, and displayed through the testing and calibration of Al-2024. Finally, most of metal plasticity assumes that yield is symmetric in the deviatoric stress plane (i.e. uniaxial tension and compression). Bai and Wierzbicki (2008) removed this limitation upon evidence that yield and fracture occurs asymmetrically (i.e. dependent on a Lode angle).

Both Xue (2007) as well as Bai and Wierzbicki (2008) showed several limiting cases for Lode Angle Parameter which can be found via classical material tests. They also showed that in the plane stress condition (where $\sigma_3 = 0$), it is possible to relate triaxiality and Lode parameter with the following equation:

$$\bar{\theta} = 1 - \frac{2}{\pi}\cos^{-1}\left(-\frac{27}{2}\eta\left(\eta^2 - \frac{1}{3}\right)\right)$$

Bai, Teng and Wierzbicki (2009) implemented the use of unique grooved plate specimens which varied in Lode Angle Parameter, but remained at a near constant stress triaxiality, to show plasticity and fracture dependence on Lode Angle. Further, they displayed that the

dependency on Lode was material dependent. In particular, it was shown that the fracture of DH36 steel was Lode independent (however, plasticity was dependent on Lode).

2.4.4 Other Invariants Effects

As previously stated, Lode angle parameter is simply a non-dimensionalized form Lode angle. Lode Angle itself is a function of the of the second and third invariants of the s_{ij} deviatoric stress tensor, described as follows.

$$\bar{\theta} = \frac{27}{2}\frac{J_3}{\left(\sqrt{3J_2}\right)^3}$$

Where: $J_3 = det(s_{ij}),\ J_2 = \frac{1}{2}s_{ij}s_{ij}$

As the first deviatoric invariant is simply zero, it Lode Angle Parameter indirectly describes all deviatoric stress contributions. There is however other work which directly addresses the contribution of each invariant, including those of the Cauchy Stress Tensor. Again, the pre-existing knowledge was generated by the rock and soil industry, particularly the work completed by Bardet (1990) and the Sandia GeoModel by Fossum and Brannon (2006), both of which consider triaxiality and all five stress invariants. The work completed by Bardet (1990) included consideration of many yield functions and failure surfaces, which consider the first and second stress invariants along with Lode angle. The Sandia GeoModel in particular is formulated in the space of both nontrivial deviatoric invariants, J_2, J_3 as well as the first Cauchy invariant, I_1. Further, the model considers rate dependence and couples the elastic and plastic deformations. The latter point is necessary due to the microphysical

material science which results in the brittle material becoming increasingly elastic with increased plastic strain.

In terms of ductile fracture, it remains to be seen if the inclusion of the other stress and direct inclusion of deviatoric stress invariants is worth considering for practical use, however it is possible to design tests to consider their influence. Further, strain rate is clearly impactful for brittle fracture, however for ship collisions, it is unlikely that the change in loading rate would cause any change in the resulting fracture capacity. Finally, temperature consideration is clearly important when considering standard ship building steels and other applications with large temperature ranges. However even at the extreme for these materials such as use on vessels participating in Arctic/Antarctic transit, it is unlikely that the temperature will have a large effect on material failure in a laboratory setup for idealized plate samples. Temperature and strain rate were considered in preliminary selection of relevant factors however ultimately not tested due to experimental limitations and as such future work should be completed to ensure the assumption that they are not a major factor.

2.5 Finite Element Standards

This section provides background knowledge regarding modelling fracture induced by moving loads. This includes the industry standards and common practices for collision as well as the inclusion of triaxiality and Lode angle in computation. This latter in particular focuses on the recent development of a specific program, LS-DYNA due to familiarity and ease of use.

2.5.1 Plasticity

Updating yield functions to include triaxiality and Lode angle in a numerical model was completed by Malcher et al (2014). The authors presented an implicit integration method depending on the Newton-Raphson algorithm to use the model presented by Bai & Wierzbicki (2008). The author prepared three finite element model cases of a flat groove specimen, the first with a basic Von-Mises equivalent stress yield function, the second using an updated yield function accounting for the pressure effect and the third, both Lode angle dependence and triaxiality. The error in the reaction displacement curve was reduced from 17% for the simplistic Von-Mises yield criteria, to 13% (which was similar to the results found by Drucker Prager models) to 2% through the inclusion of both triaxiality and Lode Angle when comparing the numerical results to an experimental validation test. As the focus of this work is fracture, these functions will not be further developed in this work.

2.5.2 Fracture

Various attempts to improve failure criterion or update standard failure criterion, the implementation of a known effective plastic strain to fracture, in finite element analysis have been completed. Alsos (2008) condensed the major works to the Bressan-Williams-Hill (BWH) criterion and the combined Royce-Tracey damage, Cockcroft-Latham damage criterion (RTCL). Both criteria include the influence of triaxiality and were shown to improve prediction of fracture in numerical specimen. The BWH uses a concept known as failure level as determined by Hill's work to describe local necking and thus relates the onset of failure to strain hardening for the material. The work also served to identify a major difficulty and ongoing issue with fracture prediction in numerical simulations; mesh

sensitivity. It was noted that at the large deformations necessary to incite fracture, elements were extremely size dependent and concluded that the study of mesh sensitivity was as important as the fracture criterion itself.

Other major works on modelling fracture includes the extension of GISSMO (Generalized Incremental Stress State dependant damage MOdel) (Basaran et al. 2010). GISSMO itself uses a damage evolution parameter and a failure curve formulated in the space of triaxiality and plastic strain. The extension of this function involves the inclusion of Lode Angle Parameter in the damage evolution, through incorporating the work of Xue & Wierzbicki (2005). Although GISSMO has shown to be an accurate method for predicting fracture of idealized sample specimen, its development and implementation is outside of the scope of this work and therefore is not further elaborated.

The implementation of triaxiality and Lode angle has also been achieved recently through the use of specific material models, such as MAT224 in LS-DYNA. This material card, formulates the stress states in the space of plastic strain, strain rate and temperature and further divides the material response into plastic and element failure. The stress state during plastic level loadings is defined by the Von Mises yield criterion, which itself is dependent on the strain hardening, rate effects and thermal softening (LS-DYNA Aerospace Working Group 2017). For damage accumulation and element failure, the material card requires four inputs. The first is the definition of the failure space via a load curve defining plastic failure strain for a given triaxiality range for shells or a table of curves defining plastic failure strain as a function of triaxiality and Lode Angle Parameter for solid elements. The remaining parameters are load curves which relate plastic failure strain to strain rate,

temperature and element size. From these inputs a failure criterion based on accumulated damage is tabulated and when it reaches 1 for a given element, the element has failed and is deleted. Further work is required to ensure that it is necessary for complicated loading scenarios of ship plating to include the parameter. At this time, the lack of implementation forces the user to use an exceptionally fine mesh, which is computationally expensive to incorporate Lode Angle parameter for common ship plating damages.

It should be noted that prediction of stationary fracture for a ship hull sample has been completed accurately using a range of methods as shown in (Ringsberg et al. 2018). Here an experimental result of a ship like structure test was given to 15 contributors who were asked to accurately replicate the result numerically. The reference structure and experiment were similar to a typical double hull side shell subjected to a 90° collision with a bulbous bow. Due to test apparatus limitations, the structure was 1/3rd scale of similar full-scale structures. The contributors used different stress/strain relations and failure criterion. In particular, the five that most accurately predicted the experimental results used three separate failure criteria; initiation and evolution, shear failure and effective plastic strain to fracture. The first of these three criterion is the most complicated, using both a shear criterion to predict onset (i.e. pressure dependent failure) and a post failure damage evolution model. The latter is simple implementation of a singular fracture strain value at which the elements are deleted from the model. The accuracy of both methods is an important finding as it indicates that ideal, stationary collisions which occur orthogonally to the ship hull sample can be modelled accurately without the implementation of pressure or Lode dependent failure or evolution. As situations like this are perfectly ideal and

compared to experimental result, it is unlikely that prediction of fracture for real world analysis can be completed using the same simplistic methodology. However, one of the main goals of research in this area should be both an accurate and accessible method to predict generalized fracture for shell elements in real world situations. As such, simplified methods should not be dismissed until shown to be insufficient to accurately predict behaviour of more complicated loading situations.

2.6 Knowledge Gaps in Literature

From the literature of moving loads, ship collisions and tearing, it is clear that the ultimate goal of the work is to accurately assess bottom damages of full ship structures (hull plating, frames, etc.) through either analytical, empirical or numerical methods, with development of the latter allowing for accurate characterizations of a range of complex collision events. Most of the work focuses on either a very specific situation, such as the analytical and empirical analysis of tearing or the quarter scale double hull tests by Rodd & Sikora (1995) or is the macroscopic energy behaviour and doesn't discuss the translation after initial impact, such as the collapse mechanisms outlined in the Rosenblatt (1975). Additionally, the two works by Quinton (2015) and Hong & Amdahl (2012), which do address moving loads, only consider plastic damages. The work by Alsos (2008) most closely addresses the problems acknowledged in this thesis, specifically moving loads, as well as fracture and implementation numerical modelling. However, the work itself does not address the actual quantification of the loss in fracture capacity due to horizontal translation.

With regard to the tearing/fracture scenario from Simonsen (1998) and Simonsen & Wierzbicki (1998) and all related work, the experiments resulted from an in plane collision.

Therefore, the "initial loading phase" which consisted of just the loading normal to the plate specimen in the work by Quinton (2015) and this thesis was omitted. As such, the work is heavily focused on the resistance (or horizontal force) whereas that is a secondary concern compared to the vertical force response for both stationary and moving loads in this thesis.

With regard to the significant literature on numerical stationary loads resulting in fracture, in particular the work by Ringsberg et al. (2018), it was shown clearly that many different methods could result in the accurate modelling of a fracture event. These methods ranged from considering post necking and pressure dependency to the simple implementation of an *effective fracture strain*. However, the study did not extend the concept for moving loads and therefore is significantly different than the work in this thesis. It should be noted that both simplified and complex methods resulted in accurate prediction of fracture, however, why this is possible is not investigated. As such this is briefly discussed in the numerical section of this thesis.

Overall, this thesis aims to confirm that the moving load effect exists for loads which incite fracture through physical experimentation, extending the work completed by (Quinton 2015). Further, various factors related to a simplified collision are to be investigated. Following this, moving loads are investigated through numerical models to determine the validity of using an *effective fracture strain* to capture the behaviour of a moving load for varying stress states. Finally, observations will be made as to the necessity of including more complex material models, accounting for the stress state and therefore triaxiality and Lode Angle Parameter, and the validity of each method for the varying stress states observed in this work.

Chapter 3 Experimental Setup

3.1 Experimental Approach

Bao and Wierzbicki (2004) developed a locus to predict fracture for various ductile metals using fracture strain and triaxiality, with Xue and Wierzbicki (2005) extending the locus to include Lode Angle Parameter. The methodology developed showed dependence on both variables for A710 steel and Al 2024, which was then extended by Bai & Wierzbicki (2008), for many types of metals, particularly, A710, DH36, 1045, TRIP 690 & 780. Of these tests, DH36 remained relatively constant for varying Lode Angle and therefore thought to be independent of Lode parameter regarding fracture.

Additionally, Quinton (2015) showed that the plastic structural capacity of steel plates and frame samples were significantly reduced due to the load translation when compared to stationary loads. Due to the path dependent nature of fracture and plastic damage, it was posited that fracture would also be dependent on moving loads for ductile ship steels. If the hypothesis was confirmed it was desired to explore the relationship between the fracture parameters due to load translation, given the research by Bai and Wierzbicki (2008) and link the current state of the art material science to the proven concept of moving loads for ship steel. This goal was ultimately not achieved as it was not possible within the scope of work for this thesis.

3.2 Experimental Objectives

The laboratory experiments had several key objectives as follows:

- Investigate the influence of moving loads on fracture initiation for plates made from ship steel;
- Explore the response of the plate samples due to the moving load for two distinct indenter shapes;
- Identify the minimum indentation depth to cause fracture for moving loads; compare with similar stationary load; and quantify the overall ultimate capacity loss due to the load movement;
- Investigate the influence of indentation depth, and translation speed on moving load effects;
- Identify the influence of the start location on fracture;
- Acquire the necessary data to calibrate corresponding numerical models for further investigation of coupled moving load and fracture events.

These objectives are centered on determining the fracture capacity for various conditions or scenarios and then comparing the results to a similar stationary loading. To do so the novel Moving Load Apparatus developed by Quinton (2015) was used. Additionally, the experimental work was significantly augmented by the past experience and knowledge from Quinton (2015).

3.3 Moving Load Apparatus

The Moving Load Apparatus is a novel experimental setup designed by Quinton (2015) to display the existence of moving load effects on plastic structural capacity for plate and frame samples. It was developed around the existing infrastructure in the Thermal Lab's cold room at Memorial University of Newfoundland.

The complete assembled apparatus can be seen in Figure 3.1 with major components labels and descriptions as follows (further explanations of the indenters in the sections that follow):

- Carriage: Plate sample is attached to the bottom side of the carriage by 70 bolts and lug nuts, in addition to the sandwich ring; which was designed to hold the sample through friction and not the shear resistance of the bolts. It should be noted that this setup differed slightly from the original tests by Quinton (2015) who also used keystock to ensure that the plate samples did not move. Keystock was not used for these experiments due to the thinness of the test samples, making the keystock setup impractical to implement.
- Roller Rail System: Holds and guides the carriage and sample horizontally over the test span via a hydraulic horizontal ram between the two parallel rails. Horizontal ram allows for precise control in the lateral direction.
- Swing Arm: Supports the indenter. It is attached to the support structure via load cells (to measure the horizontal reaction loads) and is seated on the MTS frame on the other. The swing arm rotates from minimum (-77.6mm at -1.7° to the vertical) to maximum (+77.6mm at 1.7° to the vertical) extension of the vertical ram.
- Indenter: Transfers the vertical loading from the ram to the plate sample via a specific geometry or shape. Particularly useful for altering the state of stress (thus allowing for fulfillment of the experimental objectives). For the experiments in this thesis two indenters were used, a large rolling wheel indenter and a narrow cutting wheel indenter.

- Vertical Ram & MTS Frame: Existing infrastructure which provides vertical load to the swing arm and indenter system. MTS frame system is self-contained. The vertical ram can output a maximum of 500 000 kN.
- Support Structure: The structure surrounding and supporting the other components. Provides the necessary structure to support the system and is self-contained.

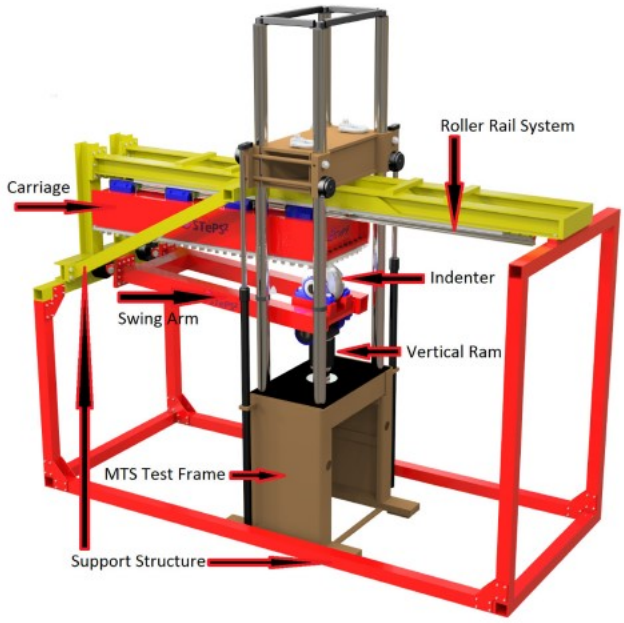

Figure 3.1: Moving Load Apparatus (Used with permission, ((Quinton 2015))

The test apparatus was designed to incorporate the existing infrastructure available, mainly the MTS test frame in the cold room. The MTS frame is the ideal machine to apply and measure vertical loads, while the cold room allows for control of temperature during testing. The other components were designed to apply and accurately measure loads in the horizontal direction while supporting the test samples.

3.3.1 Indenters

As the experimental objectives involve determining the impact of varying stress states, and thus triaxiality and Lode angle, it was necessary to develop a new indenter. Thus two separate indenters, a rolling wheel indenter designed by Quinton (2015)and a new narrow cutting indenter were used.

3.3.1.1 Rolling Wheel Indenter

The rolling wheel indenter was originally designed and used by Quinton (2015). The wheel itself (Figure 3.2) is made of QT100 steel, with a yield stress of 690 MPa. The shape is a 4in (10.16cm) thick section of a 10in (25.4 cm) diameter sphere and was designed to rotate to avoid sliding friction.

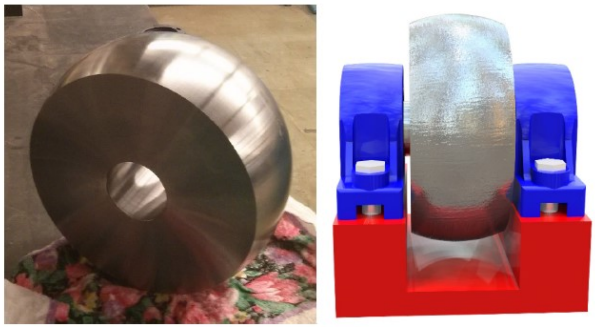

Figure 3.2: Rolling Wheel Indenter (Used with permission,(Quinton 2015))

3.3.1.2 Cutting Indenter

The cutting indenter was designed based on preliminary numerical tests to ensure that the indenter would not yield under conservative loading conditions. The wheel itself (Figure 3.3) is made of 5150 oil quenched, hardened steel, with a yield of 910 MPa. The shape is similar to that of the rolling wheel, with a diameter of 10in (25.4cm) at the base, narrowing

to a radius of 0.0277in (0.07cm) at an angle of 29.75°. The width of the indenter was 1.75in (4.445cm). The cutter was designed to fit into the pillow block bearings used in previous testing.

Figure 3.3: Cutting Wheel Indenter

3.4 Specimen

3.4.1.1 Specimen Design

As the objectives were all based on the study of steel fracture, simple plate samples were selected. Plate sizing was originally selected to as a variable as to compare to previous work (Quinton 2015) however, this was found to be impractical both from procurement and structural standpoints, as the smaller of the thicknesses was not readily available and the larger was thought to not likely fracture under the maximum force provided by the vertical ram (500kN). Originally, the thicknesses of 1/8” (mm) and 1/4” (mm) were selected for analysis (again as to compare to the results gathered in previous work). The final thickness was selected to be 3/16”.

The type of steel was also originally selected to be a variable factor based on ABS steel specifications. Two grades were selected based on operational temperature requirements. The first operational temperature was 0°C and dictated the use of A36 steel. The second

was -20°C and the standards required DH36 steel. This was also useful for comparison to the work of Bai & Wierzbicki (2008) who calibrated fracture locus for both A36 and DH36 steels. Again, this was found to be impracticable, with a very long procurement time and high cost. Therefore, an equivalent to A36 was selected, 44/50W, with material properties given in Table 3.1.

Table 3.1: Steel Bills for A36 Equivalent

	Tensile Strength (psi) @ End	Yield Strength (psi) @ End	Elongation @ End	Tensile Strength (psi) @ Center	Yield Strength (psi) @ Center	Elongation @ Center
First Bill	76024	61236	0.34	75666	60794	0.35
Second Bill	70092	54208	0.38	69568	55394	0.39

The samples (Figure 3.4) were manufactured at Technical Services of Memorial University of Newfoundland. A total of 24 samples were prepared to fit the pre-existing apparatus. The only major change from previous experiments with the apparatus were the inclusions of cut-outs around the bolt holes of the plate at the recommendation of several participants from the original experiments. These cut-outs were added from the original moving load tests to allow for removal of the plate after heavy deformation, which had caused the plate to catch on the bolt pattern of the carriage and required time consuming removal through the use of a grinder.

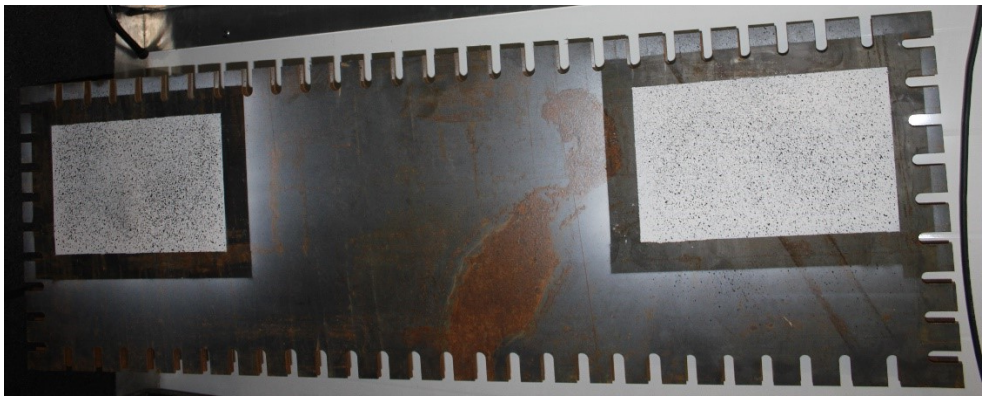

Figure 3.4: Steel Plate Specimen

From the dimensions, it should be noted that the plate samples can be considered long plates (Hughes, Paik, and Béghin 2010) as the ratio of length (*a =1500mm*) to width (*b=400mm*) is equal to 3.75, above the minimum 2 dictated for clamped plates. Therefore, the theory predicts the sample will undergo cylindrical bending (known as 1D bending henceforth) in the region of ± *b* about the center (*a/2*) of the plate and 2D bending elsewhere in the plate (i.e. near the plate's short ends). Therefore, any events which occur in the region of ((*a/2*) ± *b*) = 350mm to 1150mm are solely due to the effects of moving loads on an infinitely long plate.

3.4.1.2 Specimen Installation

The samples were installed to the carriage via a sandwich ring and series of 70 bolts and lug nuts. The sandwich ring holds the plate via friction instead of shearing on the bolts which result in local plate deformation and a change in the boundary conditions of the test. Each bolt was tightened to 325 N through the "3-2" method which was found by Quinton (2015) to be sufficient. This method allows for each nut to be tightened twice, ensuring that the boundary is even across the entire sample.

3.5 Data Acquisition

The data collected from the tests was primarily in two forms, visual and sensor data collected by the equipment outlined in this section. It should be noted that all tests were performed at a data acquisition rate of 2048 Hz. The main data recording was completed through the use of the MTS test frame and connected devices.

3.5.1 MTS Devices

The setup included the use of five instruments to collect the necessary data, some of which were used to implement the experiment depending on the control type. The measuring devices are described as follows:

- MTS Linear Variable Differential Transducer (LVDT) – LVDT is built into the MTS test frame and measures the vertical displacement of the ram and indenter.
- MTS Load Cell: Model 661.2E-01 – Vertical load cell mounted between the vertical ram and swing arm and measures the vertical force applied by the ram and thus indenter.
- Tovey Load Cell L – Model: SW20-50K – Mounted on the self-contained support structure to support the left side of the swing arm. Measures the horizontal load applied to the specimen by the indenter in conjunction with the right load cell.
- Tovey Load Cell R – Model: SW20-50K - Mounted on the self-contained support structure to support the right side of the swing arm. Measures the horizontal load applied to the specimen by the indenter in conjunction with the left load cell.
- Horizontal Linear Position Transducer (“yo-yo pot”) – Attached to the carriage via a magnet clip and measures the horizontal displacement of the carriage throughout the experiment.

3.5.2 Visual Data Recording

The visual data was collected during and after the experiment had been completed. A video of each test was recorded from at least one angle, the leading edge of the indenter outside the carriage. Photos were taken after the test, usually after the plate was removed.

All video was recorded through the use of a series of GoPro cameras. For every test, one camera was installed outside the carriage on the swing arm, facing the front edge of the indenter. In addition, for many tests, a camera was mounted inside the carriage at a similar position. The inside of the carriage was illuminated through the use of several 12V DC LED strips. For all tests, a GoPro Hero 2 was used for the outside position and a GoPro Hero 3 was used for the tests with video inside the carriage. While the two cameras are similar, the GoPro Hero 3 has a larger lens angle then the Hero 2 (170° vs 127°). The video is recorded at 1080p and 30 frames per second.

All pictures were taken through the use of a Cannon EOS Rebel T5 camera. Photos were taken of the sample, and entire apparatus throughout testing. Photos of the sample were primarily taken after the plate had been removed, to capture the damage from various angles with superior lighting in comparison to when fixed in the frame.

3.6 Experimental Methodology

The experimental design was based on the initial investigation into moving loads using the apparatus by Quinton (2015). The factors initially selected for observation included steel type, thickness, temperature and indenter geometry.

It should be noted that the indentation depth was not initially selected as a factor as fracture was the desired outcome. Initially, a preliminary test was to be performed to ensure that a moving load effect existed for loads that induce fracture. From here, a depth which resulted in fracture during the horizontal portion of loading but not in the vertical loading was to be selected and used as the basis of the remaining tests.

Due to various circumstances it was impossible to test the temperature, steel thickness and steel type factors. Instead the test parameters were changed so as to determine the moving load fracture capacity of the plates based on percentage of the maximum displacement or force necessary to induce vertical fracture for the two main regions of the plate (i.e. 1D vs 2D bending areas). Additionally, several rate tests (i.e. tests at various indenter speeds) with the cutting indenter were performed to determine the impact of strain-rate on the moving load fracture effect but provided no usable data due to an extreme amount of signal noise in the resulting data. The loading control was also varied, although not out of desire to examine its effect. For the first 11 tests, the loading was completed via displacement controlled loading, where a specific displacement was inputted and maintained throughout the test (or varied for test 11). For the last 11 tests, the loading was completed via force control, where the ram maintained a specific loading on the plate.

3.6.1 Steel Type

The steel type was initially desired to mirror common ship steels used in the industry, and therefore ABS steel grades A and DH were selected. These steel grades are used in vessels operating in ice infested waters (ABS 2016). A is exclusively used in Class 1 or secondary structural members. Additionally, A steel is only used in thin plates ($t \leq 0.39$”) in the

warmest of the classified temperatures (-20°C to -25°C). DH steel is a mid-level steel found in all three classes, particularly in Class 1 at medium thicknesses and low temperatures, Class 2 at medium temperatures and thicknesses and Class 3 for the high temperatures and thicknesses. Therefore the steel type is widely used in ice-going vessel construction, particularly in moderate primary structures. In addition to being applicable to marine applications, it also allows for comparisons between (Quinton 2015) and (Bai and Wierzbicki 2008); the latter, calibrated fracture loci for DH36 steel.

After an initial search for the types of steel, it was decided that the DH36 was impractical due to cost and order time and therefore omitted from the experiment. After this, it was also found that the specific grade A36 was unavailable, therefore an equivalent grade 44/50W was used (Appendix I). 44/50W is common structural steel, with structural properties between A36 and DH36 steel types. It should be noted that while the classic properties are similar to the standard shipbuilding steel types, it is not directly comparable to the tests completed by Bai & Wiezbicki (2008), where the Lode dependency of the fracture locus varied heavily with the steel type. It should also be noted that this steel type would not be suitable for low temperatures (Ch 3.6.3), as it is not recommended where low temperature fracture toughness is required.

3.6.2 Thickness

The thickness of the samples was also originally selected as a variable factor with two levels similar to (Quinton 2015) to determine if the thickness of the steel impacted the moving load fracture strength. Originally, two thicknesses were selected to be 1/8” (3.0625mm) and 1/4" (6.125mm). After the initial search for the materials, it was found

that 1/8” was not readily available in 44/50W steel. Further, upon review it was decided that ¼” would be too thick to allow for fracture with the rolling wheel indenter within the limits of the MLA. Therefore, a final thickness of 3/16” was selected for use in the experiment.

3.6.3 Temperature

The temperature of the tests was originally selected to be a variable factor with two levels similar to (Quinton 2015) based on the operational range of the original steel grades (A36 & DH36) and the design limits of the various instrumentation integrated into the MLA. The limiting minimum temperature for the MLA was -10°C based on the manufacturer specifications for the rolling rail system. Therefore, the two levels were selected to be -10°C and 24°C (room temperature). Due to unforeseen downtime of the refrigeration unit of the Cold Room at the Thermal Laboratory at MUN, it was impossible to vary the temperature and therefore only an experimental temperature of 24°C was used.

3.6.4 Test Start Location

The test start location was varied to determine the impact of the fixed boundary on the moving fracture capacity of the plate samples. Due to the nature of the specimens (i.e. long plates) there is a one-dimensional region about the center of the plate. To examine the impact of the transition from 2D (at the ends) and 1D bending, the starting location was varied. In reference to the plate sample (Figure 3.4), the 1D region tests start between ±350mm (550 & 900mm with respect to the end of the plate), while the 2D tests begin at ±550mm (200 & 1300mm with respect to the end of the plate). The start location of ±550mm (200 &1300mm from the end of the plate) was selected as to allow for maximum

travel for the indenter while not interfering with the sandwich ring or carriage (Quinton 2015).

3.6.5 Horizontal and Vertical Load Rate

The load rate of the indenter was also added as a factor, both in the vertical and horizontal directions for both the force controlled and displacement controlled tests. There were two levels of this variable, which were coupled: high values of 20 & 175 mm/s, and low values of 4 & 80 mm/s; for the horizontal and vertical directions, respectively. The high values were found to be the maximum sustainable values of the ram based on preliminary testing.

The load rate was also varied for several force control tests, however force control was only possible for the vertical loading phase. This was selected as it was desired to maintain constant movement along the horizontal loading of the plate. The vertical force loading rate was selected to be 18 kN/s based on the observed average loading rate of displacement controlled tests. It should be noted that although the average load rate was comparable for both displacement and force controlled tests, each resulted in a different loading rate, to maximum load during the vertical portion and a different level of force or displacement for displacement and force control respectively and therefore is difficult to compare. Further, a high speed force load rate was determined to be 180 kN/s.

After review of the experimental data for the various rate tests, it was concluded that the data was unusable and thus omitted from analysis. This was due to the lack of PID calibration for the faster speeds. An example of this can be seen in Figure 3.5 below, which gives the horizontal displacement plotted against the vertical force for a high speed test

which was force controlled through the use of a 'if' loop and target force. Clearly, in comparison to a normal test, the force varies wildly.

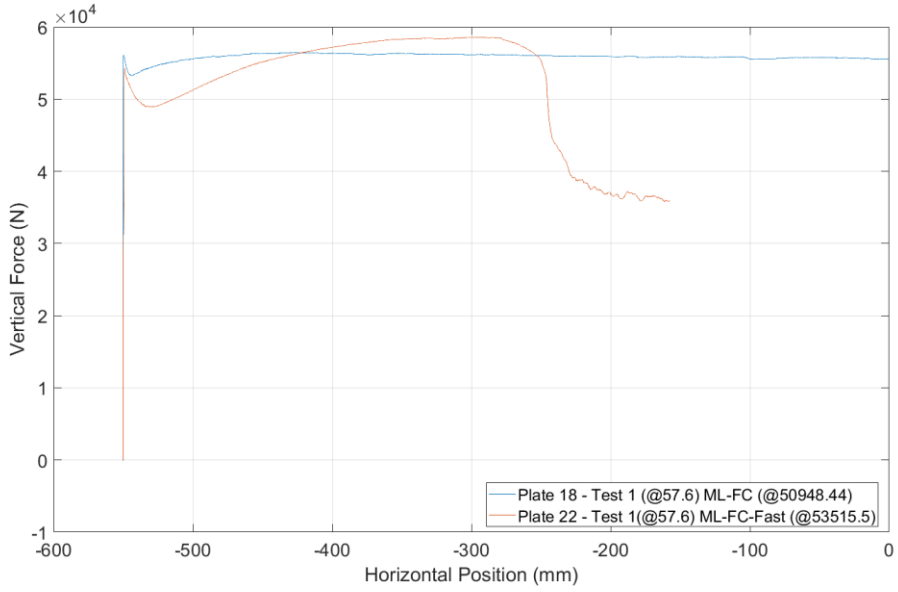

Figure 3.5: High Speed versus Normal Speed Force Control Test

3.7 Test Plan

The original test plan can be seen in Table 3.2, while the completed test regime can be seen in Chapter 4.

Table 3.2: Original Test Plan

Run	Plate Thickness	Plate Grade	Temperature	Indenter	Replications
1	0.25	A	20	CW*	2
3	0.125	A	20	RW**	2
5	0.125	A	20	CW	2
7	0.25	AH36	20	CW	2
9	0.125	AH36	20	RW	2
11	0.125	AH36	20	CW	2
13	0.25	DH36	20	CW	2
15	0.125	DH36	20	RW	2
17	0.125	DH36	20	CW	2
19	0.25	A	-25	CW	2
21	0.125	A	-25	RW	2
23	0.125	A	-25	CW	2
25	0.25	AH36	-25	CW	2
27	0.125	AH36	-25	RW	2
29	0.125	AH36	-25	CW	2
			Total Runs:		30

* Cutting Wheel (CW)

** Rolling Wheel (RW)

3.8 Experimental Procedure

3.8.1 General Procedure

For the experiments, the test procedure was as follows:

1. Install and connect internal and external cameras (if used internal was used)
2. Install specimen with installation procedure
3. Check initial values for start position, and positions of interest with ram (if necessary).
4. Bring indenter to horizontal starting position of test.
5. Move indenter to touch plate specimen.

6. Record test notes and create new specimen file on MTS control computer.
7. Activate video cameras
8. Load test profile.
9. Complete test.
10. Take post-test pictures.
11. Remove plate specimen.

Chapter 4 Experimental Results

The experimental results are divided into two separate sections, for both the displacement and force controlled tests. This is due to the differing nature of the loading that makes the results of the two incomparable. Further the actual test parameters that were measured using the outlined data acquisition devices can be seen in Table 4.1 and Table 4.2, which provide a summary of the test factors for each of the experimental divisions.

Table 4.1: Displacement Control Test Summary

Sample	Indenter	Horizontal Start Location (mm)	Vertical Indentation (mm)	Max Vertical Force ($Nx10^5$)
Test 1	RW*	-550	10-75	NA
Test 2	RW	-550	75	4.7
Test 3	RW	-550	70	4.3
Test 4	RW	-550	67.5	4.1
Test 5	RW	-550	1-10	NA
Test 6	RW	-550	69	4.6
Test 7	RW	-275	69	4.3
Test 8	RW	-550,0,550	68.3,74.7,68.7	4.9,4.9,4.9
Test 9	RW	-200	69	3.9
Test 10	CW**	0,550	Max	0.92,0.96
Test 11	CW	-550	22.5	0.83
Test 12	CW	-350	35.9	0.66

Sample	Vertical Fracture Force ($N x10^5$)/ End Force	Horizontal Distance to Fracture (mm)	Notes
Test 1	NA	NA	Calibration
Test 2	2.5	-506.4	
Test 3	2.2	-72.8	
Test 4	2.5	NA	No Fracture
Test 5	NA	NA	Elastic
Test 6	2.5	-100	
Test 7	2.5	43.4	
Test 8	NA	NA	Stationary, Max Ind.
Test 9	2.5	NA	No Fracture
Test 10	0.93,0.96	NA	Stationary
Test 11	0.57	NA	No Fracture
Test 12	0.66	215.8	Ramp Test

* Cutting Wheel (CW)

** Rolling Wheel (RW)

Table 4.2: Force Control Test Summary

Sample	Test	Location (mm)	Vertical Force (N x10^4)	Fracture Force (N x10^4)	Vertical Indentation (mm)	Distance to Fracture (mm)
Test 13	1	550 (BWD*)	8.8	8.2	27.3	14.3
	2	-550 (FWD**)	6.9	6.5	28.7	59.8
	3	-200 (FWD)	7.0	6.6	29.2	43.9
Test 14	1	-550 (FWD)	6.0	5.8	28.9	153.7
	2	-200(BWD)	5.8	5.6	29.0	235.2
Test 15	1	-550 (FWD)	5.2	NA	25.2 (max)	NA
Test 16	1	-200 (FWD)	6.8	6.3	28.4	60
	2	550 (BWD)	5.6	5.5	29.5	201.4
	3	-550 (FWD)	5.4	NA	28.9 (max)	NA
Test 17	1	-550	Max	9.6	27.1 (@ fracture)	NA
	2	0	Max	9.3	28.7 (@ fracture)	NA
Test 18	1	-550(FWD)	5.6	NA	28.8	NA

* Backwards Direction of Horizontal Travel (BWD)

** Forwards Direction of Horizontal Travel (FWD)

4.1 Displacement Controlled Tests

The displacement controlled tests were based off experience from the initial tests completed with the apparatus by Quinton (2015). Twelve tests were performed with various combinations of parameters, including start conditions as per Table 4.1. The tests were also further sub-divided by indenter type for analysis.

4.1.1 Rolling Wheel Displacement Control Tests

There were a total of nine rolling wheel, displacement controlled tests completed with varying starting conditions to observe the impact of the boundary conditions on the moving load capacity of the plate specimens. The tests were mostly performed to determine the necessary fracture indentation to cause fracture, to compare the influence of horizontal starting position (and therefore type of bending) and finally, to explore the influence, if

any, movement of the load had on plate fracture. This was completed with four tests to determine the fracture indentation over the full plate length (2D bending), two over the middle section of the plate (1D bending), an initial calibration test, and a stationary maximum capacity test. Finally, a series of elastic tests based on the recommendation for future work by Quinton (2015) were performed to observe the load level which the moving load effect could be observed.

Of the nine tests, three did not result in fracture on the first loading (subsequent loadings were not included in this work). It is also worth noting that fracture did not occur due to the overloading of the plate's membrane capacity, but instead due to the shearing action of the edge of the indenter wheel. This fact is instrumental in how the results of these tests are interpreted. This is further addressed in the recommendations of Chapter 6. Finally, the legend for the plots is in the format of "Test# - Vertical Target Displacement – Horizontal Start Position". Where omitted, the horizontal start position is the end or -550mm.

4.1.1.1 Indentation to Induce Fracture

Four displacement controlled tests were performed to explore the relationship between indentation to induce fracture for full length tests and determine the applicability of moving load effects to ductile fracture. The results of these tests can be seen in Figure 4.1, Figure 4.2 and Table 4.3**.** The presence of moving load effects was confirmed in Test 2 with an initial static, vertical indentation of 75mm, resulting in a force of 474 kN. The sample then fractured at 43.6 mm from the starting position laterally during the horizontal movement phase, at a vertical force of 248 kN. Clearly from the results of the Test 2, the fracture capacity of the plate specimen is greatly reduced.

Table 4.3: Induced Fracture Test Summary

Sample	Indenter	Location (mm)	Vertical Indentation (mm)	Max Force ($kNx10^5$)	Fracture Force ($kN\ x10^5$)/ End Force	Distance to Fracture (mm)
Test 2	RW	-550	75	4.7	2.5	43.6
Test 3	RW	-550	70	4.3	2.2	476.2
Test 4	RW	-550	67.5	4.1	2.5	NA
Test 6	RW	-550	69	4.6	2.5	450.0

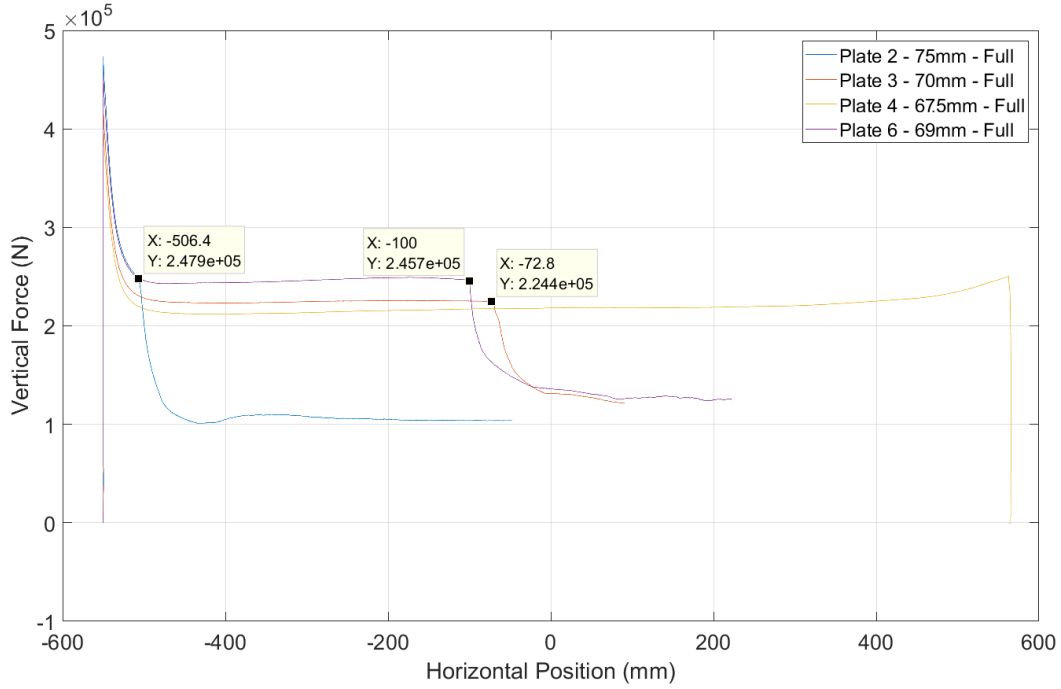

Figure 4.1: Rolling Wheel Fracture – Vertical Force vs Horizontal Position

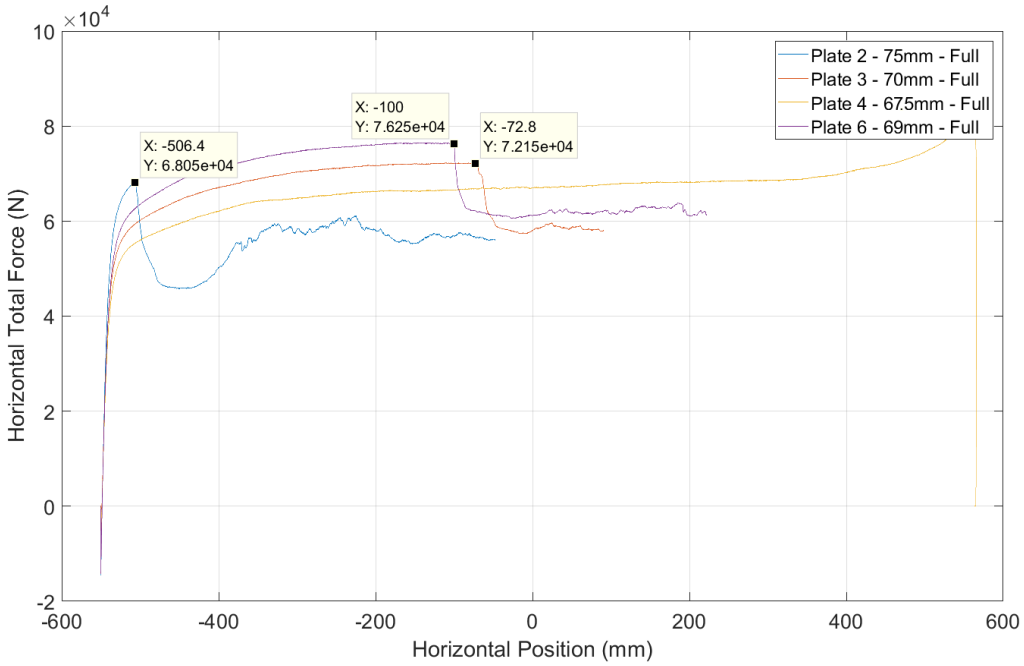

Figure 4.2: Rolling Wheel Fracture – Horizontal Force vs Horizontal Position

After the moving load fracture effect was confirmed for moving loads, the minimum depth to induce fracture was explored to determine the total capacity loss of a plate loaded critically to fracture. These tests saw several limitations. Mainly the geometry of the rolling wheel indenter bearing, allowed a maximum vertical indentation of ~75mm before the bearing came into contact with the plate during testing and therefore skewing results. An example of this can be seen in Figure 4.3, which shows post test scoring on the plate specimen. Due to this, it is likely that the reading of vertical and horizontal forces in these cases were artificially high in these cases and as such the results should be used only to display the phenomena of decreased force to fracture and not to model the relationships.

Figure 4.3: Bearing Contact Damage (shown to the right of the fracture)

Figure 4.1 shows the vertical force exerted by the plate on the rolling wheel indenter. The center of the plate was adjusted to correspond with 0 mm horizontal displacement, while the horizontal start position for the tests was -550 mm. From the plot, three tests, Test 2, Test 3 & Test 6 resulted in fracture. Based on the tests, the fracture was achieved at a minimum moving vertical force of 224 MN for the full sample tests which occurred at a vertical indentation depth of 69mm. It is worth noting that Test 6 provided inconsistent results when compared to the other three tests, with a vertical force history comparable to that of the 75mm plot, however the sample fractured at a much larger horizontal displacement. It was speculated that this was due to some deficiency or variation between the plate samples.

Figure 4.2 shows that the specimen's ability to resist horizontal movement reduces with the initial level of vertical indentation and thus vertical force. This is further illustrated when comparing the horizontal distance to fracture for the full samples tests. Test 2, Test 3, Test 6 respectively resulting in 43.6, 476.2 and 450 mm to fracture in the horizontal direction.

Due to the limited number of data points, and the non-consistent results found in Test 6, it is not possible to characterize this relationship.

4.1.1.2 Loss in Fracture Capacity

To quantify the loss of fracture capacity, three stationary vertical tests were completed to determine the fracture capacity of the plate without the identified moving load effect. The test was unsuccessful as the load capacity of the vertical hydraulic ram was reached, therefore trigging an end condition for the program and thus ending the test. The results and maximum forces & indentation achieved can be found in Table 4.4. As the necessary stationary force was not found, it was impossible to quantify the total fracture capacity loss for the rolling indenter, however the results clearly confirm a loss in capacity with horizontal translation when compared with the results of Chapter 4.1.1.1 as expected from previous study of moving loads. With the numbers available it is possible to say that the loss in capacity is in excess of 50% for both the 1D and 2D bending regions for the rolling wheel tests.

Table 4.4: Stationary Maximum Vertical Indentation Tests

Sample	Indenter	Horizontal Location (mm)	Vertical Indentation (mm)	Maximum Vertical Force (Nx10^5)
Test 8-1	RW	-550	68.3	4.9
Test 8-2	RW	0	74.7	4.9
Test 8-1	RW	550	68.7	4.9

Also of note was a slight permanent deformation of the Moving Load Apparatus, which resulted in a residual maximum deformation at the mid-point approximately 1 mm on each side Figure 4.4. Due to this, rework of the remaining plates was required to fit on the

apparatus. The size of the bolt slots were increased by 25% to allow for proper installation. The overall impact is explained with other experimental issues and errors in Chapter 6.

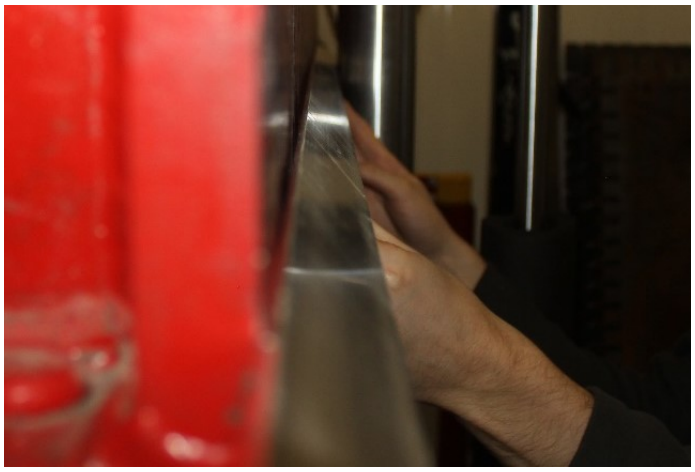

Figure 4.4: Apparatus Deformation

4.1.1.3 Influence of End Conditions

After a target vertical displacement to cause fracture was identified to be 69mm, the second factor, the initial position of the indenter in the horizontal direction, was investigated. In addition to the first four tests which were completed over the maximum horizontal test range (−550 to 550mm), two tests were performed starting from horizontal locations of −275 mm and −200 mm respectively.[1] The resulting specimen behaviour can be seen in Figure 4.5 and Figure 4.6, which compares the three tests performed at a constant initial, vertical displacement 69mm. Table 4.5 shows a summary of the relevant parameters.

[1] The initial starting location for one dimensional bending (Test 7) was selected based on observation of the vertical force from full length tests – i.e. where the vertical force no longer decreased with horizontal translation. Later (Test 9 & later), the two dimensional region was selected based on (Hughes, Paik, and Béghin 2010)(Hughes, Paik et al. 2010) which dictated the two dimensional region from -550 to -350.

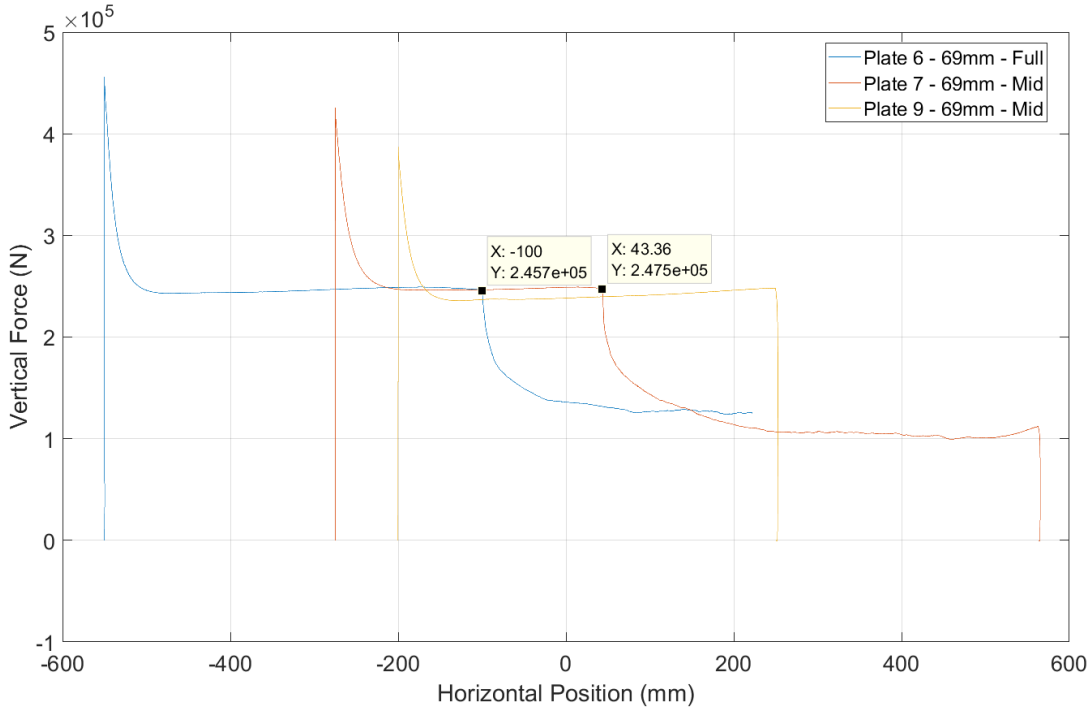

Figure 4.5: Horizontal Position vs Vertical Force for Varying Start Conditions

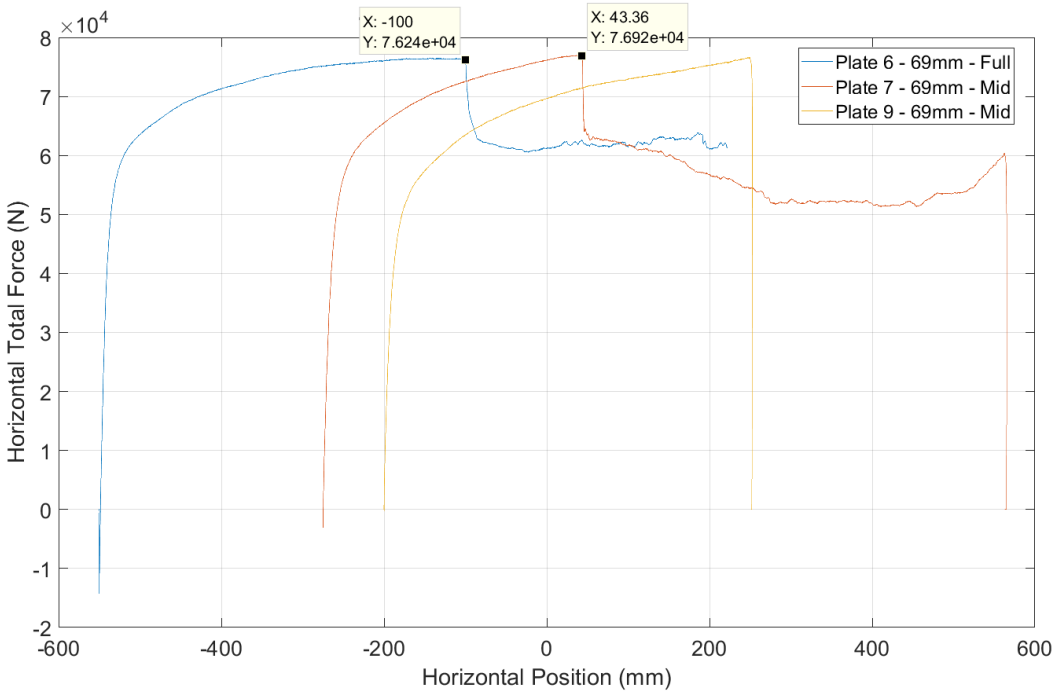

Figure 4.6: Horizontal Position vs Horizontal Force for Varying Start Conditions

Table 4.5: Summary of Start Condition Tests

Sample	Horizontal Start Location (mm)	Vertical Indentation (mm)	Maximum Vertical Force (kNx10^5)	Vertical Fracture Force (N x10^5)	Horizontal Location of Fracture (mm)	Notes
Test 6	-550	69	4.6	2.45	-100.0	
Test 7	-275	69	4.3	2.48	43.6	
Test 9	-200	69	3.9	NA	NA	No Fracture

From Figure 4.5 and Table 4.5, the fracture forces were almost identical however horizontal displacement at fracture decreased for the 2D bending test. As the vertical force at fracture is nearly identical at both start locations, this suggests that the vertical capacity of the plates are not impacted by the start position, for this level of initial vertical indentation. However, it should also be noted that this was only confirmed for vertical displacements which allowed for fracture in the observed 2D bending region (i.e. region of constant or near constant force response).

In addition to the Tests 6 and 7, a supplementary test, Test 9 was performed with the same initial vertical displacement (69mm) and horizontal starting position of -200 mm. This test did not result in fracture. Figure 4.6, shows that the vertical force achieved was 246 kN due to the same loading is slightly lower than that of the other two tests at 245.7 kN & 246.8 kN. There are a number of possible explanations for this difference, however the most likely source of error was the deformation event which occurred during the maximum vertical loading tests, where the carriage itself deformed 1mm inward at the midpoint (see Figure 4.4). The experimental problems and errors are covered in detail in Chapter 6.

Figure 4.6 shows the horizontal capacity of the plate specimens which were all performed with an initial, vertical displacement of 69mm. The resulting maximum, horizontal force is

nearly identical (76.4 kN, 76.9 kN, 76.6 kN) for each of the three tests however, only Test 6 and 7 resulted in fracture. As it Test 9 was after the bending event, comparison to earlier tests can be omitted. As the horizontal total forces were identical, this suggests several things. Primarily, the horizontal start location (and thus boundary condition) has little bearing on the maximum horizontal force induced in the sample as observed in Test 6 and 7. Following this, horizontal force is also independent of horizontal distance to fracture and is instead a function of the horizontal start location (or bending condition).

4.1.1.4 Elastic Tests

In addition to the nine rolling wheel fracture tests, nine tests were completed to show that the moving load effect was negligible for elastically loaded plates. This work was completed based on the recommendation for future work by Quinton (2015) as to determine the required loading to observe the moving load effect on hull structures. For the purposes of this work, this recommendation was observed for a plate specimen which were loaded sequentially until a moving load was observed. It was believed that the moving load effect was negligible for elastic deformations, and practically negligible for low, localised plastic strains (i.e. small plastic deformation). To explore this, a series of tests were conducted on a single test sample for increasing levels of vertical indentation. This can be seen in Figure 4.7, while a summary of the resultant forces can be seen in Table 4.6. Note data labels were omitted for clarity from Figure 4.7.

Table 4.6: Summary of Elastic Tests

Vertical Displacement (mm)	Vertical Force @ 550mm (kN)	Vertical Force at -550mm (kN)	% Difference of Vertical Force Response
1	1.5	1.3	17%
2	3.1	2.8	10%
3	4.9	4.6	7%
4	6.8	6.4	6%
5	9.3	8.6	8%
6	12.6	11.6	8%
7	17.6	16.0	10%
8	25.5	22.8	11%
10	42.2	34.1	21%

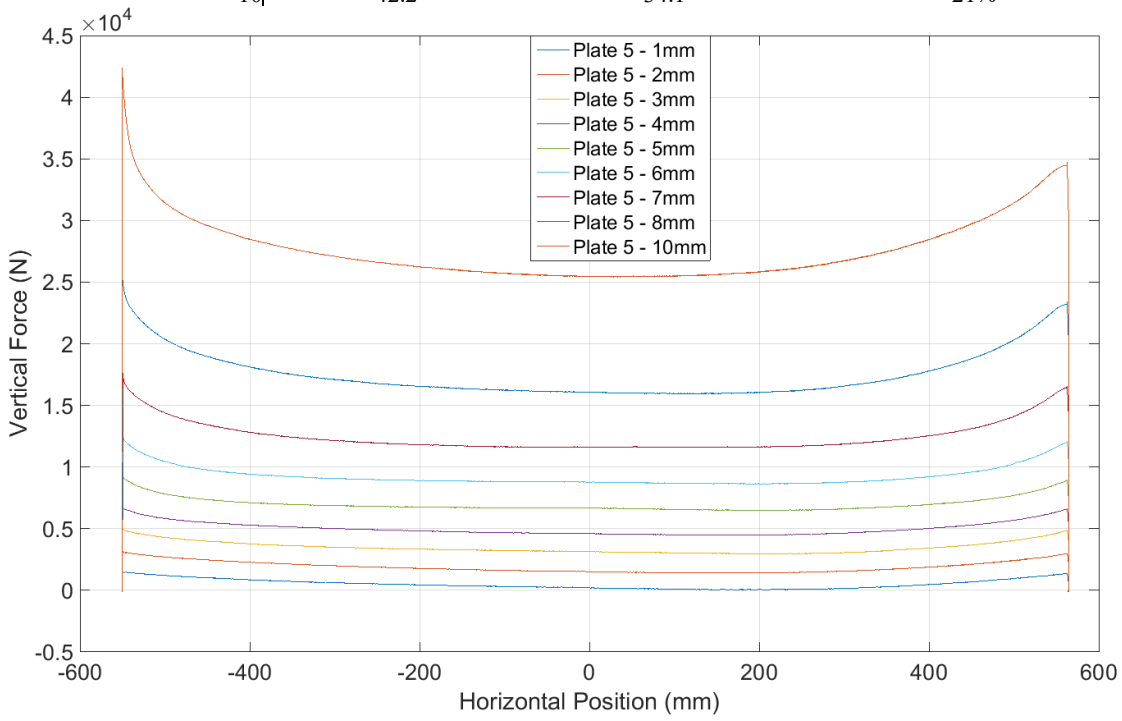

Figure 4.7: Vertical Force vs Horizontal Position for Elastic Tests

From Figure 4.7, it can be seen that the specimen response is uniform about the midpoint for the vertical indentation levels 1mm to 5mm. After this, a slight loss in vertical capacity can be observed, where the loss is defined as the difference between the maximum stationary vertical load (i.e. initial force before translation) and the force at the corresponding point. For these tests, the starting horizontal position was selected to be -550

mm, and the corresponding end point at 550mm. As the plate is constrained on the ends, it is necessary that symmetrical points about the center are selected as to ensure that the contributions due to the boundary conditions are identical for both the stationary and laterally translating measurement points. This allows for a direct comparison of the loss in capacity solely due to the horizontal component of translation. Figure 4.8, shows the loss in response as a percentage of the stationary response plotted against the initial vertical displacement. From this plot, the results are as predicted with exception to the 1mm and 2mm vertical indentation tests. Both of these tests appear to have resulted in significant vertical capacity loss when compared to all other tests. This can be practically explained due to the extremely small levels of force measured in these tests. The 1mm test resulted in a vertical force response of only 1501 N for the initial stationary, vertical displacement, which is less than 0.5% of the vertical capacity of the measurement device. The observations that the loss in capacity is negligible for elastic deformations is confirmed with small losses for 3 mm to 5 mm. After this occurs, the losses increase with vertical displacement for the remaining tests, from 5 mm to 10 mm.

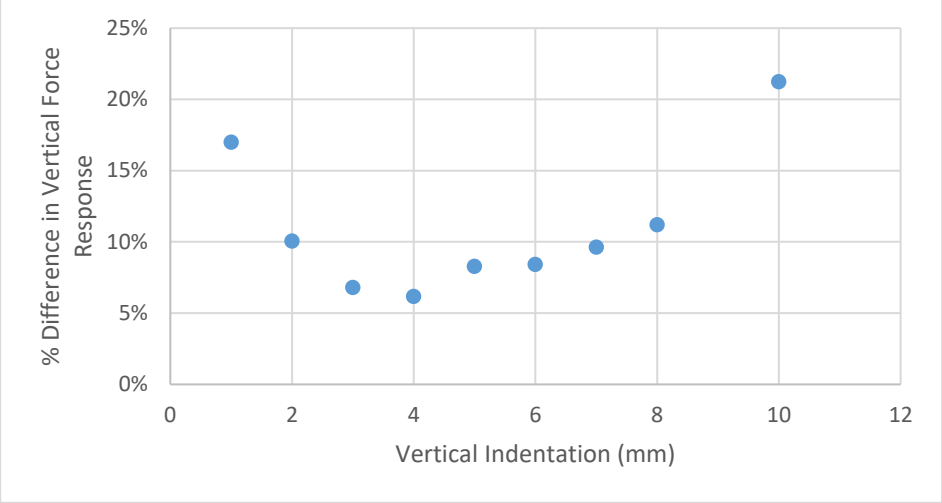

Figure 4.8: Percent Loss of Moving Load Response as Compared to Static Response

4.1.2 Cutting Wheel Displacement Control Tests

Displacement control tests were also performed for the cutting wheel indenter. Initially, the maximum vertical, stationary capacity was assessed and found to be 92.6 kN at 28.7 mm vertical indentation for a horizontal starting position of -550, and 96.1kN at 27.1 mm vertical indentation for a horizontal starting position of 0mm. Following this, a full length (horizontal movement from -550mm to 550mm) was performed at a vertical displacement of 22.5 mm (~85% of vertical capacity) of indentation which, incorrectly, was predicted to cause fracture based on the rolling wheel tests. The results of these tests can be seen in Figure 4.9 and clearly show that for constant displacement tests, the response is much less susceptible to the moving load effect for fracture than the rolling wheel tests. This is due to the change in indenter geometry and thus the stress state induced in the plate sample. This indicates that the moving load effect for fracture (the reduction of vertical, fracture capacity experienced during a horizontal displacement) is dependent on the stress state induced by the indenter. Further, it became apparent that the plate would not fracture for displacement

controlled tests, while fracturing for force controlled experiments which induced displacements on the same magnitude as the displacement controlled tests. This is believed to be due to the tests not reaching a required minimum force to induce fracture, which is relatively "close" to the stationary, vertical force to fracture due to the cutting wheel geometry and thus incited stress state. Despite the lack of fracture, this clearly shows that the moving load effect for plastic level damages is present for the cutting wheel, with a reduction in vertical force response at symmetrical points about the center of ~35%,

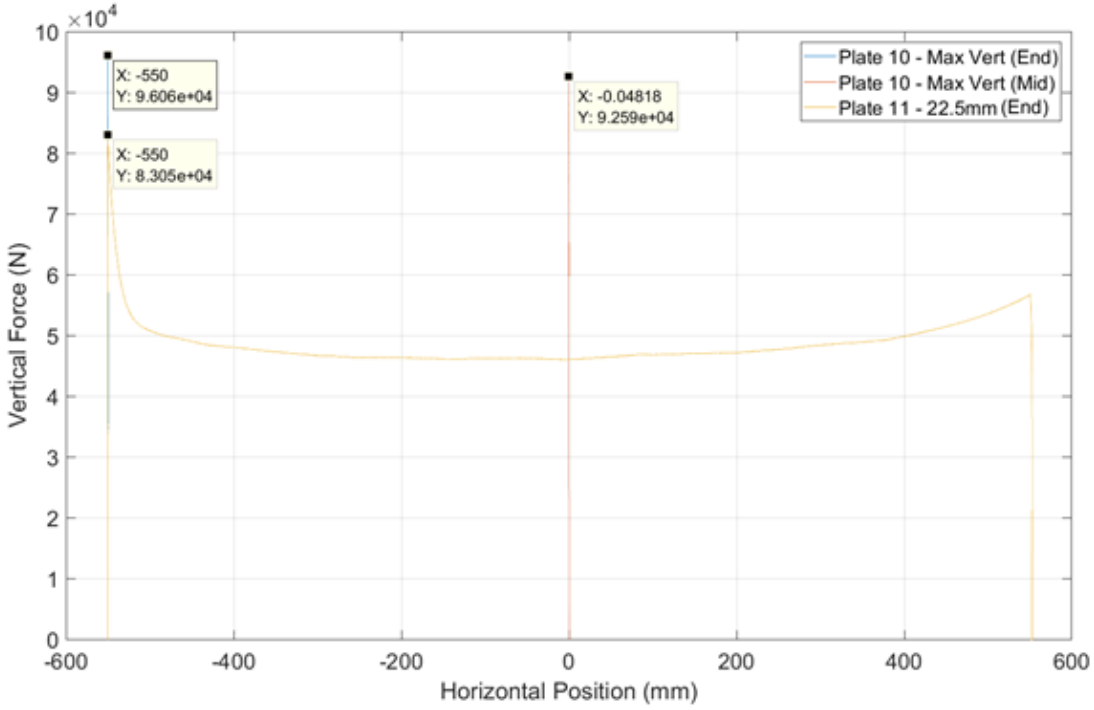

Figure 4.9: Preliminary Cutting Wheel Test Results

4.2 Force Control Tests

From the cutting wheel displacement tests, it was shown that the relative capacity loss for the cutting indenter was smaller than the rolling wheel therefore making displacement control tests more difficult to perform. It was decided to switch to force control to assess

any potential capacity loss for the cutting wheel indenter. These force control tests were done as a function of the maximum force capacities determined from the stationary displacement controlled tests. Additionally, similar to the displacement control, rolling wheel tests, the impact of horizontal starting location was also analyzed. Further, the impact of force on horizontal distance to fracture was also explored. Finally, several tests were performed with increased strain rates, however (as above for similar tests) the results are highly suspect and thus omitted from analysis due to the tuning of the PID control for a lower speed. The format of the legend of the moving load plots follows "Plate# - Test# (@Horizontal Start Location (mm)), while the stationary plots follow "Plate# - Max Vert (Horizontal Start Position) ML-FC (@Vertical Target Force)".

4.2.1 Plate Deformation between Tests

Due to the limited number of plates, multiple tests were completed on the same plate, if possible, with the cutting wheel. This was generally possible due to the small localized bending generated by most of the cutting wheel tests, in comparison to the rolling wheel test (see Figure 4.10). From the pictures, at the extents of the specimen which has been deformed with the cutting wheel, there is negligible damage in comparison to the extents of the specimen deformed with the rolling wheel. Further, to ensure that the deformations were small and the tests valid, the initial vertical starting position was measured before and after a number of tests, with the results showing no deformation.

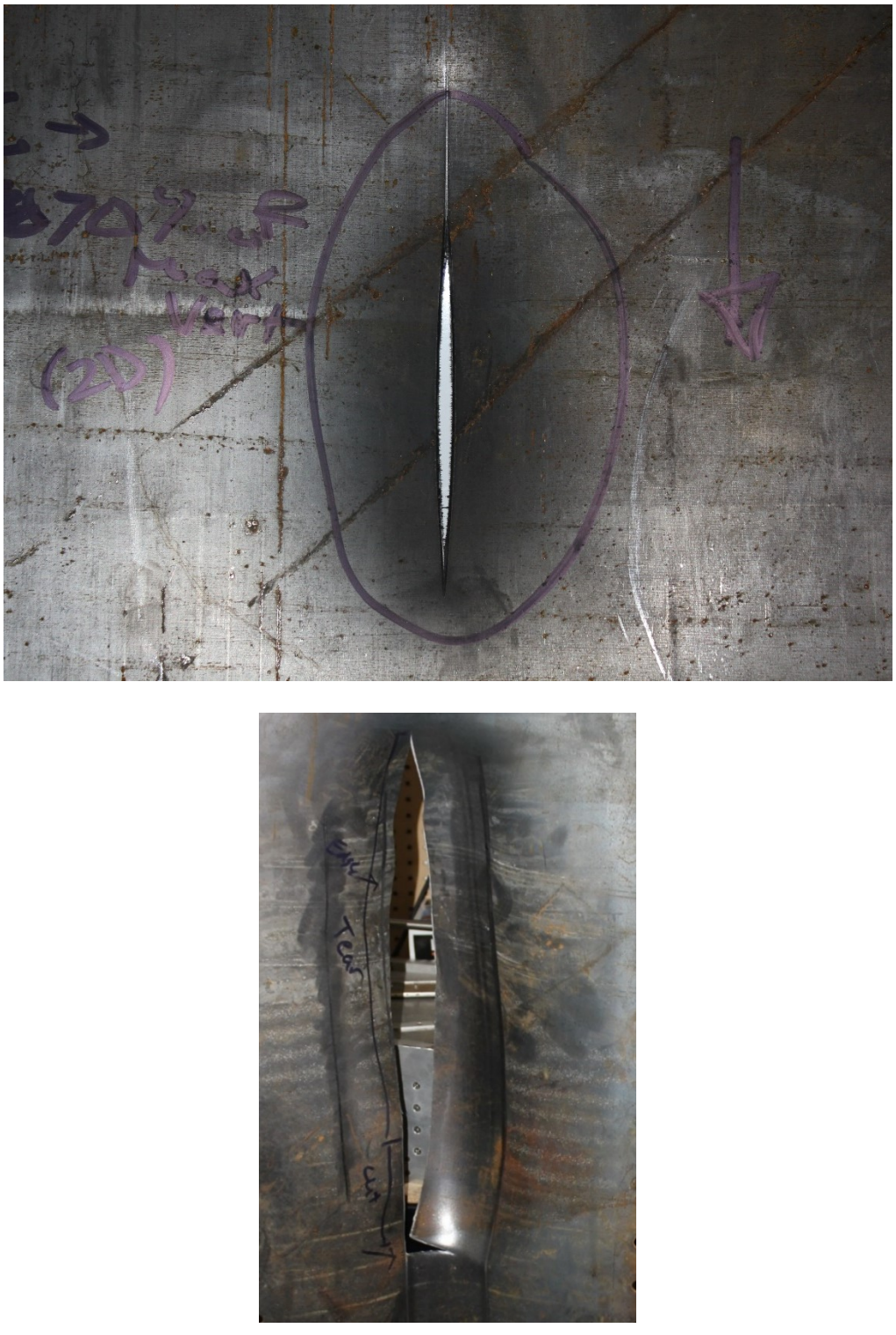

Figure 4.10: Global Damage Comparisons (Top – Cutting Wheel, Bottom – Roller Wheel)

4.2.2 Vertical Stationary Capacity

The vertical stationary capacity was assessed through two tests on one plate sample. One test was completed at -550mm (horizontal start location), with one test at 0mm (center of specimen). This was completed as to measure the capacity loss for both the 2D and 1D loading tests which were assumed to be from horizontal regions of ±550mm to ±350mm and ±200mm to 0mm respectively. The results of these tests are given in Table 4.7 below, and graphically shown in Figure 4.11, which shows that the 2D bending region had a larger capacity then the 1D tests.

It should be noted that the vertical force to fracture for the cutting wheel is significantly lower than any of the responses during stationary loading for the rolling wheel which did not result in fracture. From this, it can be surmised that the stationary, vertical force to fracture is lower for the cutting wheel geometry than the rolling wheel despite the inability to directly measure the latter. This is due to the change in stress state due to the change in indenter geometry. The cutting indenter induces significantly less bending before reaching a stress state which allows for the onset of fracture to occur. This is further addressed in Chapter 5, through the use of a numerical models to predict stationary capacity and compares numerical results for both indenter geometries.

Table 4.7: Stationary Vertical Indentation Tests

Sample	Test	Location (mm)	Fracture Force (N x10^4)	Vertical Indentation (mm)
S10	1	-550	9.6	27.1 (@ fracture)
	2	0	9.3	28.7 (@ fracture)

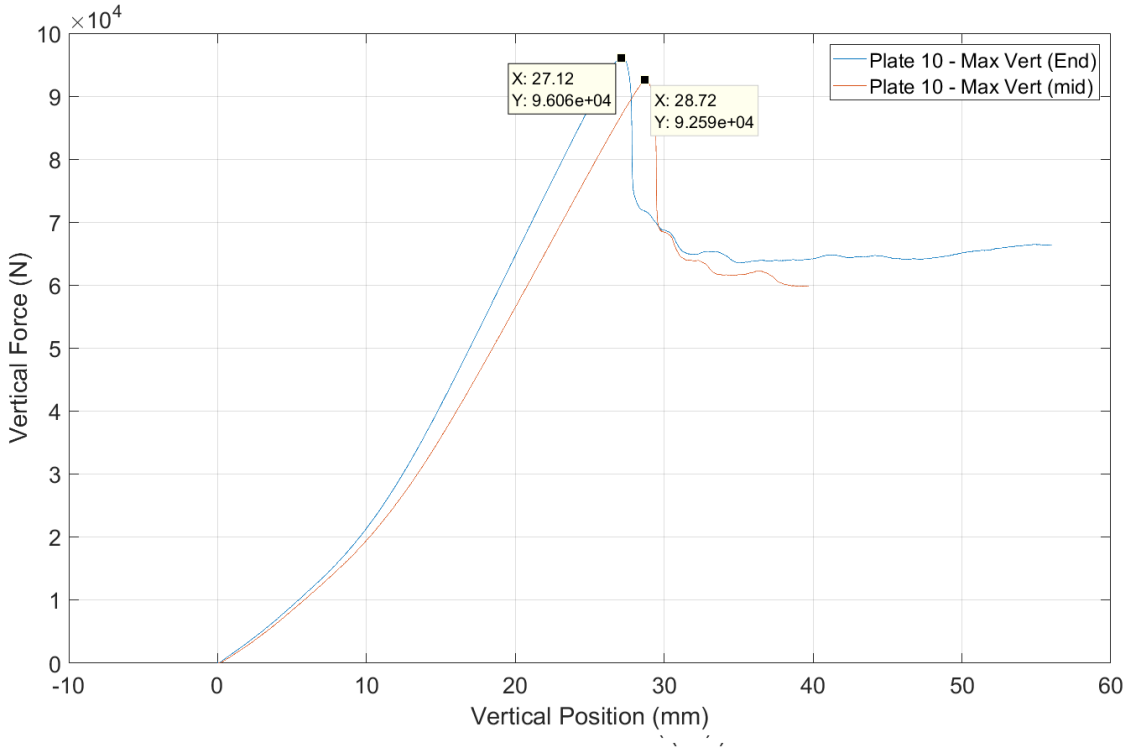

Figure 4.11: Vertical Force vs Vertical Position for Stationary Capacity Tests

4.2.3 Two-Dimensional Cutting Wheel Capacity Loss Tests

The cutting wheel capacity tests were completed by starting at the two symmetrical starting points (±550mm) and running the test towards the midpoint of the plate. Due to the relatively small fracture distances, multiple tests could be performed on each plate assuming that minimal bending occurred in the preliminary tests. This was checked by comparing the initial vertical location of the indenter before the first test and subsequent tests at that horizontal location for a number of tests.

In total, six tests were performed, five with a horizontal starting position of -550 mm and two with a horizontal starting position of 550mm and target vertical forces ranging from 83.4 kN to 46.3 kN, which corresponds to 90 & 50% of the stationary, vertical fracture

force determined through the displacement control tests. The results can be seen in Figure 4.12, Figure 4.13 and Figure 4.14 which give the vertical force vs horizontal position, vertical displacement vs horizontal position and horizontal force vs horizontal position respectively. It should be noted that the tests with the starting position of 550 mm, have been transposed to -550 mm for the purposes of visual comparison, however are clearly marked in the legend of each plot. Table 4.8 gives the target vertical force, actual vertical force at fracture (if applicable), the maximum horizontal force and maximum displacement for each test.

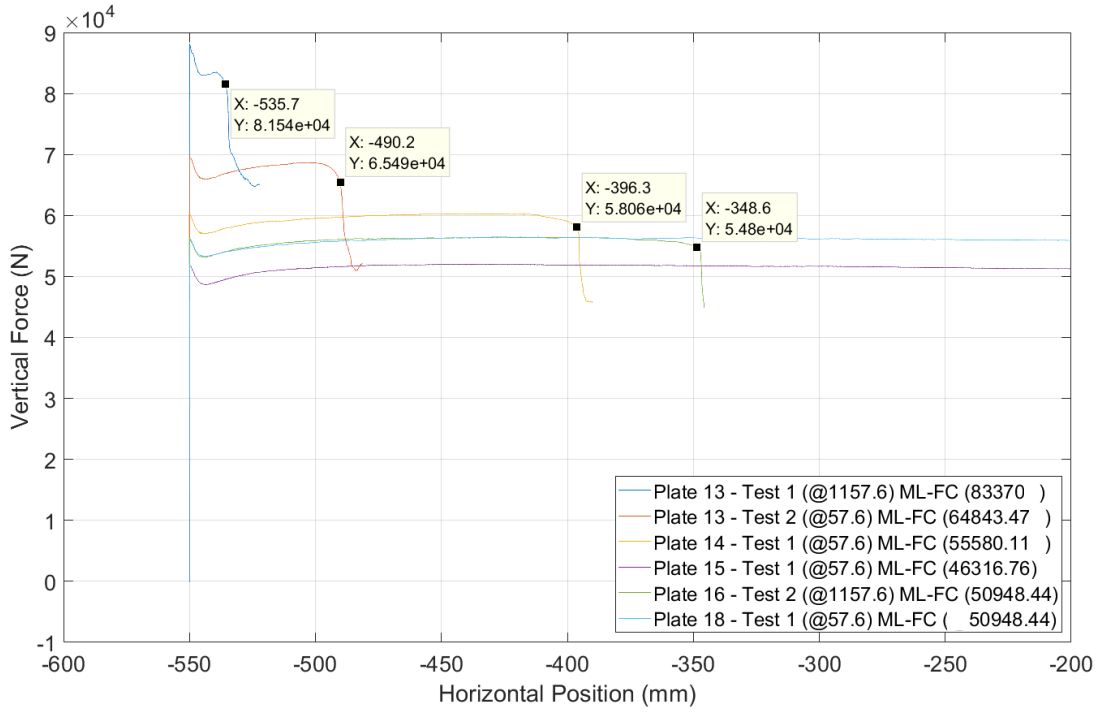

Figure 4.12: Vertical Force vs Horizontal Position for 2D Cutting Tests

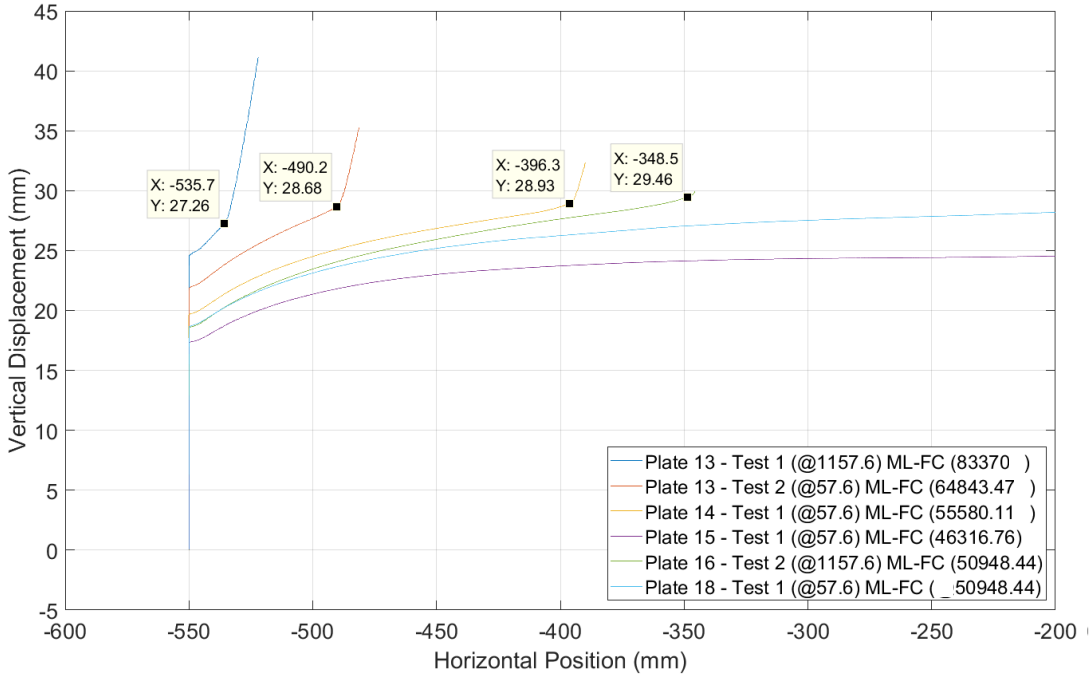

Figure 4.13: Vertical Displacement vs Horizontal Position for 2D Cutting Indenter Tests

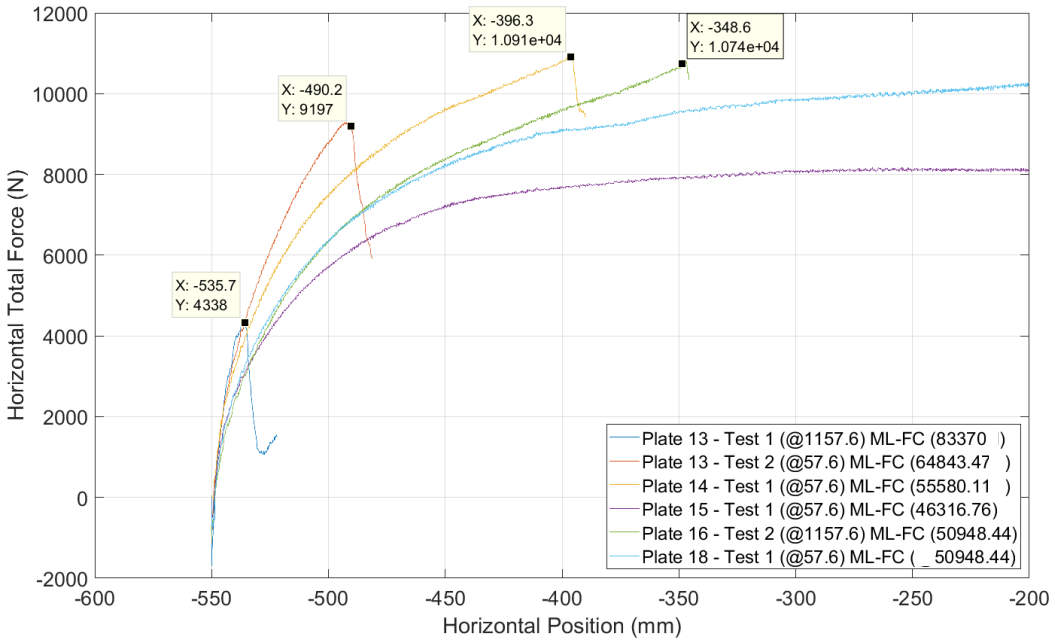

Figure 4.14: Total Horizontal Force vs Horizontal Position for 2D Cutting Indenter Tests

Table 4.8: Summary of Results for 2D Bending Cutting Wheel Tests

	Target Force (kN)	Force at Fracture (kN)	Vertical Displacement at Fracture (mm)	Horizontal Displacement at Fracture (mm)	Horizontal Force at Fracture (kN)
Plate 13-1	83.4	81.5	27.3	14.3	4.3
Plate 13-2	64.8	65.5	28.7	59.8	9.2
Plate 14-1	55.6	58.1	28.9	153.7	10.9
Plate 15-1	46.3	NA	NA	NA	NA
Plate 16-2	50.9	54.8	29.5	201.4	10.7
Plate 18-1	50.9	NA	NA	NA	NA

Figure 4.12 shows that fracture occurs in several tests at much lower forces showing a moving load capacity much lower than the stationary test, again confirming the applicability of the moving load effect for fracture, with both indenters. Additionally, the minimum force to induce fracture, and thus the maximum capacity loss, was quantified with respect to the maximum stationary vertical force. This was determined through Test 15-1 and Test 18-1 which did not fracture, reaching peak, moving vertical forces of 52 kN, and 56.4 kN respectively. However, Test 16-2 reached a peak moving, vertical force of 56.3 kN and fractured at 54.1 kN. This corresponds to a 43.6% loss in capacity as compared to the vertical, stationary, 2D bending test fracture force. This displays the variability of fracture and its dependence on material differences and flaws.

Additionally, Figure 4.13 displays the relationship between the specimen's ability to resist vertical displacement and horizontal position. From the figure, a clear point of inflection occurs, which indicates the point at which the specimen could no longer resist vertical indentation (i.e. ultimate failure & fracture). In general, at lower forces the specimen fractured at higher vertical indentation. It should be noted, that the range difference of

vertical indentation to cause fracture was extremely small in comparison to the rolling wheel specimen tests. This was likely due to the shape of the indenter inducing different stress states. In comparison to the vertical stationary tests, it is clear that the necessary indentation to induce fracture increases due to the moving load effect. Further, with decreasing vertical forces the vertical indentation at fracture increases. This is shown in Figure 4.15, where the vertical capacity as a function of the stationary capacity is plotted against the vertical indentation at fracture.

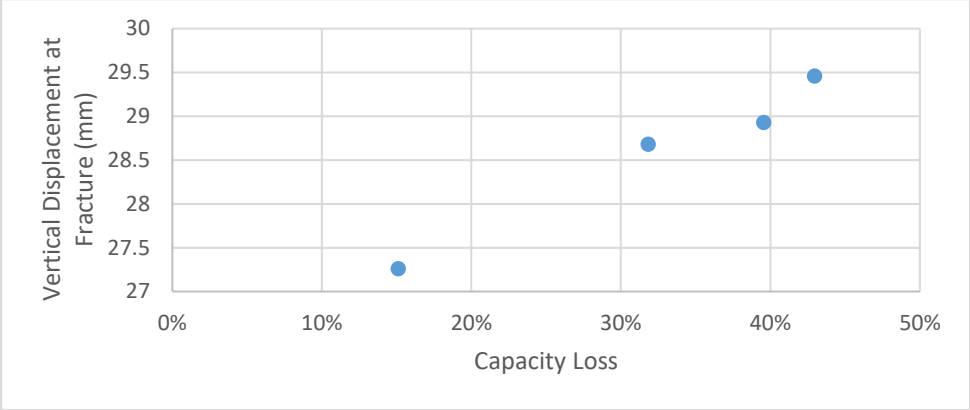

Figure 4.15: Vertical Indentation to Fracture vs Force Capacity

Figure 4.14 shows the horizontal force response for the two-dimensional bending tests. As expected, the horizontal force increased rapidly, until the target vertical force was reached at an approximate horizontal location of -500 mm in all tests resulting in fracture, with exception to Test 13-1. The specimens then carried this relatively constant horizontal force until fracture which then drops significantly when the specimen reaches steady state fracture. From Tests 15-1 & 18-1 where fracture did not occur, the constant horizontal force is reached at an approximate horizontal location of -300 mm and until the influence of the boundary causes an increase in the measured forces at an approximate horizontal location

of 300 mm. It should be noted that this is similar to the behaviour experienced by the Test 4 where fracture failed to occur for the rolling wheel, however due to the large bending deformations, the impact of the boundary conditions is greater and causes the effective one-dimensional bending region to be smaller.

Regarding the remaining tests that resulted in fracture, the horizontal forces climbed to a peak loading, with the highest target vertical force of 83.4 kN in Test 13-1 inducing the smallest horizontal force of 4.3 kN. This was simply due to the fracture occurring early in the test period thus not allowing for bending and resistance in the horizontal direction. Finally, as expected the rate of change of the horizontal forces is approximately constant for all tests.

Also of note is the horizontal distance to fracture as compared to the vertical force. As expected, the distance to fracture is directly related to the vertical force, with the largest of Test 13-1 causing fracture in 13.5 mm, while the lowest, Test 16-2 causing fracture in 201.4 mm. While Tests 18-1 and 15-1 did not result in fracture, only 18-1 does not follow this pattern, inducing a significantly lower force horizontally then expected.

4.2.4 One-Dimensional Capacity Tests

The one-dimensional tests were performed over the horizontal region from -250 mm to 250 mm and with a range of target vertical forces from 80.3 kN to 53.5 kN. As fracture occurred extremely quickly in most cases, multiple tests were performed on each plate, after concluding that the previous tests did not impact the specimen at the new test locations. Two tests were completed at horizontal locations of 200 mm and one at 0 mm. The results of the one-dimensional tests can be found in Figure 4.16, Figure 4.17 and Figure 4.18 as

well as Table 4.9. Again for convenience, the tests have been superimposed at a horizontal location of -200 mm with actual locations given in the legend.

Table 4.9: One Dimensional Capacity Results for Cutting Wheel Tests

	Target Force (kN)	Force at Fracture (kN)	Vertical Displacement at Fracture (mm)	Horizontal Displacement at Fracture (mm)	Horizontal Force at Fracture (kN)
Plate 13-3	64.8	65.8	29.2	43.9	8.7
Plate 14-2	53.5	56.3	29.0	235.2	11.5
Plate 16-1	62.4	62.6	28.4	60.0	9.5

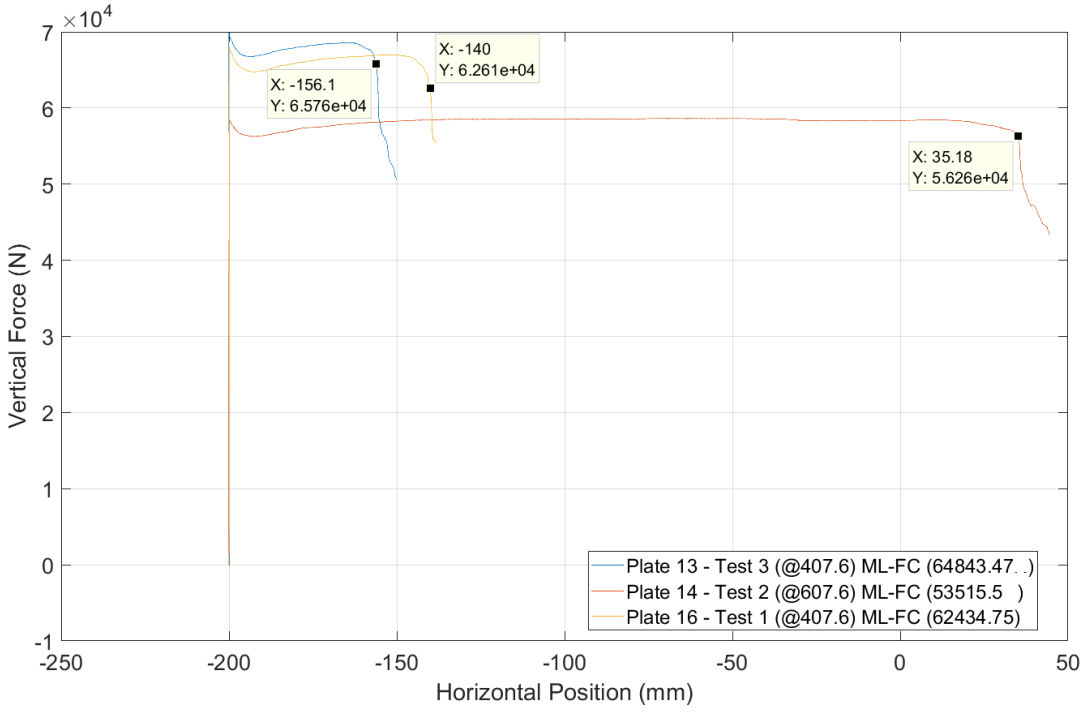

Figure 4.16: Vertical Force vs Horizontal Position for 1D Bending Tests

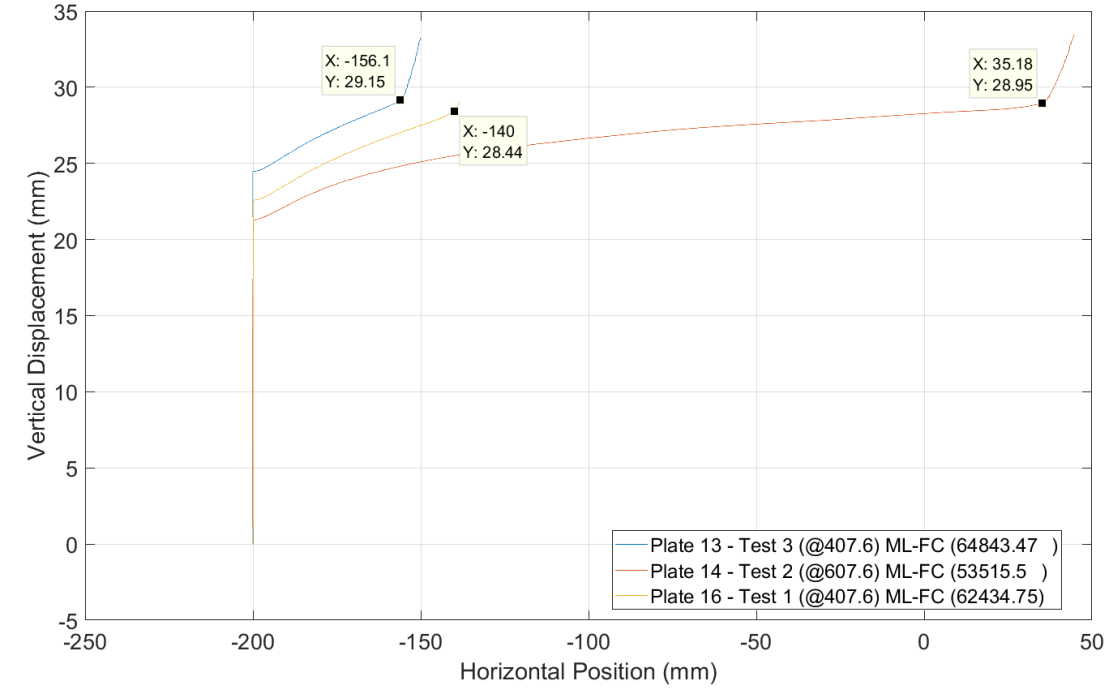

Figure 4.17: Vertical Displacement vs Horizontal Position for 1D Bending Tests

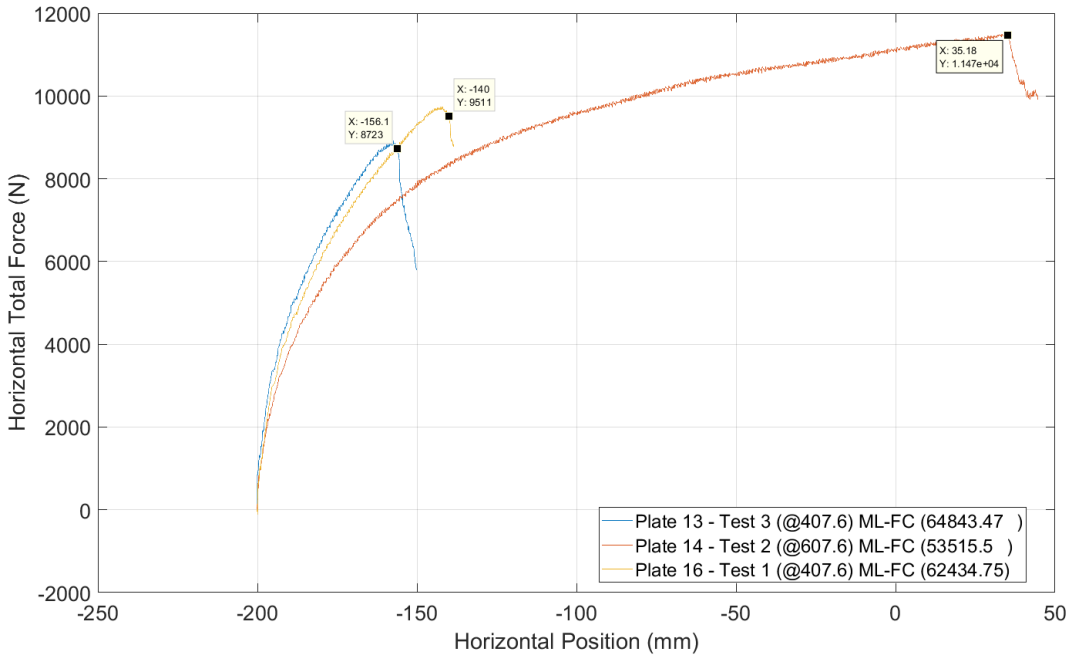

Figure 4.18: Total Horizontal Force vs Horizontal Position for 1D Bending Tests

Figure 4.16 displays the vertical force plotted against the horizontal positioning for each of the tests. The specimen exhibited similar trends to the two-dimensional test specimens where a much lower vertical force resulted in fracture in every test. The highest vertical fracture force during testing was Test 13-3 at 65.8 kN, which fractured the plate in 43.9 mm of horizontal translation. The horizontal distance to fracture decreased with vertical force, similar to the previous results for all for of the tests, with the longest fracturing in 235.2 mm. This horizontal distance to fracture corresponded to the largest loss in capacity at 32.3%, which was smaller than the 2D bending tests.

The vertical displacement at fracture is shown in Figure 4.17, which shows a decrease in vertical indentation at fracture with decreasing force. This is the inverse of what was observed in the one dimensional bending tests, however it is of note that the total difference between all tests is less than 1mm and that all values are within 1mm of the 2D bending tests. This suggests that the boundary condition at the end is the cause of the increasing indentation at fracture.

Additionally, the horizontal force is shown in Figure 4.18 and follows a similar trend to the two-dimensional bending tests. The horizontal force increases rapidly and begins to taper to a constant value as the force is allowed to develop. The lowest horizontal force, 8.7 kN, corresponds to the largest target vertical force of 64.8 kN as it fractures quickly in relation to the other tests. Conversely, the horizontal force is allowed to develop the most in Test 14-2 due to the lower vertical target force of 53.5 kN and fractures at a maximum horizontal force of 11.5 kN.

4.2.4.1 Horizontal Start Location Dependence

Fracture dependence on horizontal starting position was again compared through, in this case with two tests of the same target vertical force with horizontal starting positions of -550mm and -200mm. Only one test was performed with the same target vertical force of 64.8 kN, the results of which are compared in Figure 4.19, Figure 4.20 and Figure 4.21 below. Again they have been superimposed for ease of comparison.

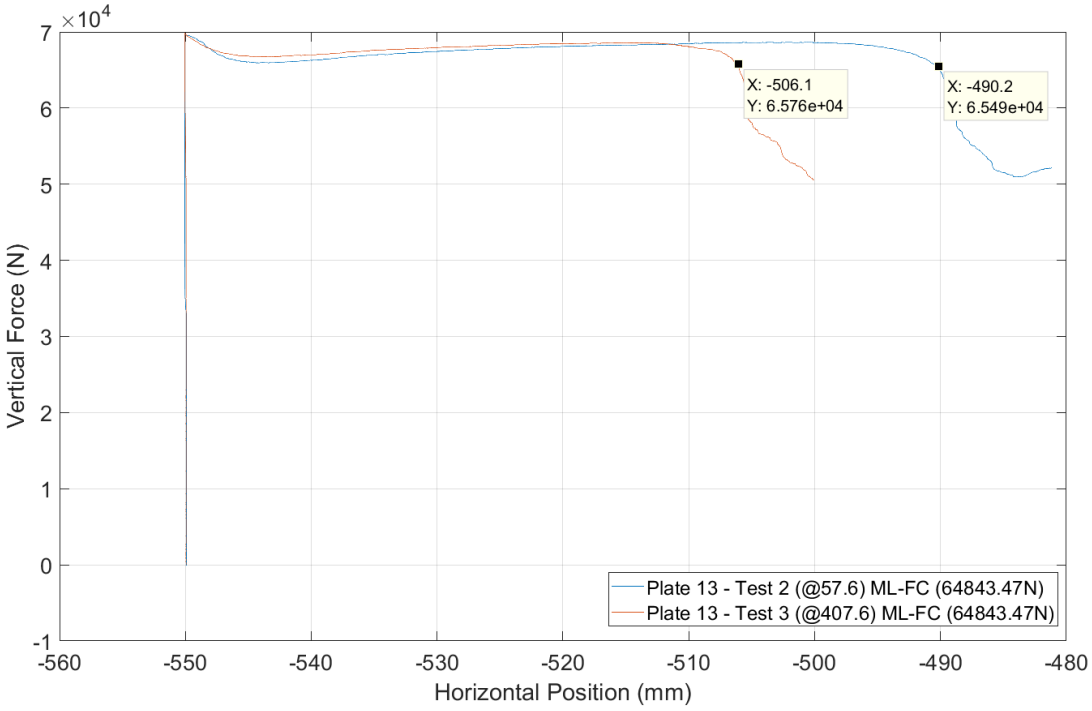

Figure 4.19: Vertical Force vs Horizontal Displacement for Starting Location Comparison

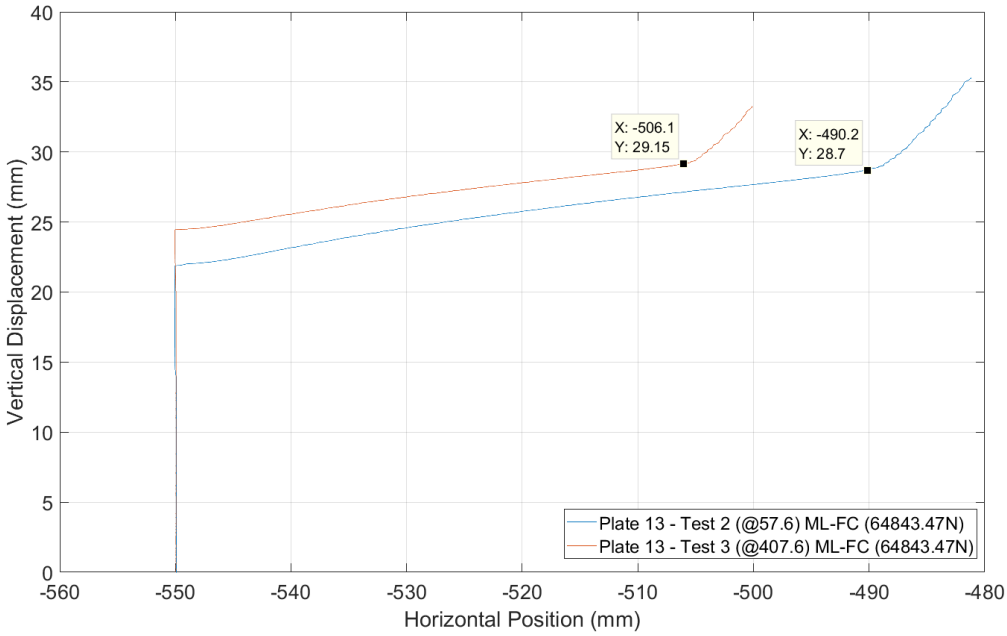

Figure 4.20: Vertical Displacement vs Horizontal Position for Starting Location Comparison

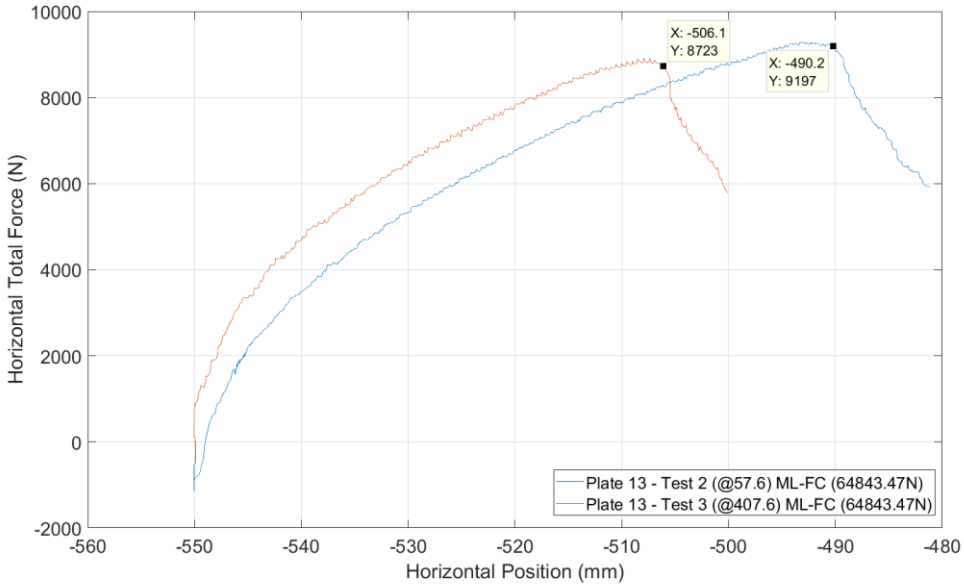

Figure 4.21: Total Horizontal Force versus Horizontal Displacement for Starting Location Comparison

Due to the limitation of sample size, it is difficult to confirm any trends, however, similar to the rolling wheel tests, the distance to fracture decreased in the one dimensional bending region. Additionally, similar to the rolling wheel tests, the peak horizontal forces were lower for the two-dimensional bending tests with 9.2 kN & 8.7 kN for Test 13-2 and 13-3 respectively. Also of note is the vertical indentation to fracture which increased slightly in the two-dimensional bending region, however was extremely small and therefore likely negligible. The initial vertical indentation to target force was lower in the one-dimensional bending region which was expected due to the influence of the boundary conditions at the end of the plate.

Chapter 5 Numerical Experimental Results

To further explore the moving load phenomena for fracture, a series of numerical experiments were completed corresponding to a rolling case, Test 6 and a cutting case Test 13-2. The methodology used in preparation and results of the models are discussed in the following section. It is worth noting that due to time constraints, the models were prepared using a single *equivalent fracture strain* value that is independent of the effects of triaxiality and Lode parameter. This is a commonly accepted method of analysis in the shipping industry and is confirmed to give accurate results for stationary loading to fracture (Ringsberg et al. 2018). However, as detailed in Chapter 2.4, the research put forth by Bao & Wierzbicki (2004), Bai & Wierzbicki (2008) and others displayed that fracture is dependent on both triaxiality and Lode angle parameter. As it was hypothesized that the change in parameters with the horizontal load movement was causing the resulting decrease in fracture capacity, it was expected that the results of these numerical tests would show the inability of the *equivalent fracture strain* method to accurately predict fracture for the moving load scenario. This method was achieved through calibration about a known point in fracture through comparing the vertical force response of the experimental, vertical stationary test and corresponding numerical simulation, and referred to as the calibration method henceforth.

5.1 Scope and Objectives

The scope and objectives of the numerical experiments were to:

- Develop calibrated/validated numerical simulations of two experimental tests: one rolling wheel (Test 7); and one cutting wheel (Test 13-2)
- Investigate the accuracy of the commonly used *equivalent fracture strain* technique to model fracture due to moving loads. This technique involves simply calibrating a singular *equivalent fracture strain* value to existing tests, which has been proven (Ringsberg et al. 2018) to be accurate for stationary loading conditions.
- Investigate and observe triaxiality and Lode angle at the experimental point of fracture to determine if their inclusion would impact results.
- Ensure that multiple tests on one plate specimen were valid for the cutting wheel indenter.

5.1.1 Methodology

The model was prepared using the standard methodology determined by Quinton (2015); except for the inclusion of a fracture strain parameter in the plastic, kinematic material model.

5.1.1.1 Model Geometry & Meshing

Similarly to Quinton (2015), the testing apparatus was assumed to be rigid for simulation purposes, and thus only necessary to model the plate specimen pictured in Figure 5.1 due to the negligible difference of the inclusion of the plate beneath the stiffener ring. It should be noted, that as the carriage actually deformed horizontally during the stationary, vertical rolling wheel test and therefore is not actually rigid in all cases. However, as these deformations were small in relation to those experienced by the plate and only in the

horizontal direction, it was assumed that this response had no real impact on the modelling of sample and boundaries. The plate was given a mesh edge length of 5mm.

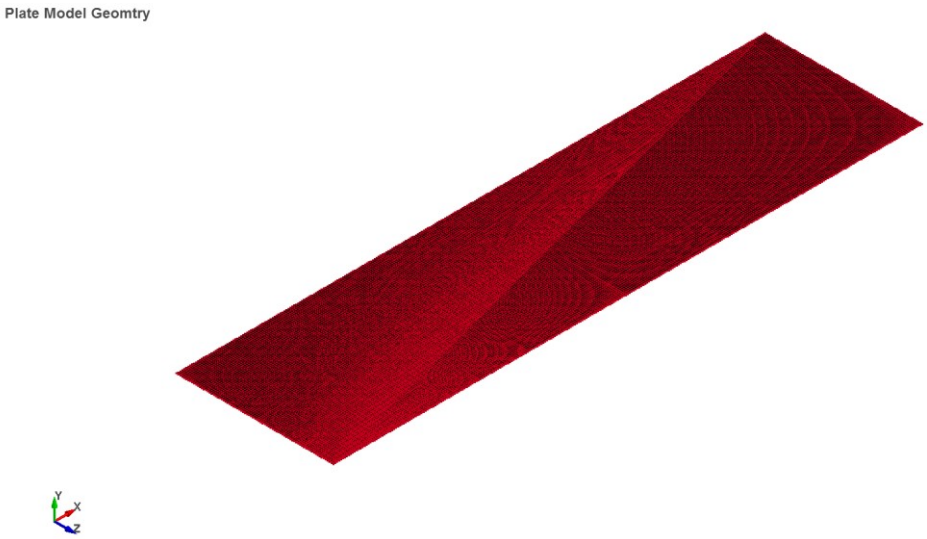

Figure 5.1: Plate Model Mesh for Calibration Method

Different from the work by Quinton (2015), the indenter wheels both vary from the previous geometric models. The roller wheel used in the physical tests is the same, however, Quinton (2015) only modelled a small wedge of the whole indenter due to the relatively small vertical indentation. As was observed in the physical tests, the straight vertical sides contacted the plate specimen and therefore was necessary to model numerically. The indenters were meshed using first the shell mesher and then extruding this mesh using the element generation tool. The mesh dimensions are 3mm in width and length, 2.5mm in depth. The rolling wheel can be seen in Figure 5.2. Additionally, the second indenter, the cutter wheel was modelled and meshed using the same methodology, however, like the original moving load experiments only a small wedge was modelled due to the lower vertical travel during these tests. The element dimensions are 7mm in width

and length. 5mm in depth. This can be seen in Figure 5.3. The indenters were both given rigid material properties as detailed in Chapter 5.1.1.3.

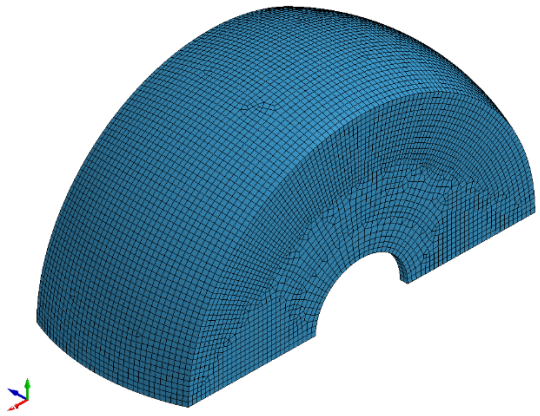

Figure 5.2: Rolling Wheel Mesh

Figure 5.3: Cutting Wheel Indenter Mesh

5.1.1.2 Loading

The loading was completed in two separate ways, force and displacement control to determine the impact if any, it had on the results. The vertical portions of the force control tests were completed through the direct utilization of the vertical force history from the

experimental results at 2048 Hz, while the displacement control used the experimental vertical displacement time history. In both cases, the data was loaded into the DEFINE_CURVE card directly with no reduction in frequency. This was done to ensure that indenter motions were correctly characterized as accurately as possible. For the force control simulations, the load was then applied using the LOAD_RIGID card, which simply applies a load to the rigid body (indenter) using the specified curve. The displacement control simulations were given a vertical motion using the BOUNDARY_PRESCRIBED_MOTION_RIGID card.

For both the force control and displacement controlled tests, the BOUNDARY_PRESCRIBED_MOTION_RIGID card was used to define the horizontal motion. The horizontal motion curve was a displacement history in both cases, collected from the experimental data at 2048 Hz.

5.1.1.3 Material Model

The material model parameters were predominantly taken from the two material steel bills received during fabrication of the plate samples. However, due to the mixing of the samples during testing, two sets of numerical simulations were completed for each of the tests to determine which of the two more closely matched the experimental results.

Further, a series of experiments were conducted to calibrate the fracture strain for the plate specimens for the calibration method as fracture strain is dependent on element size. Finally, the density, Young's Modulus and Poisson's Ratio were taken from previous experiments and standard material property datasheets for 44/50W structural steel (Chapel Steel 2018). The material constants can be found in Table 5.1 below.

Table 5.1: Material Model Parameters for Calibration Test Simulations

	Density (kg/m^2)	Young's Modulus (GPa)	Poisson's Ratio	Yield Strength (MPa)	Tangent Modulus (MPa)	Beta (Strain Hardening Parameter)	Fracture Strain
First Steel Bill	7850	207	0.33	374	432	1	0.265
Second Steel Bill	7850	207	0.33	422	157	1	0.285

It should be noted that the tangent modulus and resulting fracture strain for the calibration method generated numerical results which did not comply with the observed experimental results. Therefore, the parameters were changed until agreement with the experimental results was observed. This was done by first finding a tangent modulus that resulted in agreement during the plastic damage portion of loading (with an *effective fracture strain* of zero), followed by calibrating a new *effective fracture strain* to match the experimental point of fracture. This is elaborated in Chapter 5.2.1. The final tangent modulus was given to be 585 MPa, while the determined fracture strain was found to be 0.243. Additionally, the indenters were given a rigid material model with the properties found in Table 5.2. Rigid materials in LS-DYNA are not allowed to deform, however the material properties are necessary when observing contact.

Table 5.2: Rigid Indenter Material Model

Density (kg/m^2)	Young's Modulus (GPa)	Poisson's Ratio
7850	207	0.33

5.1.1.4 Contact

The contact between the two models was modelled using the AUTOMATIC_SINGLE_SURFACE algorithm as the formulation to detect contact between the elements, and the FORCE_TRANSDUCER_PENALTY card to read and write the forces experienced by the indenter and plate during contact. The later has absolutely no impact on the results of the simulation but measures the forces on the specified master and slave components as defined by the user. For the purposes of these numerical experiments, the contact was defined through a middle section of the plate and the whole indenter as shown in Figure 5.4, while the contact forces were measured separately for the indenter (master) and expected plate contact area (slave). The plate contact section was limited to a narrow band in the vicinity of the indenter, so as to decrease run time, as the algorithm checks for contact in all specified elements at every timestep.

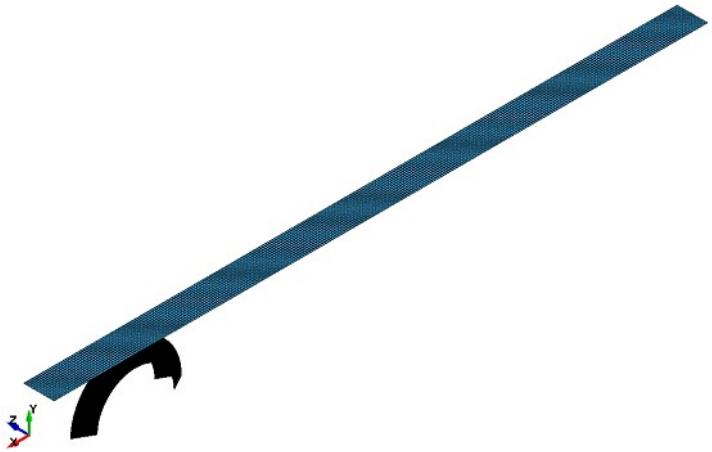

Figure 5.4: Master (Indenter) and Slave (Plate Contact Area) for Cutting Wheel Numerical Tests

It should also be noted that the contact method selected will choose the larger of the element edge length or the contact thickness. This should not be an issue for these simulations as the plate thickness of 3/16" (4.597mm) is smaller than the element edge length (5mm), however to ensure contact occurs in the proper spot, a contact thickness was defined using the PART_CONTACT card.

5.1.1.5 Boundaries & Constraints

Usually in a numerical simulation, one or more parts are fixed in place using the BOUNDARY_SPC card. However, due to the study completed by Quinton (2015), it is known that the plate is not rigidly fixed in the vertical direction, but instead moves with the elastic deformation of the carriage portion of the MLA. To achieve proper vertical compliance discrete linear springs were implemented. First, the edges of the plate are specified as a constrained nodal rigid body (CNRB) which fixes the motion of the plate edges. Following this, the motion of the CNRB is restricted for all motions with exception of vertical translation. Finally, four discrete springs at each corner are applied. This methodology was employed for the work in these thesis, as well as the observation that the k value for the spring constants was found to have a non-linear response when compared to vertical stationary force. Therefore, two spring constants were used; 6.338×10^6 N/m^2 for the lower vertical force response tests (i.e. cutting wheel) and 2.57×10^7 for the tests which had a higher magnitude of vertical force (i.e. rolling wheel). It should be noted that while sufficient for the scope of this thesis, following the same methodology employed by Quinton (2015) in developing a fully descriptive response surface would produce superior results and allow for easier and more accurate calibration of the model. Addition, during

testing the carriage of the MLA saw permeant deformation inward, deforming significantly in the center of the carriage. This is not a concern for the numerical simulations of the experiments which followed this deformation as the discrete springs ensure vertical compliance, not lateral. As the bolt slots of the plate specimens were re-drilled to allow not compression of the specimen during installation, the rigid lateral boundary condition is sufficient for the purposes of these simulations.

The indenter wheel also has a set of constraints and is loaded using the BOUNDARY_PERSCRIBED_MOTION_RIGID card. Additionally, the motion is limited in all translations and rotations with exception to the x (horizontal) direction for the horizontal motion definition, and the y (vertical) for the vertical motion definition.

5.1.1.6 Element Selection

The shell element formulation used in these simulations is the default, Belytschko-Lin-Tsay as per the sensitivity study completed by Quinton (2015). Also determined and used for these simulations was a suitable shear factor of 5/6 and number of through thickness integration points of 5. It should be noted that the number of through thickness integration points directly influenced the horizontal force readings and increasing this number would result in greater horizontal agreement and a longer solution time. For the purposes of this thesis it was deemed unnecessary.

5.2 Cutting Indenter Numerical Results

One set of calibration tests to determine a suitable *effective fracture strain to failure* was completed, followed by one displacement controlled moving load test. The stationary

calibration test was selected to be Test 10-2. For the moving load cutting indenter test specimen that was selected was Test 13-2 as it exhibited the expected result, fracturing during the horizontal translation portion of the loading despite being under a significantly lower vertical load then the stationary tests (31.8% at fracture). The following sections outline the results of the numerical experiment and comparison to the experimental results.

5.2.1 Vertical Stationary Results

There were many vertical stationary tests performed to calibrate the models to the desired point of fracture. Due to the relative accuracy of using *effective plastic strain to fracture* to model simple stationary capacity tests to fracture (Ringsberg et al. 2018) as compared to more complicated damage models, this method was used to calibrate the *effective plastic strain to fracture* for comparison in the various moving load tests. As outlined above, fracture strain is element size dependent and thus it is unsuitable to simply use the material elongation from the material bill. The use of the *effective plastic strain to fracture* method also clearly tests the belief that the moving load effect for loads which incite fracture is dependent on both Lode Angle parameter and triaxiality. If the *effective plastic strain to fracture* method of modelling fracture provides results which cannot be validated through the experimental test work, then the moving load effect is clearly dependent on the two parameters.

The material properties for both steel bills can be found in Table 5.1 above, with determined fracture strains of 0.265 & 0.285. It should be noted that the point of fracture noted by LS-Dyna is the point when the effective plastic strain of the through thickness points in an element reaches the dictated effective plastic strain to fracture. Matching these nominal

times to fracture with the observed result experimentally resulted in a vertical load profile that peaked significantly lower than the experimental data. Thus, the curve was fitted based on peak force, which gave better agreement with the experimental data. The loading profile was also compared and can be seen in Figure 5.5 and Figure 5.6 for material bills 1 and 2 respectively.

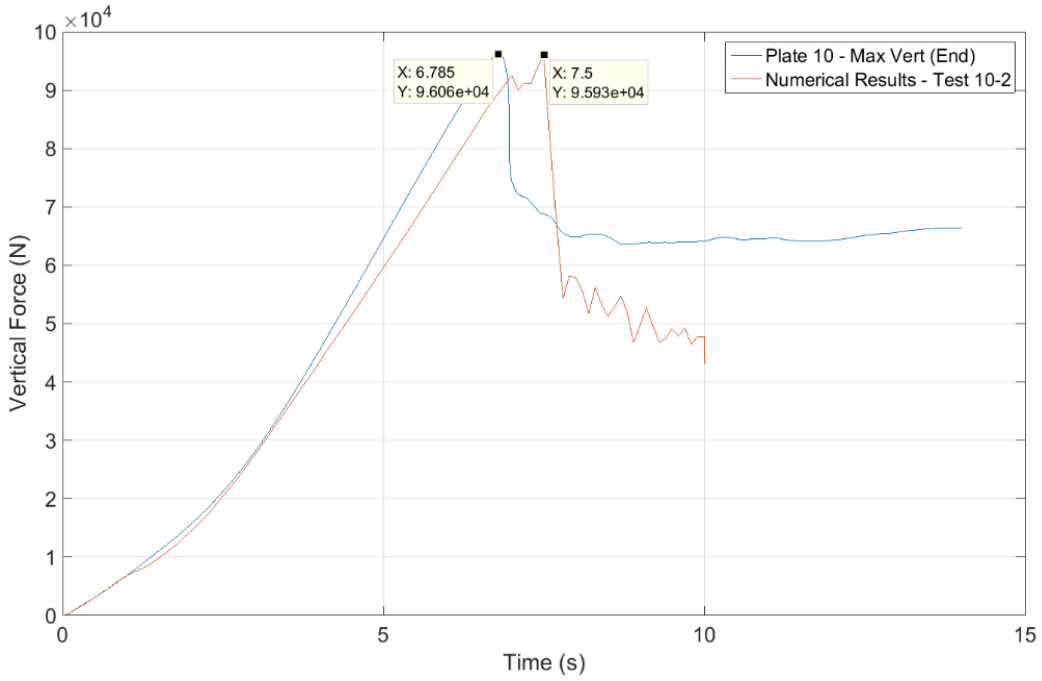

Figure 5.5: Numerical Force History for Material Bill 1

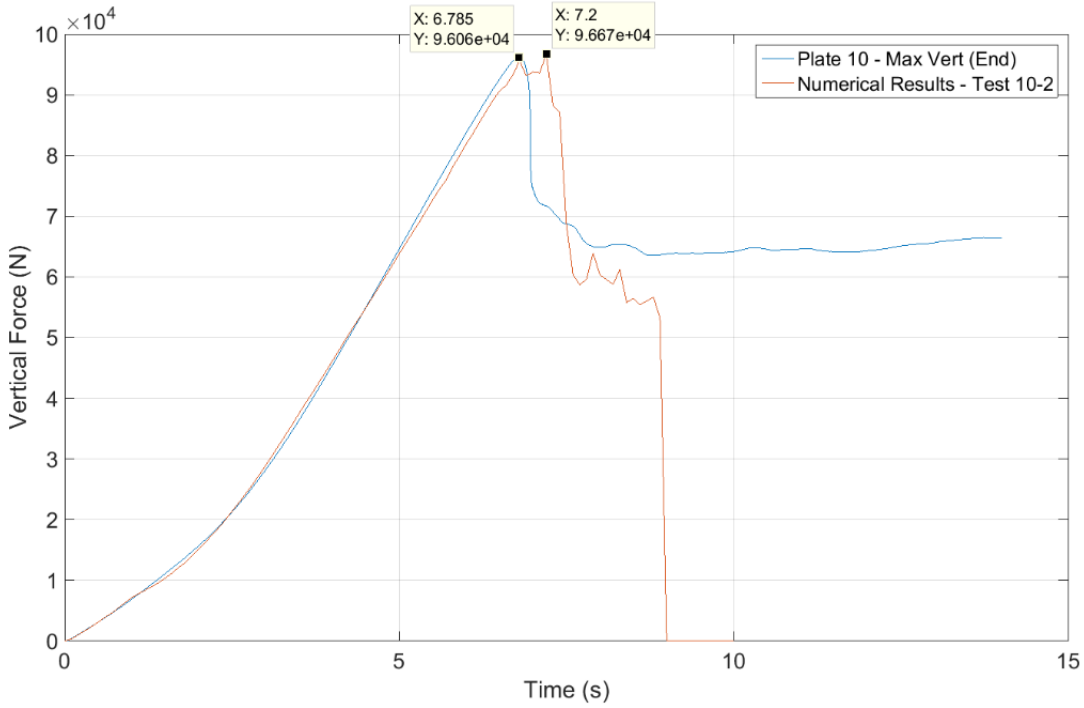

Figure 5.6: Numerical Force History for Material Bill 2

From the plots, the agreement with the experimental data is poor for the plastic level of damage and the sample stopped resisting vertical force 0.75s after the experimental result for the first steel bill and 0.45s after for the second. Additionally, an unexpected valley can be seen near the peak force value. These tests simply calibrated an *effective plastic strain to fracture* about a known point of fracture with all other material properties fixed, including element size and tangent modulus. As it is clear that the post yield behaviour, particularly before fracture did not agree with the experimental results, the tangent modulus was first varied, until agreement was found for all damages not resulting in fracture. After this, a new *effective plastic strain to fracture* was found until agreement with the experimental results was achieved for use in the other numerical simulations. This process resulted in good agreement with the experimental results, mainly the time to fracture, agreement during the plastic deformation portion of loading and reduction of the unexpected valley at the peak vertical force. It should be noted that this was completed purely by sequential changing of the tangent modulus and fracture strain with no statistical modelling. The new tangent modulus was determined to be 585 MPa with a fracture strain of 0.243. The new material model resulted in a vertical force history in Figure 5.7 below, which again are matched against the experimental results for Test 10-2 for vertical force agreement.

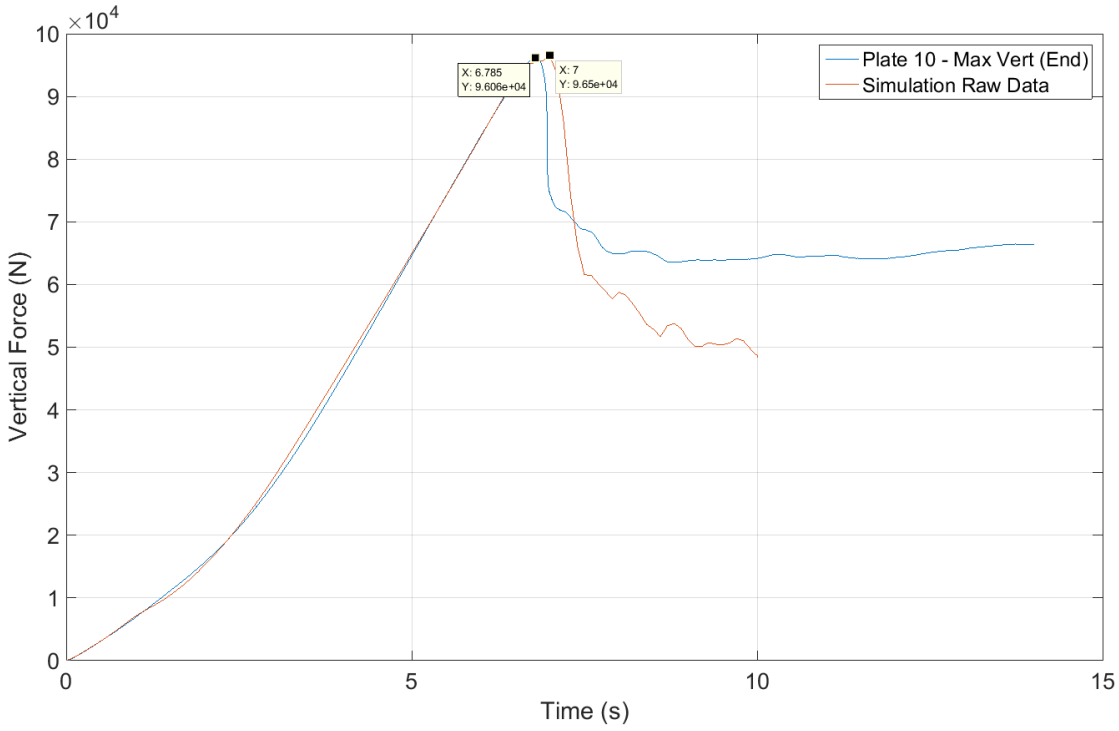

Figure 5.7: Vertical Force vs Time for Stationary Numerical and Experimental Tests

From the Figure 5.7, good agreement with the experimental data for the elastic, plastic, fracture force and relatively close time of fracture were achieved. The numerical simulation achieved a maximum force of 96.5 kN, while the experimental tests 96.06 kN, for a difference of 0.4%. While this is extremely small, it should be noted that the time of fracture was slightly different, with a numerical time of 7s and an experimental time of 6.785s. This can be explained by how fracture is treated by LS-DYNA. As each of the through thickness control points reach their fracture capacity, they simply stop supporting any load which is a downfall of how fracture is treated in numerical simulations and should be further investigated. Similarly, the post fracture behaviour is completely erratic and not in agreement with the experimental data. This is due to the treatment of element failure used

in simulation where the element is simply deleted upon the average effective plastic strain to fracture through all the control points reaching the defined fracture strain. Various post necking formulations exist to correct for this, however their use is outside the scope of this work.

5.2.2 Moving Cutting Indenter Results

The moving load tests were completed using the calibrated tangent modulus and fracture strain from the vertical stationary testing. These tests were completed through applying the vertical and horizontal displacements obtained directly from the experimental tests at 2048 Hz. It should be noted, that both the displacement defined motion and force control generated identical results and as such are not presented in this thesis. It's very likely that this is an abundance of data and unnecessary, however there was no real time penalty for implementing this and ensures that any extremely fine changes which influenced fracture were characterized in the numerical experiments. The results of the numerical test can be seen in Figure 5., 5.9 and 5.10 below. Note that in Figure 5.8, the data tip indicates the point at which horizontal translation begins for both experimental and numerical tests. In Figure 5.9, the data tip indicates the point which the material failed for both the experimental test visually, while for the numerical results it indicates the point of defined failure for the simulation. This point occurs when the average strain through all 5 through thickness integration points reaches the defined *effective plastic strain to fracture.* The actual point where the material begins to stop supporting further loading occurs at the first plateau after horizontal translation, at a horizontal location of approximately -540mm. Further, fracture occurred in the model when the effective plastic strain of the through thickness integration

points reached the defined fracture strain. With respect to this work, five integration points were used with a fracture strain of 0.243. Upon, reaching this strain, the element is deleted which means that post fracture behaviour is very poor. Further, as each of the through thickness integration points reach the defined fracture strain, they stop supporting vertical force and thus result in a reduced measured vertical capacity in the plate specimen. This is the cause of the decreasing, "piecewise" type vertical response seen in Figure 5.9 and Figure 5.10, i.e. as each of the integration points fail, the element's ability to resist vertical/horizontal force decreases. This is much different than the actual behaviour observed during experimental testing.

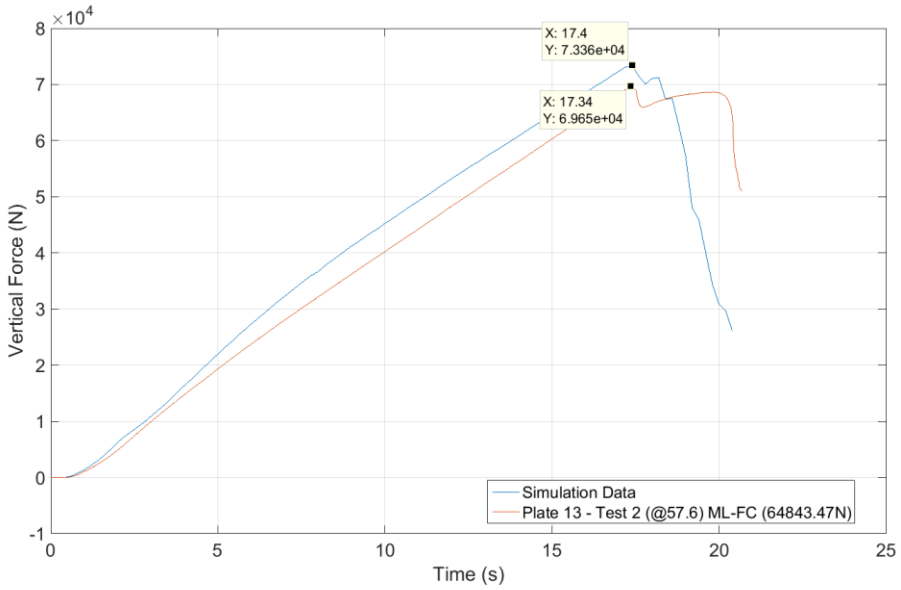

Figure 5.8: Vertical Force vs Time for Numerical and Experimental Tests

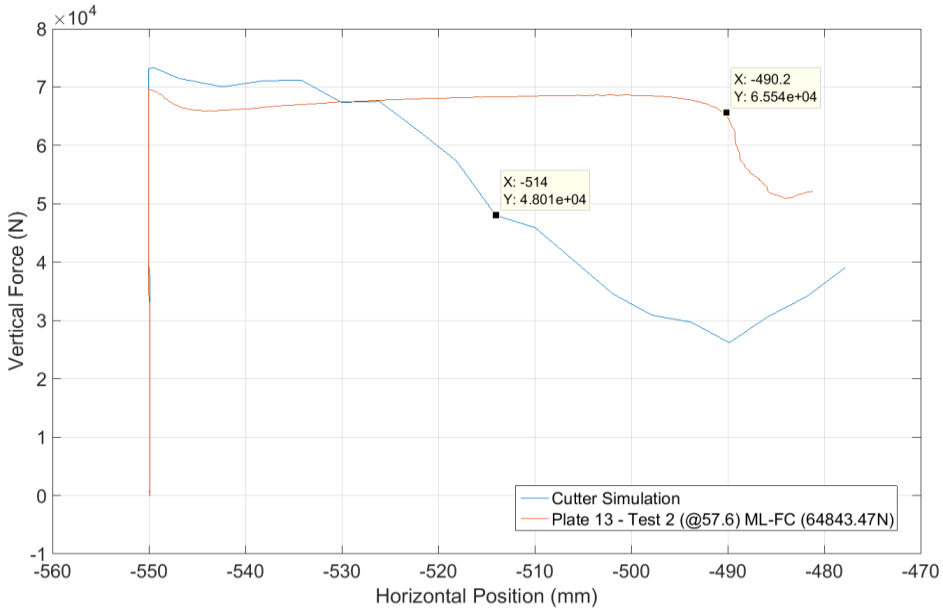

Figure 5.9: Vertical Force vs Horizontal Position for Numerical and Experimental Tests

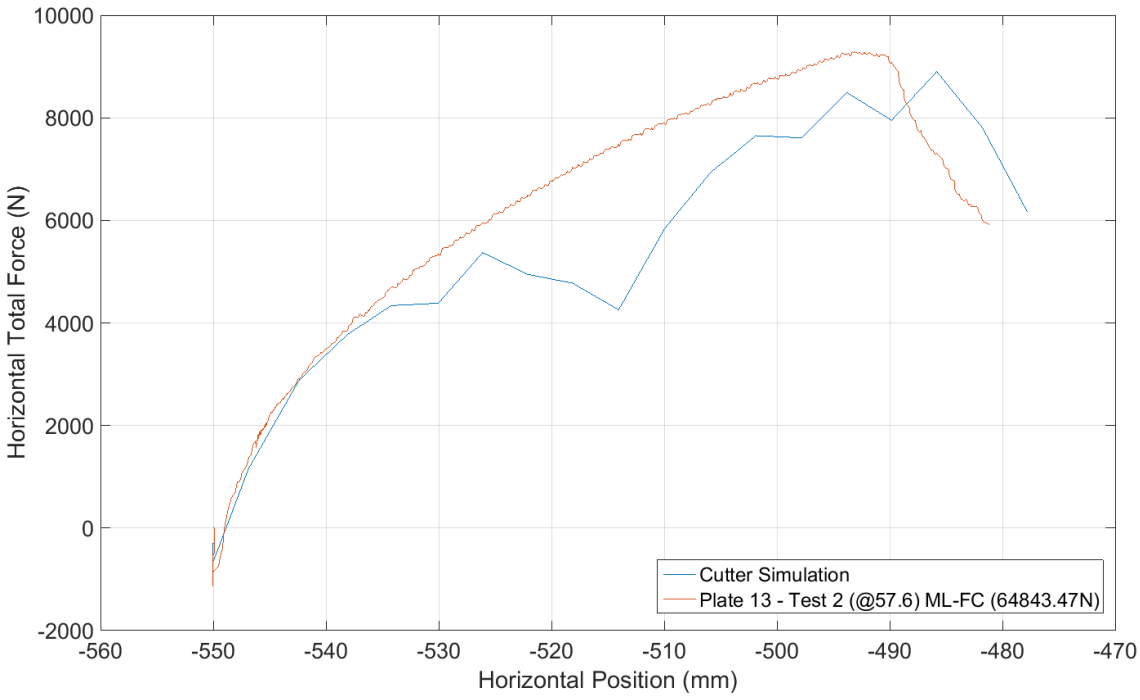

Figure 5.10: Horizontal Force vs Horizontal Position for Numerical and Experimental Tests

From Figure 5.8 the agreement with the experimental data is clearly worse than the results from stationary testing. For the vertical indentation portion of the test, the difference in peak vertical force is approximately 5% when compared to the experimental result (7.336 kN and 6.9 kN for numerical and experimental respectively). This difference is not large, however is significantly larger then difference in stationary capacity in the calibration test above. This may suggest that the plate specimen used for both the calibration test and Test 13-2 were prepared from separate batches and thus slightly different material properties.

From Figure 5.9, the simulation accurately predicts the response until horizontal translation begins. After this, the quality of results severely diminishes, with a large discrepancy in results between the simulation and actual experimental results at the expected point of fracture. However, fracture is predicted to occur during the horizontal translation phase. Despite the inability to predict the horizontal point of failure, the numerical simulation clearly shows that fracture occurs at a lower force capacity than the stationary loading. From Figure 5.10, a similar trend is observed, however, the differences between the data sets is much less than that of the vertical force plot.

Despite the differences, the results show that the numerical simulation does in fact predict fracture during the moving load portion of the test, despite the simplicity of the element fracture implemented in the model. This is not unexpected as the situation generated by the cutting wheel is very close to pure shear with minimal bending, regardless of whether the cutting wheel is stationary or moving (rolling). From (Bai, Teng, and Wierzbicki 2009), the pure shear corresponds a triaxiality and Lode Angle parameter of 0, which is logical considering the singular value of *effective plastic strain to fracture* used in analysis.

However, the analysis predicted fracture at a horizontal displacement of 36mm in comparison to the experimental result of 59.8mm found during laboratory testing. This is best seen in Figure 5.9, where the vertical capacity in the experimental data stays relatively constant until fracture occurs, while the vertical capacity decreases steadily until visual fracture occurs in the simulation. This can be explained due to the nature of the onset of fracture. In the experimental tests, fracture occurs due to a random, microscopic material defect along the length of the plate, while in comparison the plate sample is perfect uniform for the numerical simulation. Further, there is a minimal amount of bending due to the cutting wheel which makes the loading not strictly pure shear and thus shows the limitation of the *effective plastic strain to fracture* method and the necessity of including triaxiality and Lode Angle parameter in analysis of any loadings or collisions which don't exhibit pure shear.

5.2.3 Validity of Multiple Tests on One Plate Sample

To show the validity of the assumption made during experimental testing about multiple tests on a plate specimen for the cutting wheel, the displacement and therefore deformation of the plate was measured at four horizontal locations along the plate (-550, -200, 200, 550) before and after each test. Doing so allowed for the justified assumption that no plastic damage had occurred. It is possible to further confirm this assumption, using the vertical stationary numerical model and the Von-Mises stress incited throughout the plate. This can be seen in Figure 5.11.

.

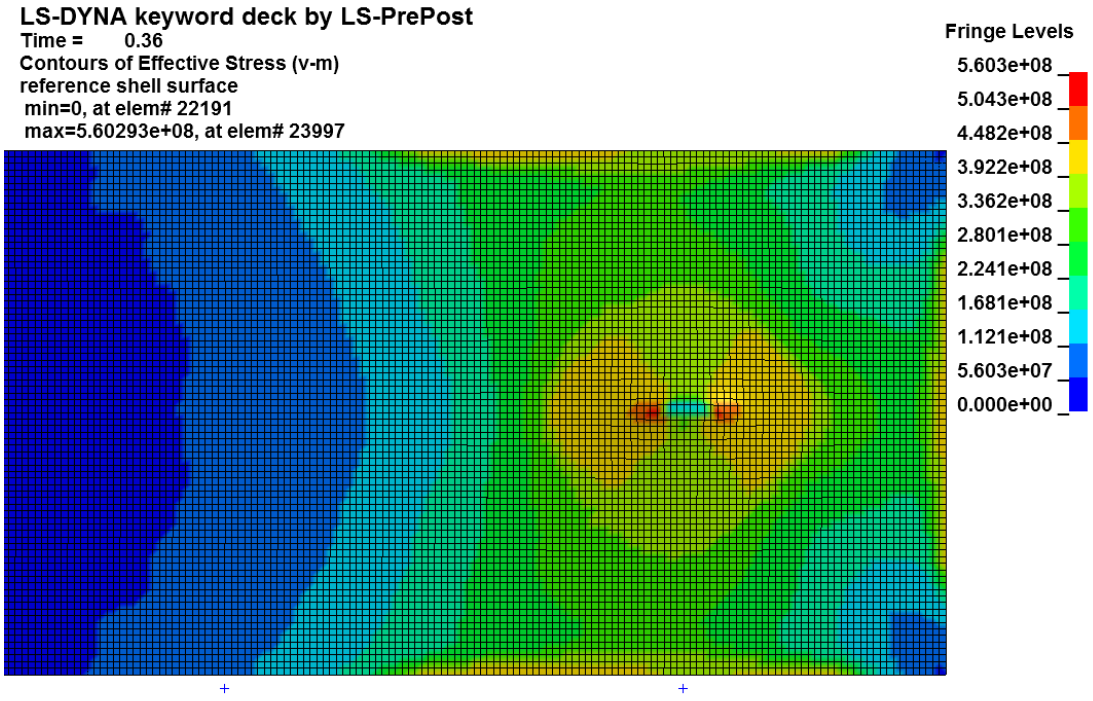

Figure 5.11: Von-Mises Stress for Vertical Stationary Cutting Wheel Test

From Figure 5.11, the non-trivial region of Von-Mises stress can be seen along with several reference points. From left to right, the first reference point is located at a horizontal location of -200mm, while the second at -550mm, both measured from the center of the plate. The Von-Mises stress at the -200m point is at maximum 121 MPa, which is well below the yield limit given by the material sheet at 374 MPa and 422 MPa for bill 1 and 2 respectively. In fact the only large deformations are extremely local to the indenter or along the horizontal edges of the plate sample.

5.2.4 Comparison of Moving and Stationary Tests

Through the use of numerical models, it is possible to observe the potential influence of triaxiality and Lode Angle parameter on the moving load effect by comparing the response during a moving load test and a corresponding vertical force during a stationary test. For

the purposes of this thesis, the vertical force at the step before the onset of fracture was observed to be 5.74 kN. Figure 5.12 and Figure 5.13 show the triaxiality at corresponding forces, while Figure 5.14 and Figure 5.15 show Lode Angle parameter at the same vertical force.

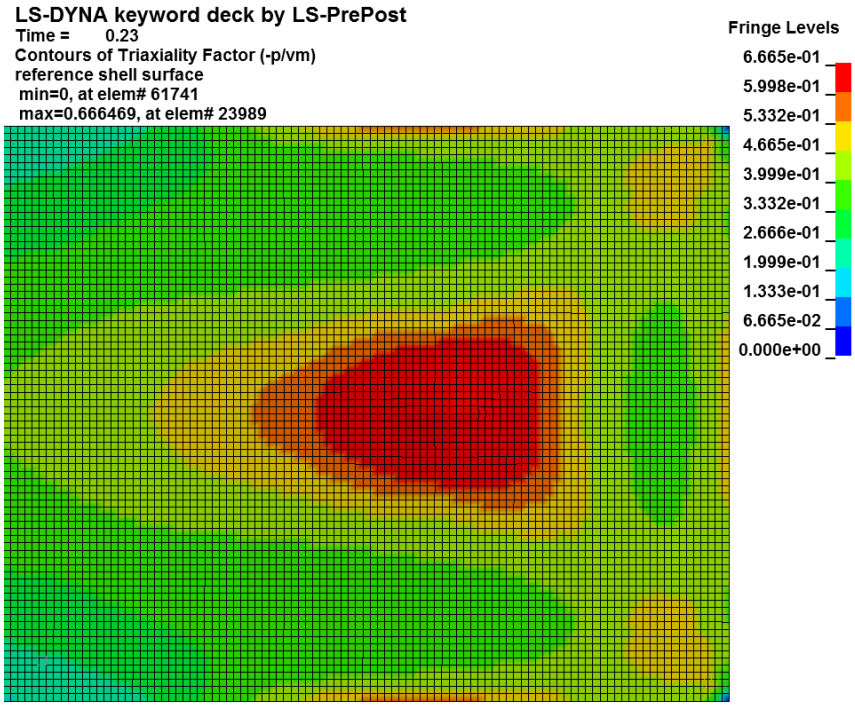

Figure 5.12: Triaxiality at 5.74 kN Vertical Force for Stationary Simulation

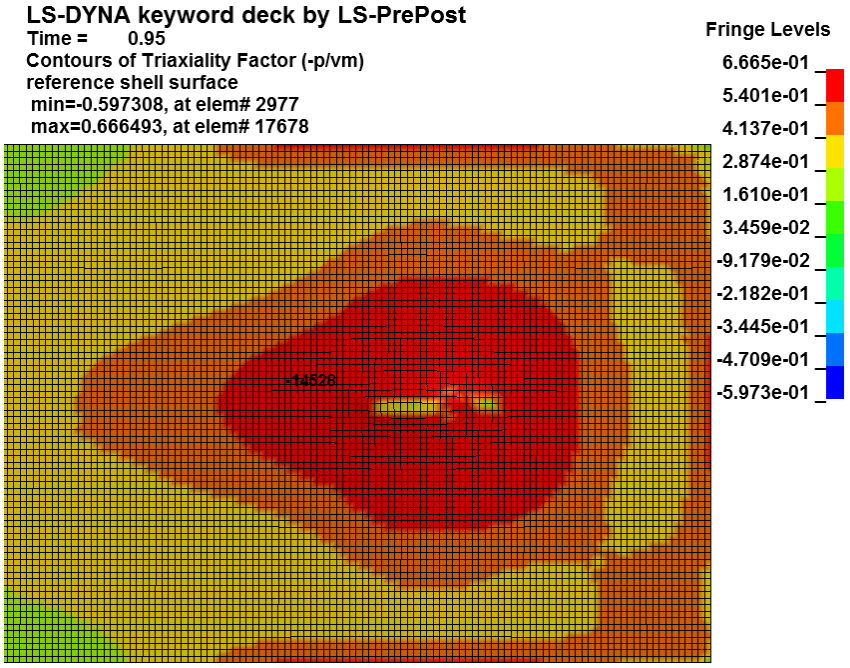

Figure 5.13: Triaxiality at 5.74 kN Vertical Force for Moving Simulation

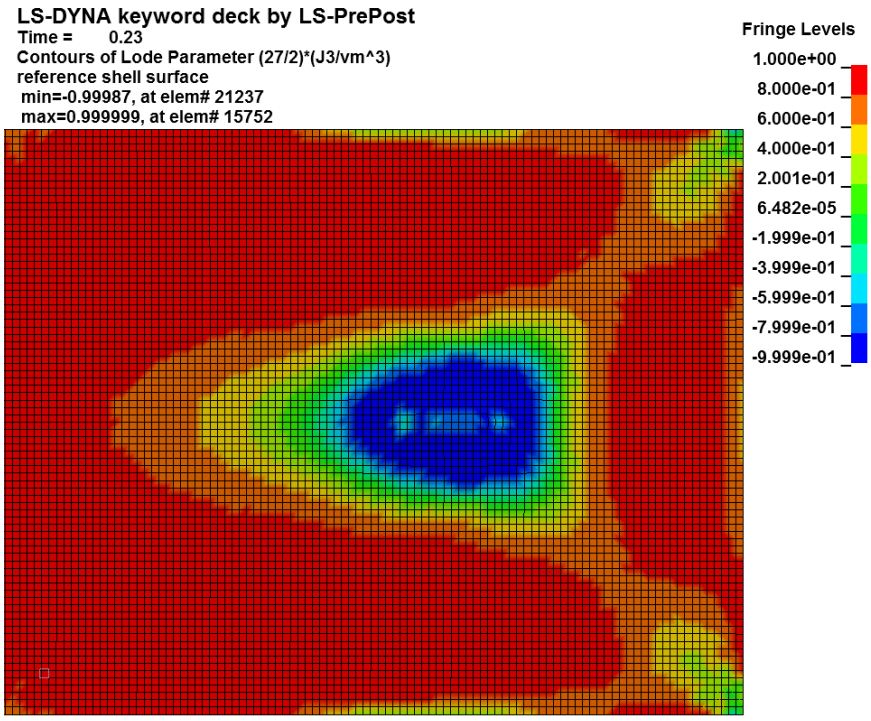

Figure 5.14: Lode Angle Parameter at 5.74 kN Vertical Force for Stationary Simulation

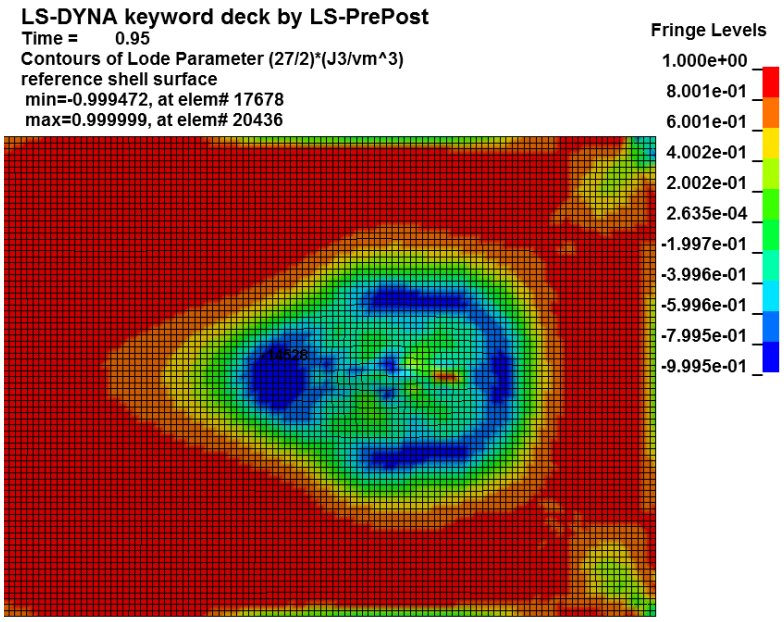

Figure 5.15: Lode Angle Parameter at 5.74 kN Vertical Force for Moving Simulation

Figure 5.13 shows a very different behaviour with respect to triaxiality. For the stationary test a zone around the indenter wheel with high triaxiality (2/3) is seen. This corresponds to a region of tension as shown in (Bai and Wierzbicki 2008). In this region there is no influence of the edge conditions from the indenter. The moving test shows similar behaviour in the region surrounding the indenter, however, the zone of high triaxiality is larger than that of that of the stationary test. Additionally, a zone of intermediate triaxiality (0.3) can be observed at the edge, with a value of ~0 found in one singular element at the peak of the indenter. Also of note is a small trailing region of high triaxiality separating the intermediate region caused by the indenter. This can be seen in Figure 5.16, which has the same fringe scale as Figure 5.13 above. From this, it appears that a slight tension is occurring on the trailing edge of the indenter.

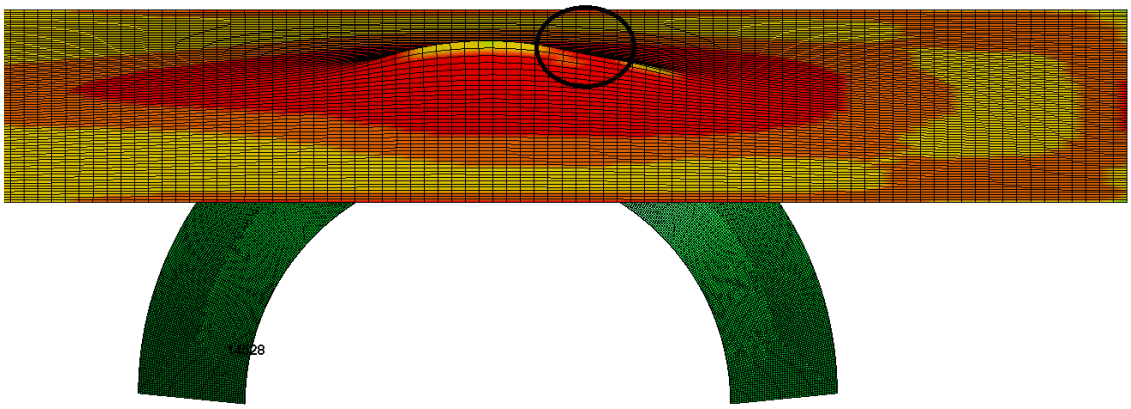

Figure 5.16: Compression on the Trailing Edge of Indenter

Similar to the observed behaviour regarding triaxiality, the resulting Lode Angle parameter is significantly different for both the stationary and moving tests as seen in Figure 5.14 and Figure 5.15. For the stationary simulation, there is a region of low (-1) Lode Angle Parameter surrounds the indenter with a small, moderately low (ranging from -0.6 to -0.8) region at the peak of the cutting wheel. The behaviour at the peak of the indenter is of particular interest, with a region of Lode Angle Parameter equal to -0.6 at the leading and trailing edge of the indenter wheel, while at the absolute peak having a value of -0.8. For the moving load test, the pattern is much more complicated. The low region (Lode Angle Parameter =-1) is significantly smaller, however encircles the majority of the indenter wheel as well as forming a small local low region at the leading edge. Moderate values (~0) can be seen in a symmetrical pattern about the majority of the indenter. The pattern shows the local stress state as the cutting wheel traverses through the plate sample. Finally, a high (~1) local region at the trailing point of contact of the indenter is seen, at the same location as the local high triaxiality region seen in Figure 5.13. The region about the indenter are described in Table 5.3 by combining the two parameters.

Table 5.3: Load States Observed During a Moving Load

Label	Triaxiality	Load Angle Parameter	Stress State
A	0.3	0	Plain strain & generalized shear
B	0	-0.2	Generalized Shear
C	0.3	1	Uniaxial tension
D	0.66	0	Plastic plane strain tension
E	0.66	-0.2	Combined tension and shear
F	0.66	-0.8 to -1	Equibiaxial tension

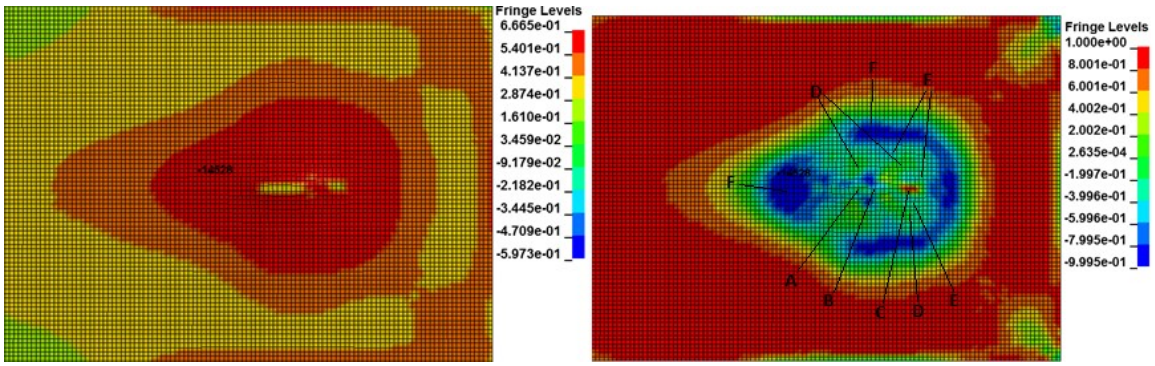

Figure 5.17: Triaxiality (Left) and Lode Angle Parameter (Right) for Moving Load Case

From the analysis, the stress state and thus Lode Angle parameter and triaxiality are clearly different for similar force responses for a moving load and stationary indentation case, however for the cutting wheel, fracture occurs at a point which is mostly under shear with a small bending (compression) component. Additionally, it can be seen that the horizontal motion causes a region of high triaxiality and Lode Angle parameter at the trailing edge as well as a region of low Lode Angle parameter at the leading edge (in a roughly constant triaxial region). This results in good agreement with the experimental results as the plastic strain at ~0 triaxiality and Lode Angle is a local minimum, and this minimum is reached at the ~0 region before the surrounding elements which are under a different stress state.

5.3 Rolling Indenter Numerical Test Results

The rolling indenter test specimen that was selected was Test 6, which exhibited fracture in a relatively short time as compared to the other tests, thus a reduced solution time. Further, the unfinished vertical stationary test was also modelled as to determine at what vertical displacement necessary to induce stationary fracture. Two non-calibration tests were completed. This section details the results of these tests.

5.3.1 Rolling Wheel Moving Indenter Results

A rolling wheel, moving load simulation was completed to compare to the experimental results as to determine the applicability of standard fracture finite element methodology for moving loads. This was completed by preparing a model identical to that of the most favorable of the experimental tests, Test 6. In this test, a plate specimen was loaded to 69mm, using vertical displacement control and translated ~450mm before fracturing.

To compare, the numerical model was prepared using the full experimental vertical and horizontal displacement loading curves, which was sampled at a rate of 2048Hz. Again, the test duration was scaled to 1/20 that of the actual experimental test as strain rate effects were not implemented in the numerical model. Additionally, as mentioned above, the k value was adjusted for forces on the scale of magnitude experienced during the roll wheel tests, based on the numerical test calibrations completed by Quinton (2015). Similar to the cutting wheel simulations, the post yield, pre-fracture behaviour was matched with the experimental results by varying the tangent modulus (690 MPa) until acceptance was achieved. Following this, the *effective plastic strain to fracture* of 0.243 found in the cutting wheel tests was used. The choice to use the calibrated *effective plastic strain to fracture* for

cutting wheel implies that the rolling wheel used in the same manner will also result in a number of incited stress states including that of nearly pure shear. It is hypothesised that if fracture can be adequately modelled while omitting triaxiality and Lode Angle Parameter then plate fracture for the following simulations should be well predicted. The results of the numerical test can be seen in Figure 5.18 and Figure 5.19.

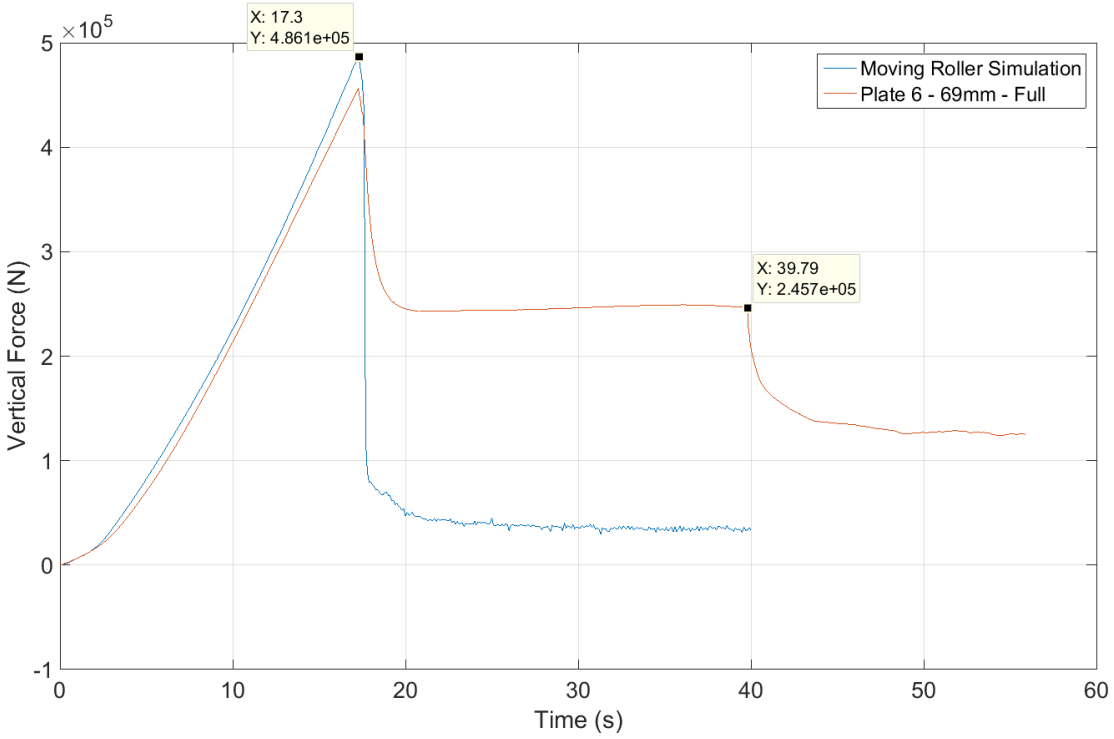

Figure 5.18: Vertical Force vs Time for Numerical and Experimental Tests

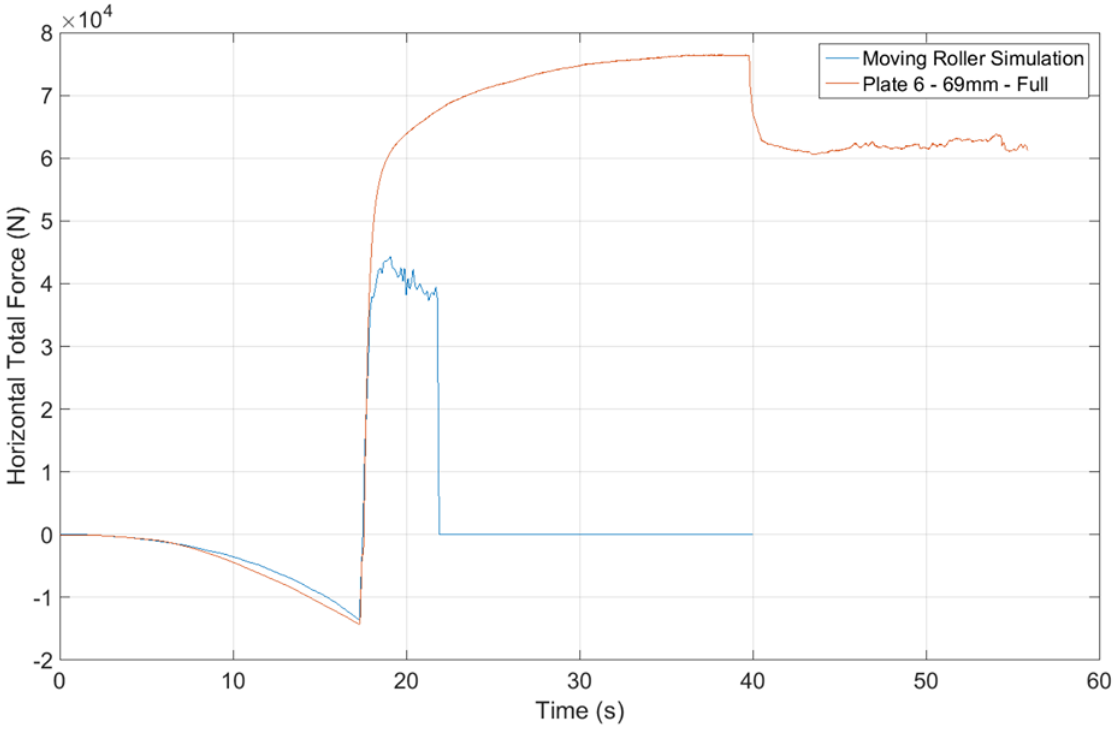

Figure 5.19: Horizontal Total Force vs Time for Numerical and Experimental Tests

From Figure 5.18 the force at fracture is overpredicted by the numerical test slightly, with good agreement during the plastic loading section of the test. However, more notably is how and when fracture occurs in the numerical model. In the experimental tests, some horizontal travel occurred in every rolling wheel test before fracture. However, in the numerical test, the sample fracture immediately upon horizontal translation, at a significantly higher vertical force.

The similar force profiles for the plastic damage section of loading suggests that the tangent modulus and boundary compliance are adequately calibrated, however, it should be noted that this was a difficult process. This could be more effectively achieved through the implementation of some analysis of variance (ANOVA) of the relevant factors (tangent

modulus, fracture strain) to create some sort of statistical model. Also of note is the greatly reduced horizontal response in the numerical test in comparison to the experimental result, seen in Figure 5.19.

Figure 5.20, which displays the first frame of element failure, which is simply when the *effective plastic strain* through all five integration points reaches the defined *effective fracture strain*. The failure occurs at the peak displacement of the plate, or the centerline of the indenter first, and then propagates diagonally at 45° to the outside edges of the indenter. This suggests that the plate failed due to exhaustion of tensile strength in the model as the elements were effectively pulled apart in the z-axis (i.e. the width of the plate). In the experimental results, drastically different behaviour was observed, which can be seen in Figure 5.21. Here, it is obvious that the plate fractures at the right side of the indenter, which is then propagated in a steady manner by the edge of the indenter, suggesting that the plate failed due to some combination of shear and tension. This aligns with the initial belief that the moving load effect incites changing values is simply a manipulation of triaxiality and Lode Angle Parameter and indicates that the inclusion of these two parameters could increase the accuracy of numerical prediction of fracture for horizontally translating loads. Finally, this shows that the current methodologies are inadequate to predict fracture due to moving loads.

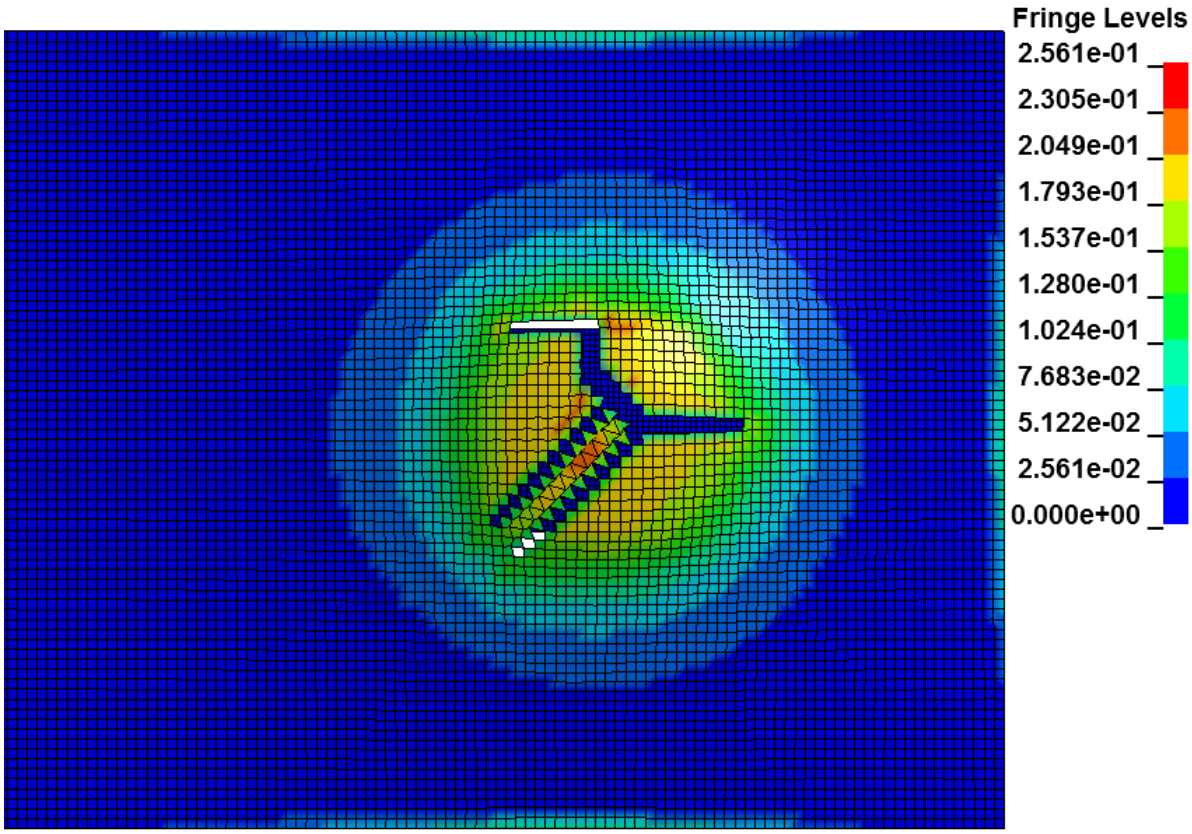

Figure 5.20: Numerical Fracture Propagation (Effective Plastic Strain Gradient). Note: Direction of indenter travel is to the left

Figure 5.21: Experimental Fracture Propagation. Note: Direction of indenter travel is down

The difference in fracture modes can be explained through the exclusion of Lode Angle parameter and triaxiality. The values of these parameters are presented in the timestep before failure and can be seen in Figure 5.22 below.

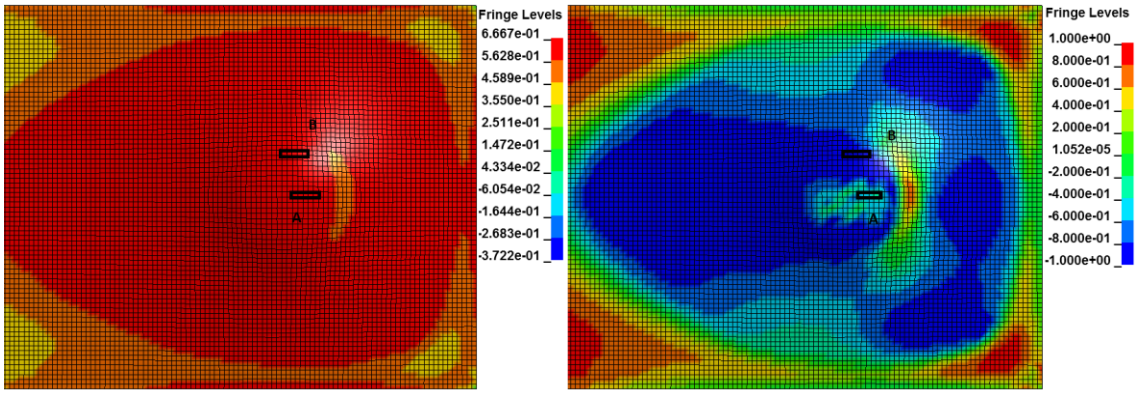

Figure 5.22: Triaxiality (Left) and Lode Angle Parameter (Right) for Rolling Wheel Moving Load, Note: Direction of travel is left

In Figure 5.22, it can be seen that where the failure occurs (section A, along the center line of the indenter wheel) is a region of high (2/3) triaxiality and approximately constant Lode Angle parameter (-0.2 to -0.4). Together, these parameters detail a complicated stress state of at the point of fracture in the numerical experiment, with large contributions due to bending. In comparison to the where fracture occurred in the laboratory experiments, (section B) experienced a range of triaxiality 2/3 and Lode Angle parameter of ~ -1. From the observed results during experimental testing, it is believed that fracture occurred at the peak of the indenter at the full width, occurring due to the shear edge of the indenter wheel in combination with a heavy bending. The large discrepancy is an inherent flaw in the *effective plastic strain to fracture* method, as the elements that are under heavy bending should fail at a relatively high effective strain (Bai and Wierzbicki 2008) as compared to a

stress state of pure shear. It should also be noted that highlighting the physical location of fracture, even with video, is extremely challenging, and future work in the area should incorporate some form of local strain measurement, or even a painted grid system with multiple internal cameras to ensure the location of fracture.

It should also be noted that the state of stress incited in the numerical specimen at the point of fracture displayed in the laboratory (region B) is not an accurate. Fracture in the lab was witnessed to be incited by the combination of a large amount of bending in conjunction with the shear edge of the indenter, however, the state of stress given from the model is equibiaxial tension. This behaviour is function of the shell element size of the plate. The elements are as small as possible to be valid for shell elements in numerical models (thickness ~ edge length), however, is still relatively coarse in comparison to microscopic defects in actual steel, where fracture originates. Additionally, the indenter wheel edge is along element and not at an edge. As that element is strained from both the vertical and horizontal displacement, it incites the state of equibiaxial tension seen in the numerical model. This can be thought of like a small plate with a patch load starting at the center to one side of the plate. Further, as the element reaches the defined *effective plastic strain to fracture* they are simply deleted. In actuality, the patch load is a singular force at every point and instead forms a crack that aligns with the indenter wheel. Possible solutions were outside the scope of this thesis, however include solid modelling of the plate sample (thus increasing run time drastically) to allow for a finer mesh, some sort of fracture propagation modelling for shell elements, or extremely careful selection of mesh size based on contact

area. Overall, the behaviour suggests that for moving loads which incite fracture due to stress states that are not generalized shear, shell elements may not be valid for thin plates.

5.3.2 Vertical Stationary Results

The vertical stationary results used the fracture strain determined via the known fracture point of the vertical, stationary cutting indenter tests elaborated below. It should be noted as the experimental results did not reach fracture, the exact load curve could be not be used. Therefore, a simplified linear curve was defined. As strain rate effects were omitted from analysis, the overall test length was scaled by 20 (i.e. the displacement was applied 20 times faster then the actual tests were performed) as to reduce the cumulative CPU round-off error in longer explicit tests and to reduce run time. The results can be seen in Figure 5.23.

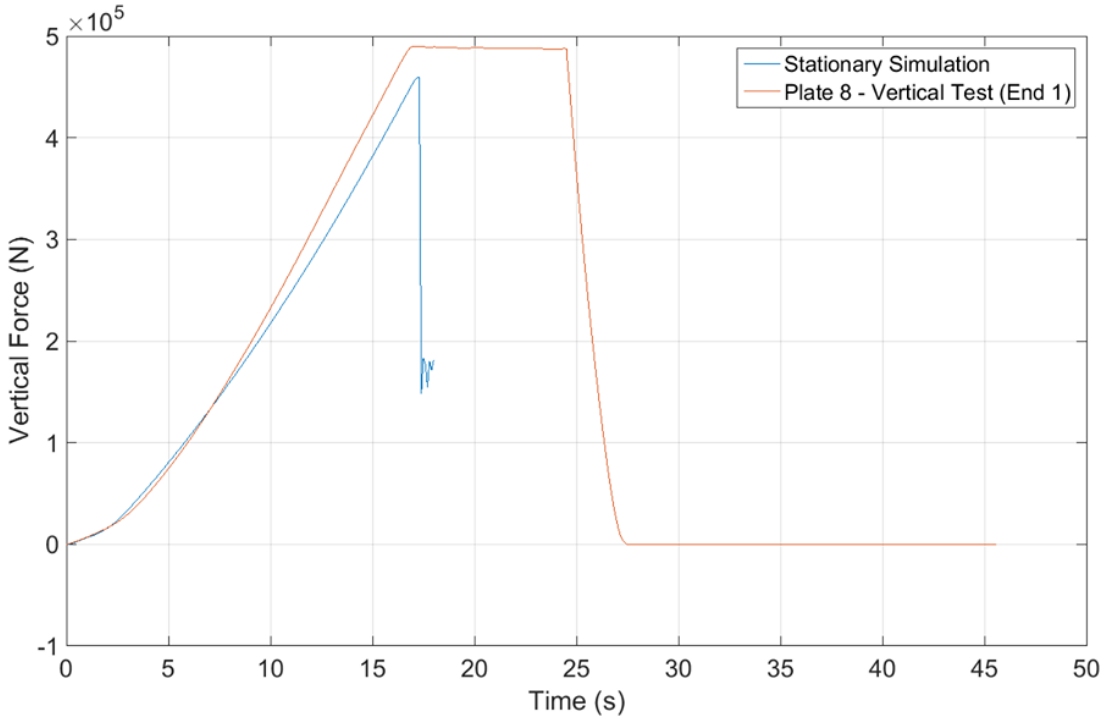

Figure 5.23: Vertical Force vs Time for Experimental and Simulation Results

From Figure 5.23, the results for the simulation show a significantly different result then the experimental testing. Primarily, fracture occurred in the stationary simulation for the rolling wheel, at a relatively lower force and displacement whereas the experimental test resulted in no fracture.

5.3.2.1 The Calibration Method and Indenter Type

As displayed in the sections above, a clear discrepancy arises between numerical and experimental results for the rolling wheel tests despite excellent agreement with the vertical, stationary calibration test with the cutting wheel. This is an expected result and clear deficiency of using a singular *effective plastic strain to fracture* value to predict fracture for various types of collisions. Clearly, the two indenters possess significantly different geometry and therefore incite significantly different stress states. From the drastically different results, it can be said that the behaviour both during plastic level damages and at failure is dependent on more than a single strain value. From the work of Bai, Teng and Wierzbicki (2009) these factors include Lode Angle parameter and triaxiality. As such the triaxiality and Lode Angle parameter were compared for both numerical stationary tests which resulted in fracture. This can be seen in Figure 5.24, Figure 5.25 for triaxiality and Figure 5.26, 5.27 for Lode Angle Parameter.

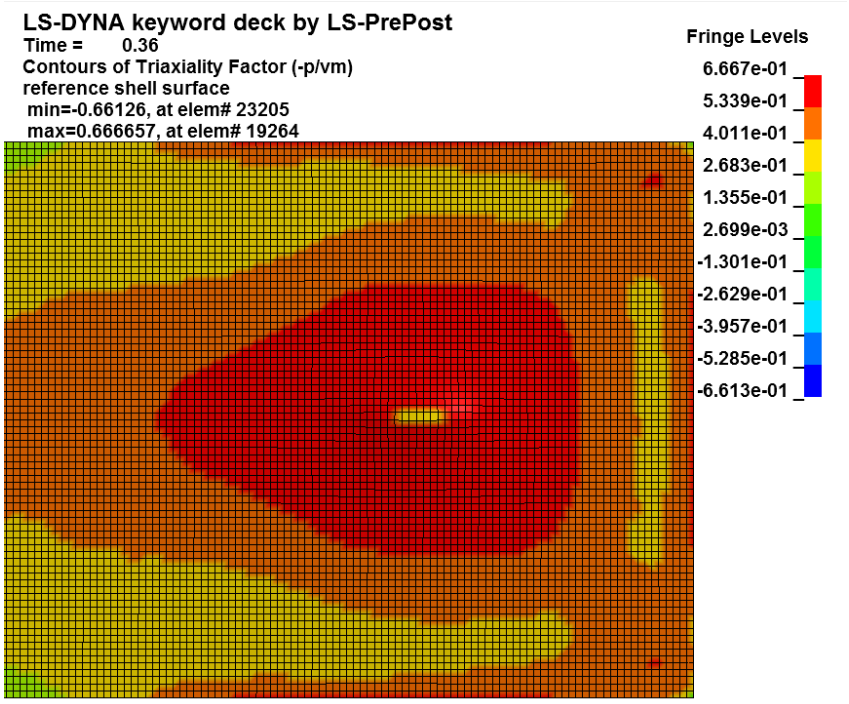

Figure 5.24: Triaxiality for Stationary Cutting Wheel Simulation at Onset of Fracture

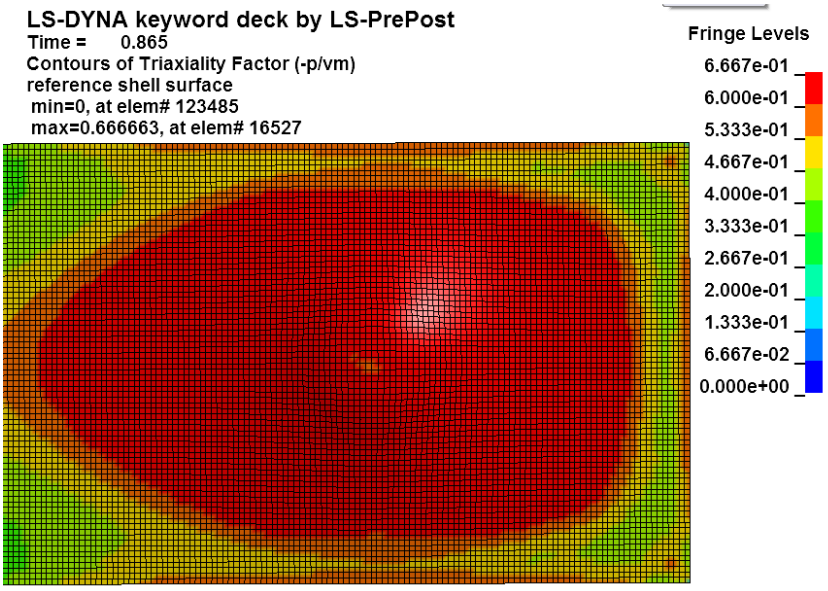

Figure 5.25: Triaxiality for Rolling Wheel Simulation at Onset of Fracture

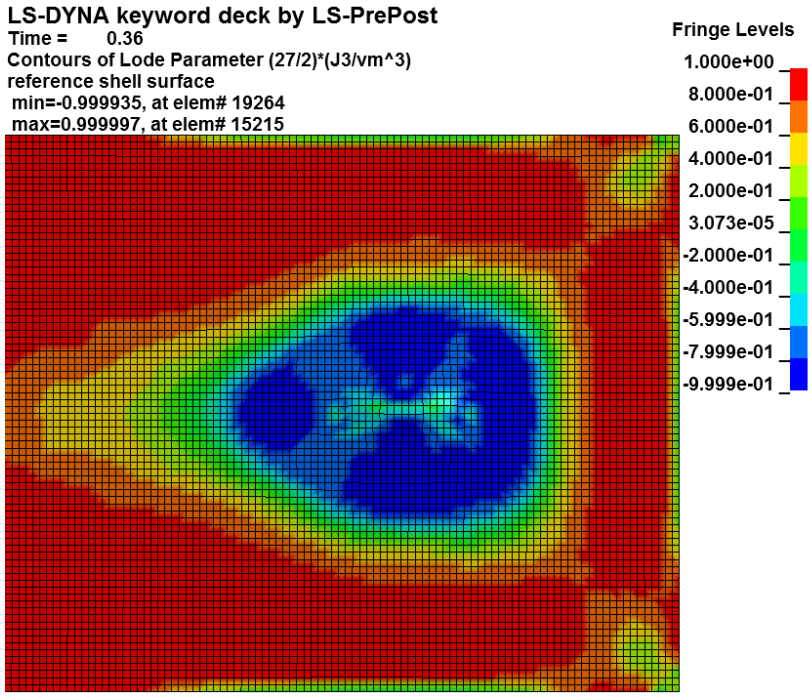

Figure 5.26: Lode Angle Parameter for Cutting Wheel at Onset of Fracture

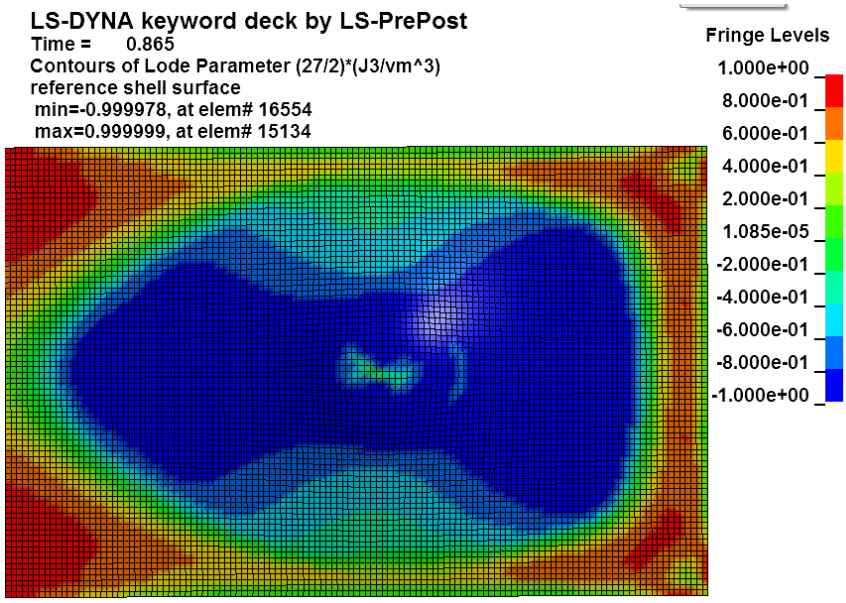

Figure 5.27: Lode Angle Parameter for Rolling Wheel at Onset of Fracture

Figure 5.24 and Figure 5.25 show very different behaviour in the triaxialities at the point of fracture for both indenters. For the cutting wheel, a small, local low region is generated

at by the smaller edge of the indenter, while the majority remains a constant region equal to 2/3 all around. The rolling wheel shows just a constant area of 0.5-2/3 in a similar pattern as the cutting wheel around the indenter due the lack of small edge. Further, the pattern of triaxiality equal to 2/3 is much larger for the rolling indenter.

Similarly, Figure 5.26 and Figure 5.27 show different behaviour at fracture for the cutting and rolling wheel respectively. The difference between the observed Lode Angle parameter contours are similar to that seen for triaxiality, with the edge of the cutting wheel causing a small local high region, centered in a large region with a value of -1. The rolling wheel on the other hand has a larger region of Lode Angle parameter of -1 with a small region of ~0 centered about the peak of the indenter where fracture occurs.

When combining these two parameters, the cutting wheel fractures clearly due to shear, as expected by the sharp peak. Contrary to this, the rolling wheel apparently fails numerical in a state of plane strain.

Chapter 6 Recommendations & Conclusions

6.1 Conclusions

In this thesis, moving loads were shown to have a clear influence on the initiation of fracture for steel plate samples through experimental testing. Contributions on moving load effect due to other factors including the vertical indentation depth, start location (boundary condition) and indenter shape were also analyzed. Due to various difficulties, contributions due to horizontal translation speed were not identified. Following this, the secondary goal of this work was met; preparing and comparing a numerical model to corresponding experimental data. Here it was shown that the use of the *effective plastic strain to fracture* method is insufficient to capture the behaviour at fracture during a moving load event for both indenter types. Further, the difficulties in preparing a model were shown through using material steel bills from manufacturers. Models were prepared in two distinct methods; using the calibration and scaling techniques, however both required significant change to the tangent modulus and plastic strain to comply with the observed experimental results.

In addition to the two main objectives of this work, several other conclusions can be made as to the nature of moving loads, particularly for the plate samples in the MLA experimental setup and numerical modelling using the *effective plastic strain to fracture* method. These are as follows:

- Minimum indentation to fracture during a moving load for the rolling wheel was found to be ~6.9cm, which is significantly lower then a stationary load (undetermined due to reaching the limit of the load cell). The cutting wheel test

was found to not exhibit a lower minimum indentation to fracture and instead was loaded with force control to show the moving load effect. This shows that the geometry of the indenter (and thus stress state incited) has a clear impact on the reduction of vertical displacement capacity observed. Further, it can be said that this reduction in vertical displacement capacity is related to the increased bending found during the rolling wheel tests.

- For the rolling wheel, the maximum reduction in vertical force capacity was found to be in excess of 54% when compared to the maximum achieved vertical stationary force. It was impossible to quantify the maximum stationary vertical force capacity for the rolling wheel and selected plate thickness with the current MLA.
- For the cutting wheel, the maximum reduction in vertical force capacity was found to be 43.6% when compared to stationary vertical force capacity. Additionally, the reduction in vertical force capacity correlated with an increased displacement at fracture.
- The horizontal start position, or influence of the boundaries of the carriage were found to have negligible impact on fracture during a moving load effect for both the rolling and cutting wheel tests for the levels of vertical indentation tested.
- The elastic and small plastic deformation behaviour was observed over nine experimental tests for the rolling wheel. The tests showed that the moving load effect for loadings inciting this level of damage was small or non existent.

- Numerically, an *effective plastic strain to fracture* accurately captures the behaviour of a stationary vertical when compared to the experimental results.
- Using a singular *effective plastic strain to fracture* can effectively simulate any constant stress state, for example the moving load induced by horizontally translating the cutting wheel.
- Using a singular *effective plastic strain to fracture* cannot adequately model a moving load where the stress state changes. For example, the moving load induced by horizontally translating the rolling wheel resulted in a variable state of stress where fracture is possible in any of the induced states of stress.
- Calibration of an *effective plastic strain to fracture* is extremely sensitive to mesh size. Additionally, capturing complicated stress states of combined bending and shear is extremely difficult numerically, potentially possible with shell elements.
- The stress state and therefore Lode Angle parameter and triaxiality are drastically different for stationary loads with different indenter type at fracture.
- The stress state and therefore Lode Angle parameter and triaxiality are drastically different for both moving and stationary loads causing the same vertical force induced by the same indenter. An extreme amount of variation and complication in the behaviour of the plate sample with respect to Lode Angle in particular can be seen in comparison.

6.2 Recommendations for Future Work

There is a significant amount of potential further work necessary to further the understanding of fracture during a moving load event and to accurately model an event resulting in fracture. These topics include:

- The influence of strain rate, temperature, steel type, steel thickness was not observed due to impracticalities or issues in setup. As much study of fracture for A36 and DH36 steel exists, temperature and thickness for these types are particularly relevant for study.
- During testing, the plate samples from two different batches were mixed creating difficulties when numerically modelling. If it all possible, the samples should be prepared from the same batch and if not carefully tracked during experimental testing.
- The *effective plastic strain to fracture* method was used to develop models which were compared to the experimental work. It is clear that this is insufficient to model moving loads. A more sophisticated failure and damage model should be investigated for moving loads which incite fracture, with particular focus on Lode Angle and triaxiality dependence.
- The numerical models were prepared using the calibration method. Future work should include some form of local material testing to eliminate or reduce the amount of sequential change in order to achieve agreement with experimental results. In lieu of this, a statistical based design of experiment should be performed to determine the relevant parameters. For the *effective plastic strain to*

fracture method, the tangent modulus, *effective plastic strain to fracture* (calibration), yield stress and spring constant k of the apparatus, are the likely relevant parameters. Through the omission of yield stress which has a relatively low range, a response surface could be generated in as little as 15 runs.

- No attempt was made to observe mesh convergence for the numerical studies due to the inherent relationship between *effective fracture strain* and element size. To mitigate this issue, an extremely fine mesh was used, while still being valid for shell element analysis. This is a nontrivial problem when studying fracture, however, significant time and effort would be saved through the completion of material testing. Further, testing multiple same sizes to allow for the use of Barba's Law (Davis and ProQuest (Firm) 2004) would be effective for implementation of the *effective plastic strain to fracture* method. This issue is significantly complicated for more sophisticated damage models including triaxiality and Lode Angle Parameter dependence.
- The impact of defined contact area, the coincidence of indenter element edge & plate element edge locations (i.e. node to node contact or exceedingly close instead of near the midpoint of the element) should be investigated.

Bibliography

Akita, Yoshio, Noritaka Ando, Yuzuru Fujita, and Katsuhide Kitamura. 1972. "Studies on Collision-Protective Structures in Nuclear Powered Ships." *Nuclear Engineering and Design* 19 (2): 365-401. doi:10.1016/0029-5493(72)90137-9.

Alsos, Hagbart Skage. 2008. *Ship Grounding: Analysis of Ductile Fracture, Bottom Damage and Hull Girder Response*, edited by Norges Teknisk-Naturvitenskapelige Universitet, Fakultet for Ingeniørvitenskap Og Teknologi,Institutt for Marin Teknikk Norges teknisk-naturvitenskapelige universitet, Fakultet for ingeniørvitenskap og teknologi, Institutt for marin teknikk.

Ammerman, D. J. and J. C. Daidola. 1996. "A Comparison of Methods for Evaluating Structure during Ship Collisions." *International Conference on Designs and Methodologies for Collision and Grounding Protection of Ships, San Francisco*.

Atkins, A. G. 1996. "Fracture in Forming." *Journal of Materials Processing Tech.* 56 (1): 609-618. doi:10.1016/0924-0136(95)01875-1.

Bai, Yuanli, Xiaoqing Teng, and Tomasz Wierzbicki. 2009. "On the Application of Stress Triaxiality Formula for Plane Strain Fracture Testing." *Journal of Engineering Materials and Technology* 131 (2): 021002. doi:10.1115/1.3078390.

Bai, Yuanli and Tomasz Wierzbicki. 2008. "A New Model of Metal Plasticity and Fracture with Pressure and Lode Dependence." *International Journal of Plasticity* 24 (6): 1071-1096. doi:10.1016/j.ijplas.2007.09.004.

Bao, Yingbin and Tomasz Wierzbicki. 2004. "On Fracture Locus in the Equivalent Strain and Stress Triaxiality Space." *International Journal of Mechanical Sciences* 46 (1): 81-98. doi:10.1016/j.ijmecsci.2004.02.006.

Bardet, J. P. 1990. "Lode Dependences for Isotropic Pressure- Sensitive Elastoplastic Materials." *Journal of Applied Mechanics* 57 (3): 498. doi:10.1115/1.2897051.

Basaran, Merdan, Sven David W\olkerling, Markus Feucht, and Dieter Weichert. 2010. "An Extension of the GISSMO Damage Model Based on Lode Angle Dependence.".

Calle, Miguel Angel and Marcilio Alves. 2011. *Ship Collision: A Brief Survey*.

Cazacu, Oana, Brian Plunkett, and Frédéric Barlat. 2006. "Orthotropic Yield Criterion for Hexagonal Closed Packed Metals." *International Journal of Plasticity* 22 (7): 1171-1194. doi:10.1016/j.ijplas.2005.06.001.

Chapel Steel. "**Structural, Carbon & HSLA Steel Plate**.", accessed 05/22, 2018, https://www.chapelsteel.com/csa-g4021-50w-50a.html.

Davis, J. R. (J and ProQuest (Firm). 2004. *Tensile Testing*. 2nd ed.. ed. Materials Park, Ohio: Materials Park, Ohio : ASM International.

DRUCKER, D. C. and W. PRAGER. 1952. "Soil Mechanics and Plastic Analysis Or Limit Design." *Quarterly of Applied Mathematics* 10 (2): 157-165. http://www.jstor.org/stable/43633942.

Fossum, A. and R. Brannon. 2006. "On a Viscoplastic Model for Rocks with Mechanism-Dependent Characteristic Times." *Acta Geotechnica* 1 (2): 89-106. doi:10.1007/s11440-006-0010-z.

Frýba, Ladislav. 1972. *Vibration of Solids and Structures Under Moving Loads*. Groningen: Groningen: Noordhoff International Pub.

Gurson, A. L. 1977. "Continuum Theory of Ductile Rupture by Void Nucleation and Growth: Part I—Yield Criteria and Flow Rules for Porous Ductile Media." *Journal of Engineering Materials and Technology* 99 (1): 2. doi:10.1115/1.3443401.

HÃ¤nninen, Saara and Jorma RytkÃ¶nen. 2004. *Oil Transportation and Terminal Development in the Gulf of Finland*.

Hancock, J. W. and A. C. Mackenzie. 1976. "On the Mechanisms of Ductile Failure in High-Strength Steels Subjected to Multi-Axial Stress-States." *Journal of Mechanics Physics of Solids* 24: 147-160. doi:10.1016/0022-5096(76)90024-7. http://adsabs.harvard.edu/abs/1976JMPSo..24..147H.

Hong, Lin. 2009. *Simplified Analysis and Design of Ships Subjected to Collision and Grounding*, edited by Norges Teknisk-Naturvitenskapelige Universitet, Fakultet For Ingeniørvitenskap Og Teknologi,Institutt For Marin Teknikk Norges teknisk-naturvitenskapelige universitet, Fakultet for ingeniørvitenskap og teknologi, Institutt for marin teknikk.

Hong, Lin and Jø Amdahl. 2012. "Rapid Assessment of Ship Grounding Over Large Contact Surfaces." *Ships and Offshore Structures* 7 (1): 5. doi:10.1080/17445302.2011.579003.

Hughes, Owen F., Jeom Kee Paik, and Dominique Béghin. 2010. *Ship Structural Analysis and Design*. Jersey City, N.J.: Jersey City, N.J. : Society of Naval Architects and Marine Engineers.

Kudo, H. and K. Aoi. 1967. "Effect of Compression Test Conditions upon Fracturing of Medium Carbon Steel." *Journal of Japanese Society of Technology and Plasticity* 8.

LS-DYNA Aerospace Working Group. 2017. *AWG*MAT_224 User Guide (may 8, 2017)* LS-DYNA Aerospace Working Group.

Lu, G. and C. R. Calladine. 1990. "On the Cutting of a Plate by a Wedge." *International Journal of Mechanical Sciences* 32 (4): 293-313. doi:https://doi.org/10.1016/0020-7403(90)90095-Z. http://www.sciencedirect.com/science/article/pii/002074039090095Z.

Malcher, L. and E. N. Mamiya. 2014. "An Improved Damage Evolution Law Based on Continuum Damage Mechanics and its Dependence on both Stress Triaxiality and the Third Invariant." *International Journal of Plasticity* 56: 232-261. doi:10.1016/j.ijplas.2014.01.002.

Malvern, Lawrence E. 1969. *Introduction to the Mechanics of a Continuous Medium*. Englewood Cliffs, N.J.: Englewood Cliffs, N.J., Prentice-Hall.

Mcclintock, F. A. 1968. "A Criterion for Ductile Fracture by the Growth of Holes." *Journal of Applied Mechanics* 35 (2): 363. doi:10.1115/1.3601204.

Melia, N., K. Haines, and E. Hawkins. 2016. "Sea Ice Decline and 21st Century Trans-Arctic Shipping Routes." *Geophysical Research Letters* 43 (18): 9720-9728. doi:10.1002/2016GL069315.

Minorsky, V. U. 1959. "An Analysis of Ship Collisions with Reference to Protection of Nuclear Power Plants." *Journal of Ship Research*.

MSL, Engineering. 2000. *Collision Resistance of Ship-Shaped Structures to Side Impact*, edited by Great Britain. Health and Safety Executive. Sudbury: Sudbury : HSE Books.

Norris, D. M., J. E. Reaugh, B. Moran, and D. F. Quiñones. 1978. "A Plastic- Strain, Mean- Stress Criterion for Ductile Fracture." *Journal of Engineering Materials and Technology* 100 (3): 279. doi:10.1115/1.3443491.

Paik, Jeom Kee. 1994. "**Cutting of a Longitudinally Stiffened Plate by a Wedge**." *Journal of Ship Research* 38 (4): 340.

Paik, Jeom Kee and Preben Terndrup Pedersen. 1996. "Modelling of the Internal Mechanics in Ship Collisions." *Ocean Engineering* 23 (2): 107-142. doi:10.1016/0029-8018(95)00021-6.

Pedersen, Preben Terndrup and Shengming Zhang. 1998. *Absorbed Energy in Ship Collisions and Grounding*.

Porter, V. L. and D. J. Ammerman. 1996. "Analysis of a Ship-to-Ship Collision." *PATRAM `95: 11.International Conference on Packaging and Transportation of Radioactive Materials, Las Vegas*.

Quinton, Bruce W. T. 2015. *Experimental and Numerical Investigation of Moving Loads on Hull Structures* Memorial University of Newfoundland.

———. 2008. *Progressive Damage to a Ship's Structure due to Ice Loading* Memorial University of Newfoundland.

Racherla, V. and J. L. Bassani. 2007. "Strain Burst Phenomena in the Necking of a Sheet that Deforms by Non-Associated Plastic Flow." *Modelling and Simulation in Materials Science and Engineering* 15 (1): S297-S311. doi:10.1088/0965-0393/15/1/S23.

Rice, J. R. and D. M. Tracey. 1969. "On the Ductile Enlargement of Voids in Triaxial Stress Fieldsâˆ—." *Journal of the Mechanics and Physics of Solids* 17 (3): 201-217. doi:https://doi.org/10.1016/0022-5096(69)90033-7. http://www.sciencedirect.com/science/article/pii/0022509669900337.

Ringsberg, Jonas W., Jö Amdahl, Bai Qiao Chen, Sang-Rai Cho, Sö Ehlers, Zhiqiang Hu, Jan M. Kubiczek, et al. 2018. "MARSTRUCT Benchmark Study on Nonlinear FE Simulation of an Experiment of an Indenter Impact with a Ship Side-Shell

Structure." *Marine Structures; Marine Structures* 59: 142-157. doi:10.1016/j.marstruc.2018.01.010.

Rodd, James L. and Jermone P. Sikora. 1995. *Double Hull Grounding Experiments*. Bethesda: Naval Surface Warfare Center, Carderock Division, Department of the Navy.

Rosenblatt, M. 1975. *Tanker Structural Analysis for Minor Collisions*, edited by ROSENBLATT (M) AND SON INC,NEW YORK.

Samuelides, Manolis. 2015. "Recent Advances and Future Trends in Structural Crashworthiness of Ship Structures Subjected to Impact Loads." *Ships and Offshore Structures* 10 (5): 488. doi:10.1080/17445302.2015.1009287.

Servis, Dimitris, Aa Bb, Louka T, and Voudouris G. 2002. *Implementation of Finite-Element Codes for the Simulation of Ship-Ship Collisions*. Vol. 46.

Simonsen, Bo Cerup. 1998. "Plate Tearing by a Cone." *International Journal of Mechanical Sciences* 40 (11): 1145-1158. doi:10.1016/S0020-7403(98)00015-0.

Simonsen, Bo Cerup and Tomasz Wierzbicki. 1998. "Plasticity, Fracture and Friction in Steady-State Plate Cutting." *International Journal of Impact Engineering* 21 (5): 387-411. doi:10.1016/S0734-743X(98)90004-5.

Spitzig, W. A. and O. Richmond. 1984. "The Effect of Pressure on the Flow Stress of Metals." *Acta Metallurgica* 32 (3): 457-463. doi:https://doi.org/10.1016/0001-6160(84)90119-6. http://www.sciencedirect.com/science/article/pii/0001616084901196.

Timoshenko, Stephen. 1983. *History of Strength of Materials : With a Brief Account of the History of Theory of Elasticity and Theory of Structures*. New York: New York : Dover Publications.

Tvergaard, Viggo and Alan Needleman. 1984. *Analysis of the Cup-Cone Fracture in a Round Tensile Bar*. Vol. 32. doi:10.1016/0001-6160(84)90213-X.

Vaughan, H. 1980. *The Tearing Strength of Mild Steel Plate*. Vol. 24.

Wang, G., H. Ohtsubo, and D. Liu. 1997. *A Simple Method for Predicting the Grounding Strength of Ships*. Vol. 41.

Wierzbicki, Tomasz and Liang Xue. 2005. "On the Effect of the Third Invariant of the Stress Deviator on Ductile Fracture." *Impact and Crashworthiness Laboratory, Technical Report* 136.

Wierzbicki, Tomasz. 1995. "Concertina Tearing of Metal Plates." *International Journal of Solids and Structures* 32 (19): 2923-2943. doi:10.1016/0020-7683(94)00237-Q.

Wierzbicki, Tomasz, Yingbin Bao, and Yuanli Bai. 2005. *A New Experimental Technique for Constructing a Fracture Envelope of Metals Under Multi-Axial Loading*.

Wilson, C. D. 2002. "A Critical Reexamination of Classical Metal Plasticity." *Journal of Applied Mechanics* 69 (1): 63. doi:10.1115/1.1412239.

Woisin, G. 1979. "Structural Design Against Collision." *Advances in Marine Technology*.

Xue, Liang. 2007. "Damage Accumulation and Fracture Initiation in Uncracked Ductile Solids Subject to Triaxial Loading." *International Journal of Solids and Structures* 44 (16): 5163-5181. doi:10.1016/j.ijsolstr.2006.12.026.

Xue, Liang and Tomasz Wierzbicki. 2006. *Verification of a New Fracture Criterion using LS-DYNA*.

Zhang, Shengming. 2002. "Plate Tearing and Bottom Damage in Ship Grounding." *Marine Structures* 15 (2): 101-117. doi:10.1016/S0951-8339(01)00021-1.

Zheng, Zi-Ming. 1994. "Theoretical Analyses of Wedge Cutting through Metal Plates."Massachusetts Institute of Technology.

Appendix A – Plate Sample Material Bills

12/20/16 7:14:34

EMAIL COVER PAGE

==========

Company:

12/20/16 7:14:34 Document Summary:

Cover Page: 1

Subject: MILL TEST CERTIFICATE

Order Number :03359677

Customer PO# :REQ # 040459

City : MEM. UNIV OF NFLD, S State/Province : NL

The order of the printed MTRs is as follows:

Item	Description:	Heat	MTR
.	.188 (3/16) HR PLT 44W/50W	139388	020077471

ArcelorMittal Dofasco G.P.
P.O. Box 2460
Hamilton, Ontario
L8N 3J5

TEST REPORT
RAPPORT D'ESSAI

Page 1 of 1

Attention: Jharvey
Email: jharvey@russelmetals.com
Date: 07/14/2016

-Purchase Order/Bon de Commande-
P02098098 -1 JULY
-Bill of Lading/Connaissement-
343636
-Customer/Client-
557628
-Sales Order/Bon de Commande-
PCS 359988001
-Packing Slip/Bordereau de Charge-
-Vehicle or Carrier/Vehicule ou Transporteur-
-Vendor/Vendeur-

-Sold To/Vendu A-
RUSSEL METALS INC.
28 LAKESIDE PARK DRIVE
LAKESIDE, NS.
B3T 1A3

-Ship To/Expedier A-
COILEX - VARENNES
350 RUE JEAN COUTU, SUITE DOOR #1
VARENNES, QC.
J3X 0E1
CORNER DE L'ENERGIE/JEAN COUTU

-Spec/Norm et Spec-
DOF G40.21 44W/50W FOR CONV TO PLATE (01/11)
STANDARD THICKNESS TOLERANCE
TEST REPORTS REQUIRED
CODE 64494

-Material Description/Description du Material-
PLATE-IN-COIL FOR CONVERSION
STRUCTURAL STEEL
COILS
MILL EDGE PLAIN DRY
.1890 MIN .1898 X 48 X COIL
Weight: 42580 LBS
-Test Methods/Methods d'Essai-
ASTM A370, E1019, E415

HEAT
COULEE C Mn P S Si Cu Ni Cr Sn Mo Als Alt Cb V Ti Ca N B O
139388 .06 .54 .009 .004 .02 .14 .04 .08 .006 .013 .034 .035 .027 .003 .015 .002 .0054 .0001

MECHANICAL PROPERTIES/PROPRIÉTÉS MÉCANIQUES

SERIAL NUMBER / NOMBRE DE SERIE	LIFT # / FARDEAU	DIR	TEST UNITS KSI YIELD STRENGTH RESISTANCE A LA D'ELASTICITE	ULTIMATE STRENGTH RESISTANCE A LA TRACTION	GAUGE LENGTH 2 INCH %ELONG ALLONG
L21949/88	3445713	T	57	70	31.2 (*)

(*) - Method of elongation calculation: at fracture. / Méthode de calcul de l'allongement: au point de fracture.

0200 77471

ArcelorMittal Dofasco G.P. as per Lesley Taggart - CMTL Supervisor
The Results Relate Only To The Items Tested

AMC - Atlantic Metallurgical Consulting Limited

TEST REPORT
DETERMINATION OF TENSILE PROPERTIES

Conducted By: Mechanical Testing Division
AMC - Atlantic Metallurgical Consulting

Client: Russel Metals Inc.
Halifax, NS

Date: Sept. 14, 2016

AMC Project No.: 16-AMC-314

Purchase Order No.: 02023932

Item Tested: **$^{3}/_{16}$" Coil – Lead and Centre Sections**
- Ht# 139388
- Tag# 81691

Testing Equipment:
- MTS 8500 Testing Machine with ADMET MTESTQuattro Digital Electronics, Cal Due – Aug, 2017
- Instron Extensometer, Cal Due – Aug, 2017
- Mitutoyo Digital Calipers, Cal Due – Oct. 29, 2016

Testing Procedure: All testing was conducted in accordance with the requirements of:
CSA G40.20/G40.21: General Requirements for Rolled or Welded Structural Quality Steel / Structural Quality Steel

Results: The material tested meets the minimum requirements for CSA 44W/50W.

Specimen ID.	Maximum Load (lb)	Tensile Strength (psi)	Yield Load (lb)	Yield Strength (psi)	Elong. (%)	Width (in)	Thick. (in)
Lead, Ht# 139388	19,732	70,092	15,261	54,208	38	1.530	0.184
Centre, Ht# 139388	19,491	69,568	15,520	55,394	39	1.531	0.183

Verification: THIS IS TO CERTIFY THAT THE ABOVE TESTING WAS PERFORMED ACCORDING TO REQUIREMENTS SET FORTH BY THE CLIENT AND AMC – ATLANTIC METALLURGICAL CONSULTING IN A MANNER CONSISTENT WITH STANDARD PRACTICES.

RESULTS RELATE ONLY TO THE ITEMS TESTED.

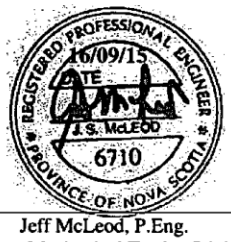

Verified By: _____
Jeff McLeod, P.Eng.
Manager, Mechanical Testing Division

AMC – Atlantic Metallurgical Consulting Limited
11 Morris Dr., Unit 106, Dartmouth, Nova Scotia, Canada B3B 1M2 Tel: (902) 405-3600 Fax: (902) 405-3601

1/16/17 10:16:45

EMAIL COVER PAGE

==========

Company: Russel Metals Inc

1/16/17 10:16:45 Document Summary:

Cover Page: 1

Subject: MILL TEST CERTIFICATE

Order Number :02067682

Customer PO# :REQ # 040460

City : MEM. UNIV OF NFLD, S State/Province : NL

The order of the printed MTRs is as follows:

Item	Description:	Heat	MTR
.	.188 (3/16) HR PLT 44W/50W	778710	020081333

	.188 (3/16) HR PLT 44W/50W	9167B4	020077461

SOLD 4000002
TO RUSSEL METALS INC.
28 LAKESIDE PARK DRIVE
LAKESIDE NS B3T 1A3

SHIPPED
TO RUSSEL METALS INC.
28 LAKESIDE PARK DRIVE
LAKESIDE NS B3T 1A3

SALES DESCRIPTION.....
.188 (3/16) HR PLT 44W/50W
.188 (3/16) HR PLT 44W/50W
72" 240.0000
CUST.ORDER# M02097476
MILL: USS

GRADE | ITEM | ORDER# | DATE SHIPPED 4/14/16
23186 | 40200570 | QTY SHIPPED 7400

TAG NO. 1998071
RELEASE
MILL NO. 4037-013116
CONTRACT
COUNTRY OF ORIGIN CANADA

HEAT NO. 778710

CHEMICAL ANALYSIS

CARBON	MANGANESE	PHOSPHORUS	SULPHUR	SILICON	COPPER	NICKEL	CHROMIUM
.0600	.5800	.0070	.0080	.0150	.0310	.0130	.0330

MOLYBDENUM	VANADIUM	COLUMBIUM	ALUMINUM	ASA	ZINC	TITANIUM	BORON
.0040	.0020	.0370	.0430	.0000	.0000	.0020	.0002

MECHANICAL / PHYSICAL PROPERTIES

ROCKWELL	TENSILE PSI	YIELD PSI	ELONGATION	SAMPLE SIZE	ONE	CEV
000	76000.000	64500.000	24.00	2.000	.0000	.0000

JOULES	FT LBS	LDH TEST	N VALUE	R VALUE	IMPACTS	BENDTEST	TEST
.0000	.0000	.000	.000	.000	00000000	00000000	16-0253C

WE CERTIFY THE HEAT ANALYSIS AND OR TEST RESULTS SHOWN ABOVE ARE TRUE AND EXACT AS CONTAINED IN THE PERMANENT RECORDS OF RUSSEL METALS INC. THESE RECORDS MAY BE EXAMINED BY YOUR PERSONNEL OR ANY AGENT AUTHORIZED BY YOU.

AUTHORIZED AGENT

B&T Steel
A Division of Russel Metals Inc.

1052 South Service Road, Stoney Creek, ON L8E 6G3
Mailing Address: P.O. Box 2105, LCD1, Hamilton, ON L8N 3R5
Toll Free: 1-800-263-6597 Tel: (905) 643-3008 Fax: (905) 643-5976

Form# 071 Rev 4 09-07-2011

ISO 9001
REGISTERED QMS

0200 81333

ESSAR STEEL

ESSAR STEEL ALGOMA INC.,105 West Street, Sault Ste. Marie,Ontario, Canada P6A 7B4

SO No.,Item & Date.: 8043207 000010 2016/06/17	Shipment No.& Date.: 1200006003 2016/06/21	TC No., Date & Time : ESA-331547 2016/06/23 - 13:38:01
Sold to Customer Name and Address :	Ship to Customer Name and Address:	Customer PO NO./Item: M02097531 / 2
RUSSEL METALS INC	RUSSEL METALS INC	BOL NO.: 1200006003
LAKESIDE PARK DRIVE 28	RUE IRWIN 6001	Cust.Part No.: 64499
LAKESIDE,Nova Scotia,Canada	LASALLE,Quebec,Canada	Carrier : C P RAIL (CAD FUNDS) - CIGX 803854
B3T 1A3	H8N 1A1	

Customer Specification : HR STEEL SHEET HSLA SQ / SS To the Chemistry of Multi Cert CSA G40.21 50W (2013) / CSA G40.21 44W (2013) Top Semi Critical Surface Improved Shape Gauge type MIN - 0/+ 0.0165 "

Supplementary Instructions : Test Cert 1:ssawh@russelmetals.com Test Cert 2: jharvey@russelmetals.com E

Insp T/R : Test Report For Info Only Cust Use : STRUCTURAL

ESSAR STEEL ALGOMA INC. HEREBY CERTIFIES THAT THE MATERIAL HEREIN DESCRIBED WAS MADE AND TESTED IN ACCORDANCE WITH THE RULES OF THE SPECIFICATION SHOWN. ALL RESULTS ARE RETAINED IN ACCORDANCE WITH THE COMPANY'S STANDARD RECORD KEEPING PRACTICES.
THIS MILL TEST REPORT MAY NOT BE REPRODUCED EXCEPT IN FULL WITHOUT WRITTEN APPROVAL OF ESSAR STEEL ALGOMA INC. IF YOU RECEIVE THIS DOCUMENT AND ARE NOT THE INTENDED RECEIVER, PLEASE CALL (705)945-4095 FOR INSTRUCTIONS ON METHOD OF DISPOSAL OF DOCUMENT. THIS TEST REPORT HAS BEEN GENERATED BY A COMPUTERIZED SYSTEM AND IS VALID WITHOUT A PHYSICAL SIGNATURE.

MEETS EN 10204 3.1
ISO QUALITY AND ENVIRONMENTAL CERTIFICATES AVAILABLE AT WWW.ESSARSTEELALGOMA.COM

ALL HEATS FULLY KILLED.
HEATS INDICATED WITH (*) FINE GRAINED.
HEATS INDICATED WITH (+) Made in Canada for NAFTA duty preference and NAFTA marking purposes

Dimensions (T x W x L)	Batch No.	Heat No-MS	Quantity	Pcs
0.1800 " x 72.000 "	LQG7393	9167B4-55	31,080 LB	1

CHEMICAL PROPERTIES

Heat No. (wt%)	C	Mn	P	S	Si	Cr	Ni	Cu	Mo	Al	Nb	V	Ti
9167B4+*	0.08	0.88	0.007	0.004	0.020	0.03	0.02	0.04	0.00	0.032	0.047	0.000	0.001

MECHANICAL PROPERTIES

Tensile Tests

Heat No.	Batch No.	SRCE	LAB	GAUGE	COND	METH	DIR	LOC	YIELD(KSI)	TENSILE(KSI)	EL SCALE	ELONG(%)
9167B4		106*	ALG	0.1800	AR	.2	T	F	69.0	77.0	2"	25

0200 77461

KASHIF REHMAN
MANAGER METALLURGICAL SERVICES

WARNING THE TEST RESULTS AND VALUES REPORTED HEREIN INDICATE ONLY THAT (1) THE PARTICULAR STEEL FOR WHICH THIS CERTIFICATE IS ISSUED MEETS THE MINIMUM SPECIFIED YIELD STRENGTH AND (2) THE ANALYSIS AND PHYSICAL PROPERTIES OF SUCH STEEL ARE IN CONFORMANCE WITH THE REQUIREMENTS OF THE SPECIFICATION INDICATED. THE RESULTS OR VALUES REPORTED HEREIN CAN NOT BE USED TO QUALIFY THE STEEL FOR ANY SPECIFICATION OTHER THAN THE ONE INDICATED AND CAN NOT BE RELIED UPON FOR ANY PURPOSE (INCLUDING DESIGN OR CALCULATIONS) AS REPRESENTING THE ACTUAL STRENGTH OF SUCH STEEL.

Date:2016/06/23 Time:14:50:08 Page no:1 of 1

AMC - Atlantic Metallurgical Consulting Limited

TEST REPORT
DETERMINATION OF TENSILE PROPERTIES

Conducted By: Mechanical Testing Division
AMC - Atlantic Metallurgical Consulting

Client: Russel Metals Inc.
Halifax, NS

Date: Sept. 6, 2016

AMC Project No.: 16-AMC-304

Purchase Order No.: 02023890

Item Tested: **$^{3}/_{16}$" Coil – Lead and Centre Sections**
- **Ht# 9167B4**
- **Tag# C1210088**

Testing Equipment:
- MTS 8500 Testing Machine with ADMET MTESTQuattro Digital Electronics, Cal Due – Aug, 2017
- Instron Extensometer, Cal Due – Aug, 2017
- Mitutoyo Digital Calipers, Cal Due – Oct. 29, 2016

Testing Procedure: All testing was conducted in accordance with the requirements of:
CSA G40.20/G40.21: General Requirements for Rolled or Welded Structural Quality Steel / Structural Quality Steel

Results: The material tested meets the minimum requirements for CSA 44W/50W.

Specimen ID.	Maximum Load (lb)	Tensile Strength (psi)	Yield Load (lb)	Yield Strength (psi)	Elong. (%)	Width (in)	Thick. (in)
Lead, Ht# 9167B4	21,390	76,024	17,230	61,236	34	1.555	0.181
Centre, Ht# 9167B4	21,774	75,666	17,494	60,794	35	1.556	0.185

Verification: THIS IS TO CERTIFY THAT THE ABOVE TESTING WAS PERFORMED ACCORDING TO REQUIREMENTS SET FORTH BY THE CLIENT AND AMC – ATLANTIC METALLURGICAL CONSULTING IN A MANNER CONSISTENT WITH STANDARD PRACTICES.

RESULTS RELATE ONLY TO THE ITEMS TESTED.

REGISTERED PROFESSIONAL ENGINEER
16/09/06
DATE
J.S. McLEOD
6710
PROVINCE OF NOVA SCOTIA

Verified By: _____
Jeff McLeod, P.Eng.
Manager, Mechanical Testing Division

AMC – Atlantic Metallurgical Consulting Limited
11 Morris Dr., Unit 106, Dartmouth, Nova Scotia, Canada B3B 1M2 Tel: (902) 405-3600 Fax: (902) 405-3601

Appendix B – GoPro HD Hero 2 & 3 Specifications

FEATURES	HD HERO 2
PHOTO – FEATURES + FOV	
MEGAPIXELS	5 MP
MODES	Single 3 photos in 1 sec Time Lapse every 1, 2, 10, 30, 60 Self-Timer
VIDEO – RESOLUTION + FOV	
1080p	1920×1080 wide (127°) FOV 30fps
960p	1280×960 FOV Wide (170°) 30fps
720p	1280×720 Wide (170°) FOV 30fps 60fps
WVGA	848×480 Wide (170°) FOV 60fps
USABILITY	
Inputs	Component port, Composite port, USB, SD, HERO Port
Battery Life (in 720p/60 mode)	2.5 hrs
Simultaneous record + charge when plugged into USB power source	yes

FEATURES	HERO 3
Optics + Lens	Ultra-sharp *f*/2.8 - 6 element lens, Ultra wide angle with reduced distortion
PHOTO FEATURES	
Megapixels	5MP
Modes	Photo Burst Photo Time Lapse
VIDEO FEATURES + FOV	
1080p (16:9)	30, 25 fps Medium FOV
960P (16:9)	30, 25 fps Ultra Wide FOV
720P (16:9)	60, 50, 30, 25 fps Ultra Wide FOV
WVGA (16:9)	60, 50 fps Ultra Wide FOV
PHOTO SPECS	
Megapixels + FOV	5MP (Wide)
Time Lapse Intervals	0.5, 1, 2, 5, 10, 30, 60 seconds
Burst Photo (Frames/sec)	3/1
ADVANCED FEATURES	
Wi-Fi Built-in	Yes
Looping Video	Yes
High Video Bitrate Capture (H.264) Mode dependent, highest bitrates supported in Protune	Up to 15/Mbs
AUDIO SPECS	
Mono Mic, AAC compression w/ AGC	No
USABILITY	
Inputs	Micro-HDMI port, mini USB, microSD, HERO Port, composite A/V (via adapter, optional accessory), 3.5mm stereo mic (via adapter, optional accessory)
Battery	1050mAh rechargeable lithium-ion

Appendix C – Cannon Rebel T5 EOS Specifications

- Large single-plate CMOS sensor with 18 effective megapixels
- ISO 100-6400
- Dedicated CMOS sensor for autofocus, 9-point AF
- Compatible with SD-SDHC-SDXC memory
- Compatible with Canon EF lenses

See:http://www.canon.ca/en/product?name=EOS_Rebel_T5&category=/en/products/Cameras/DSLR-Cameras/Entry-level#specific